



**TURUN
YLIOPISTO**
UNIVERSITY
OF TURKU

STRUCTURAL AND CHEMICAL MODIFICATIONS OF POROUS SILICON FOR BIOMEDICAL APPLICATIONS

Ermei Mäkilä



**TURUN
YLIOPISTO**
UNIVERSITY
OF TURKU

STRUCTURAL AND CHEMICAL MODIFICATIONS OF POROUS SILICON FOR BIOMEDICAL APPLICATIONS

Ermei Mäkilä

University of Turku

Faculty of Science
Department of Physics and Astronomy
Physics
Doctoral programme in Exact Sciences

Supervised by

Professor Jarno Salonen
Department of Physics and Astronomy
University of Turku
Turku, Finland

Professor Hélder A. Santos
Department of Biomedical Engineering
University Medical Center Groningen
University of Groningen
Groningen, The Netherlands

Reviewed by

Professor Jeffery L. Coffey
Department of Chemistry and
Biochemistry
Texas Christian University
Fort Worth, Texas, United States

Professor Ester Segal
Department of Biotechnology and
Food Engineering
Technion – Israel Institute of Technology
Haifa, Israel

Opponent

Professor Michael J. Sailor
Department of Chemistry and
Biochemistry
University of California San Diego
La Jolla, California, United States

The originality of this publication has been checked in accordance with the University of Turku quality assurance system using the Turnitin OriginalityCheck service.

Cover Image: Optical micrograph by E. Mäkilä and M. Kaasalainen, 2016

ISBN 978-951-29-9723-7 (PRINT)
ISBN 978-951-29-9724-4 (PDF)
ISSN 0082-7002 (PRINT)
ISSN 2343-3175 (ONLINE)
Painosalama Oy, Turku, 2024

For my late parents

UNIVERSITY OF TURKU

Faculty of Science

Department of Physics and Astronomy

Physics

MÄKILÄ, ERMEI: Structural and chemical modifications of porous silicon for biomedical applications

Doctoral dissertation, 164 pp.

Doctoral programme in Exact Sciences

June 2024

ABSTRACT

The versatility in properties of porous silicon (PSi) has enabled a broad spectrum of applications, ranging from microelectronics and various types of sensors to its use as a biocompatible material in drug delivery.

Structural properties of PSi were shown in this work to be adaptable post-fabrication using thermal annealing. Control over the average pore size of the material proved to be beneficial, when adjustments were necessary to accommodate larger biomolecules within the pores of the PSi. Furthermore, a facile method of fabricating PSi nanoparticles was introduced using a multilayer approach with a stepwise electrochemical etching process, where the comminution of the material was guided with formation of fragile, high porosity perforation layers at specific intervals. This method has been proven successful, being utilized in over 70 publications so far.

For extended control over biocompatibility and biodistribution of PSi micro- and nanoparticles, two new surface modifications based on hydrolytically stabilized PSi were introduced. Amine-terminated thermally carbonized PSi, capable of carbodiimide crosslinking for further functionalization with biomolecules, and an alkyne-terminated hydrocarbonized PSi, enabling the use of click chemistry -based addition reaction for secondary functionalization.

Solid-state properties of confined drug molecules adsorbed into PSi microparticles were also studied. As PSi is known to enhance aqueous dissolution and cellular permeability of poorly soluble drugs, more accurate information was sought on the effects of the mesoscale confinement. Small molecule drugs were observed to partially have a liquid-like behavior according to solid-state NMR analysis and participate in interactions with the pore walls, according to the availability of specific functional groups. Slight disruption in short-range order of the adsorbed drugs was also found, as the confinement appeared to reduce the true density of the drug molecules below that of a bulk amorphous state. Study over the conditions for efficient drug adsorption into the pores showed the importance of solvent and drug solution concentration selection. Optimal choices enabled high drug payload within the PSi, without precipitation of crystalline drug on the external surface of the PSi microparticles.

KEYWORDS: porous silicon, surface chemistry, nanoparticles, microparticles, confinement, drug delivery

TURUN YLIOPISTO

Matemaattis-luonnontieteellinen tiedekunta

Fysiikan ja tähtitieteen laitos

Fysiikka

MÄKILÄ, ERMEI: Structural and chemical modifications of porous silicon for biomedical applications

Väitöskirja, 164 s.

Eksaktien tieteiden tohtoriohjelma

Kesäkuu 2024

TIIVISTELMÄ

Huokoisen piin (*porous silicon*, PSi) monipuoliset ominaisuudet ovat mahdollistaneet runsaasti erilaisia sovelluksia, lähtien mikroelektroniikasta ja ilmaisimista aina tämän käyttöön bioyhteensopivana materiaalina lääkeannostelussa.

Tässä työssä osoitettiin huokoisen piin rakenteen olevan jälkikäteen muokattavissa hallitusti lämpökäsittelyn avulla. Huokoskokoja kasvattamalla mahdollistettiin tarpeen vaatiessa suurempien biomolekyylien pääsy huokosiin. Tämän lisäksi esiteltiin menetelmä huokoisen piin nanopartikkelien valmistamiseksi syövyttämällä sähkökemiallisesti huokoinen monikerrosrakenne, missä tasaisin välimatkoin sijaitsevat hauraat korkean huokoisuuden kerrokset toimivat murtumista edistävinä kohtina. Menetelmää on sittemmin hyödynnetty tähän mennessä yli 70:ssä tieteellisessä julkaisussa.

Huokoisen piin mikro- ja nanopartikkelien bioyhteensopivuuden ja kulkeutumisen hallintaan työssä kehitettiin kaksi uutta pintakemiallista muunnosta huokoiselle piille, mikä oli esikäsitelty heikosti veteen liukenevaksi. Muunnokset perustuivat vapaiden amiiniryhmien ja alkyynien saatavuuteen huokoisen piin pinnoilla. Näistä edellinen mahdollisti biologisen funktionalisoinnin karbodi-imidisilloituksen kautta, jälkimmäisen puolestaan mahdollistaen monipuolinen funktionalisointi kupariavusteisen sykloadditioreaktion kautta.

Lääkemolekyylien fysikaalista olotilaa nanokokoluokan huokosissa tutkittiin huokoisen piin mikropartikkelien avulla. Huokosiin adsorboitujen niukkaliukoisten lääkeaineiden tiedetään liukenevan tehokkaasti veteen, mutta syitä tälle voi olla useita. Pienmolekyyllilääkkeiden havaittiin olevan osittain nestemäisessä muodossa huokosten sisällä NMR-tutkimusten mukaan. Molekyylien lähijärjestys vaikutti myös osittain muuttuneen, huokosiin adsorboituneen lääkeaineen tiheyden ollessa tavallista amorfista tilaa alhaisempi.

Lääkeaineen adsorptiota huokosiin pyrittiin myös tehostamaan seuraamalla liuotimen ja lääkeaineliuoksen konsentraation vaikutusta. Sopivin parametrein saavutettiin korkea lääkkeen hyötykuorma, ilman lääkemolekyylien kiteytymistä huokoisen piin mikropartikkelien ulkopinnoille.

ASIASANAT: huokoinen pii, pintakemia, nanopartikkelit, mikropartikkelit, lääkeannostelu

Acknowledgements

With this long process of compiling the pages that follow coming to an end, I find myself pondering on the choices and priorities I set myself at a time which now feels so long ago. Would I have pursued different interests, had this been completed within a more, how would I say it, sensible schedule? As trite it may sound – I doubt it. At the very least, it probably would not have been as fun and interesting.

For pursuit of knowledge, there could not have been a better place to work than the Laboratory of Industrial Physics. Interdisciplinary research is just another day at the office. For this I am grateful my supervisor Jarno Salonen, who has provided this environment. I will extend my thanks to Hélder A. Santos who also took on the task of supervision of this rather extended project I embarked upon.

Science is rarely done by a single person. Instead, it advances as a team effort, building upon the foundation laid by those who came before us. On this journey of scientific process, I thank all my co-authors for their contributions to the original publications and also for allowing me to contribute to your research.

A large part that has made this work what it is, is the camaraderie in our laboratory. For this I thank my colleagues and friends, past and present in the Laboratory of Industrial Physics over the years, Tero Jalkanen, Martti Kaasalainen, Jaani Paski, Jaakko Lamminpää, Matti Murtomaa, Maija Nyström, Jorma Roine, Outi Alanen, Janne Peltonen, Luke Jäppinen, Rici Lindgren, Teemu Heikkilä, Mikko Tenho, Mikko Björkqvist, Mika Aarnio, Teija Sainio, Joakim Riikonen, Vesa-Pekka Lehto and all others I have accidentally forgotten to mention here. I am grateful also to my former students, Leila, Rosita, Sanna-Mari, Noora, Joonas and Markus who worked on the often silly ideas I had come up with, contributing to the pool of research regarding the miracle material, porous silicon.

Integral part for most of the research I have worked in, has been the Division of Pharmaceutical Chemistry and Technology at University of Helsinki under the stewardship of Jouni Hirvonen. Here, the members of the Santos group drove our knowledge and understanding of porous silicon in biomedicine forward with incredible pace and I can only say I am honoured to have been part of it. My warmest thanks to Luis Bimbo, Dongfei Liu, Chang-Fang Wang, Mohammad-Ali Shahbazi, Neha Shrestha, Alexandra Correia, Mónica Ferreira, Hongbo Zhang, Patrick Almeida, Zehua Liu and everyone else in this wonderful and extensive group.

Similarly important has been our long collaboration with the Laboratory of

Radiochemistry at University of Helsinki, where I extend my thanks to Mirkka Sarparanta, Anu Airaksinen, Kerttuli Helariutta, Ulrika Jakobsson and Outi Keinänen.

I am grateful for Professor Nicolas Voelcker for hosting my research visit in Adelaide at the Mawson Institute in University of South Australia. Also, I will thank Professor Kurt Kolasinski for the crash course in silicon electrochemistry over the few summers of your research sabbaticals in our laboratory, the results of which are shown in the cover image of this book.

And finally, I would like to thank the pre-examiners, Professor Ester Segal and Professor Jeffery Coffey for their helpful comments and suggestions to improve the text. For the defense, I am honoured to welcome Professor Michael J. Sailor as my opponent.

Turku, May 2024
Ermei Mäkilä

Table of Contents

Acknowledgements	vi
Table of Contents	viii
Abbreviations	x
List of Original Publications	xiii
1 Properties of porous silicon	1
1.1 From discovery to current interest	1
1.2 Fabrication of porous silicon	3
1.2.1 Prerequisites for electrochemical anodization	3
1.2.2 Electrochemical dissolution of silicon	4
1.2.3 Formation theories	6
1.3 Structural properties of porous silicon	10
1.3.1 Morphological features of porous silicon	10
1.3.2 Structural control and modification	12
1.4 Surface chemistry of porous silicon	13
1.4.1 Oxidation and Si–O -based modification	14
1.4.2 Hydrosilylation through Si–C linkage	16
1.4.3 Thermal carbonization	19
1.5 Applications of porous silicon	22
2 Biomedical use of porous silicon	27
2.1 Formulation considerations	28
2.2 Biocompatibility	33
2.3 Porous silicon as drug carrier material	34
2.3.1 Drug loading methods and on adsorption from solution	35
2.3.2 Effects of physical confinement on molecular state .	38
2.4 Biomedical and pharmaceutical applications	40

3 Aims of the study	48
4 Experimental	49
4.1 Fabrication and surface modification of porous silicon	49
4.2 Structural characterization	52
4.3 <i>In vitro</i> and <i>in vivo</i> experiments	55
5 Results and Discussion	57
5.1 Paper I	57
5.2 Paper II	58
5.3 Paper III	60
5.4 Paper IV	63
5.5 Paper V	66
5.6 Paper VI	67
6 Conclusions	72
List of References	74
Original Publications	99

Abbreviations

ALD	Atomic layer deposition
APSM	Advanced Porous Silicon Membrane
APSTCPSi	Aminopropylsilane-TCPSi
APTES	(3-Aminopropyl)triethoxysilane
ATR	Attenuated total reflectance
BCS	Biopharmaceutical Classification System
BET	Brunauer-Emmett-Teller
BJH	Barrett-Joyner-Halenda
CBM	Current burst model
CHF	Chloroform
CP-MAS	Cross-polarized MAS
CT	X-ray computed tomography
CuAAC	Copper catalyzed azide-alkyne cycloaddition
DLA	Diffusion limited aggregation
DNA	Deoxyribonucleic acid
DPP4	Dipeptidyl peptidase-4
DSC	Differential scanning calorimetry
DSSC	Dye-sensitized solar cell
DTGS	Deuterated triglycine sulfate
EPR	Enhanced permeation and retention
EtOH	Ethanol
FFA	Flufenamic acid
FIPOS	Full isolation by porous oxidized silicon
FTIR	Fourier-transform Infrared
GLP-1	Glucagon-like peptide 1
GSV	Griseofulvin
HF	Hydrofluoric acid
HPLC	High pressure liquid chromatography
IMC	Indomethacin
IUPAC	International Union of Pure and Applied Chemistry
LED	Light emitting diode
MACE	Metal assisted chemical etching
MAS	Magic angle spinning

MCF	Mesocellular foam
MPS	Mononuclear phagocyte system
NIR	Near-infrared
NMR	Nuclear magnetic resonance
PAS	Photoacoustic spectroscopy
PEG	Polyethylene glycol
PET	Positron emission tomography
PL	Photoluminescence
PSi	Porous silicon
RIE	Reactive ion etching
ROS	Reactive oxygen species
SBF	Simulated body fluid
SDS-PAGE	Sodium dodecyl sulphate polyacrylamide gel electrophoresis
SEM	Scanning electron microscopy
SOI	Silicon-on-insulator
SON	Silicon-on-nothing
SPECT	Single-photon emission computed tomography
SRAM	Static random access memory
TC	Thermal carbonization
TCPSi	Thermally carbonized PSi
TEM	Transmission electron microscopy
TG	Thermogravimetry
THC	Thermal hydrocarbonization
THCPSi	Thermally hydrocarbonized PSi
THF	Tetrahydrofuran
TOPSi	Thermally oxidized PSi
UnTHCPSi	-COOH-derivatized THCPSi
UV	Ultraviolet
XPS	X-ray photoelectron spectroscopy
XRD	X-ray diffraction

List of Original Publications

This dissertation is based on the following original publications, which are referred to in the text by their Roman numerals:

- I** Salonen, J., Mäkilä, E., Riikonen, J., Heikkilä, T. and Lehto, V.-P. *Controlled enlargement of pores by annealing of porous silicon*. *Physica Status Solidi (A)*, **2009**; 206(6): 1313–1317.
- II** Bimbo, L. M., Sarparanta, M., Santos, H. A., Airaksinen, A. J., Mäkilä, E., Laaksonen, T., Peltonen, L., Lehto, V.-P., Hirvonen, J. and Salonen, J. *Biocompatibility of Thermally Hydrocarbonized Porous Silicon Nanoparticles and their Biodistribution in Rats*. *ACS Nano*, **2010**; 4(6): 3023–3032.
- III** Mäkilä, E., Bimbo, L. M., Kaasalainen, M., Herranz, B., Airaksinen, A. J., Heinonen, M., Kukkk, E., Hirvonen, J., Santos, H. A. and Salonen, J. *Amine Modification of Thermally Carbonized Porous Silicon with Silane Coupling Chemistry*. *Langmuir*, **2012**; 28(39): 14045–14054.
- IV** Wang, C.-F., Mäkilä, E., Bonduelle, C., Rytönen, J., Raula, J., Almeida, S., Närvänen, A., Salonen, J., Lecommandoux, S., Hirvonen, J. T. and Santos, H. A. *Functionalization of Alkyne-Terminated Thermally Hydrocarbonized Porous Silicon Nanoparticles With Targeting Peptides and Anti-fouling Polymers: Effect on the Human Plasma Protein Adsorption*. *ACS Applied Materials & Interfaces*, **2015**; 7(3): 2006–2015.
- V** Mäkilä, E., Ferreira, M. P. A., Kivelä, H., Niemi, S.-M., Correia, A., Shahbazi, M.-A., Kauppila, J., Hirvonen, J., Santos, H. A. and Salonen, J. *Confinement Effects on Drugs in Thermally Hydrocarbonized Porous Silicon*. *Langmuir*, **2014**; 30(8): 2196–2205.
- VI** Mäkilä, E., Kivelä, H., Shrestha, N., Correia, A., Kaasalainen, M., Kukkk, E., Hirvonen, J., Santos, H. A. and Salonen, J. *Influence of Surface Chemistry on Ibuprofen Adsorption and Confinement in Mesoporous Silicon Microparticles*. *Langmuir*, **2016**; 32(49): 13020–13029.

The original publications have been reproduced with the permission of the copyright holders.

1 Properties of porous silicon

1.1 From discovery to current interest

With the discovery of the solid state transistor in the late 1940s by Bardeen, Brattain and Shockley [1], the interest in developing semiconductors suitable for utilization in communication technology to replace the aging vacuum tubes increased. While the initial experiments were made on germanium, in the early 1950s silicon also started to gain attention as purification methods were refined and the semiconducting nature of silicon could be better controlled [2], being enough for a Si-based transistor [3]. By the end of the decade, Si had practically replaced germanium, as it had several advantages over Ge, from physical, chemical and manufacturing standpoints [4, 5].

Since fabrication of semiconductor devices requires clean, undamaged surfaces, an accidental discovery during studies of chemical polishing of Ge and Si was made in Bell Laboratories in 1955 by Arthur and Ingeborg Uhlir [6, 7]. While emphasizing Ge, an important note of Si behavior during attempts of electropolishing was included. Under specific anodic potentials, the surface of the Si substrate did not polish tetravalently as expected with hydrofluoric acid (HF), but instead formed a matte, dark red or brown layer, with the reaction proceeding divalently and producing hydrogen. Although initially assumed by the Uhlirs as a silicon suboxide due to the presumed nature of the reaction, this discovery marked the first report of the material later to be recognized as porous silicon (PSi). Further studies related to electropolishing were carried out by Turner, similarly noting the dark film formation under certain hydrofluoric acid concentrations and anodic current densities, while suspecting the film to be possibly porous, as the formation did not disrupt the current flow [8]. The experiments also showed the anode film to lift off as flakes, if the current was sufficient for electropolishing and reacting violently on exposure to strong oxidizers such as nitric acid (HNO_3).

Another observation made at the Bell Laboratories was by Fuller and Ditzenberg, showing a dark stain forming on the Si substrate when wetted in HF with trace amounts of HNO_3 [9]. Later, Turner [10] and Archer [11] recognized the reaction with the etchant and Si to be electrochemical in nature and the forming colorful stain film to share similarities with the anode film observed by the Uhlirs. Interestingly, these early results already noted the film composition to be silicon hydrides, but also in some cases crystalline, albeit with reduced density. The film

was however considered as deposited. Further studies on anode film formation were conducted at Philips Laboratories by Memming and Schwandt [12], providing more comprehensive overview on the electrochemical dissolution mechanism, with also more evidence mounting on the nature of the film being porous and much of the Si atoms being part of Si–H structures [13]. The works of Meek [14] and Theunissen [15, 16] brought more information on the selective nature of the etching process. Watanabe and Sakai at NTT confirmed the porous nature of the anode film, when utilizing the tendency of PSi to oxidize at fairly moderate conditions to create thick insulating layers for semiconductor devices [17, 18]. Further work at NTT by Arita and Sunohara verified the retainment of crystalline structure after porosification [19].

Despite the obscurity of the material, the late 1970s and the 1980s saw considerable advances in understanding the formation mechanisms and general properties of PSi, such as the work of Pickering *et al.* who observed photoluminescence of PSi at cryogenic temperatures in studies regarding the optical properties of the material [20, 21]. It was not until the early 1990s, when two seminal papers were published regarding the quantum wire nature of microporous Si. The discovery of visible photoluminescence (PL) of PSi at room temperature by Leigh Canham [22] and theoretical basis for the formation of such structure by Volker Lehmann and Ulrich Gösele [23] brought PSi into center of sudden attention. Photoluminescence from an indirect band gap material caused a flurry of research due to the possibility of Si-based optoelectronics. The report of visible PL was soon followed by observations of electroluminescence [24–26] and chemiluminescence [27]. The concerted research effort on PSi broadened also beyond the search for Si-based LED. Berger *et al.* [28–30] and Vincent [31, 32] showed that PSi can also be applied as an optical component, utilizing the porosity based control of the refractive index as a basis, for example, interference filters, culminating in a seminal paper by Lin *et al.* [33], leading to the development of PSi-based optical biosensors. Another pivotal discovery was the apparent bioactivity of PSi, made by Canham [34]. According to the initial porosity of PSi, the material would behave either as bioinert or bioactive, promoting the growth of hydroxyapatite in simulated body fluid (SBF), or even bioresorbable, opening the field of biomedicine for PSi based applications. While the initial promise in light emission did not come into fruition, leading to waning interest in PSi luminescence, the new fields found during this initial push had taken over and are still actively pursued, over 30 years later.

The following sections touch upon the topics and methodologies employed in the included papers at the end of this thesis, providing a brief overview on the fabrication, structure and surface chemistry of PSi and basis for its application in drug delivery. For avid readers, the recent years regarding the state of PSi research have been very bountiful with several books published, such as Porous Silicon in Practice by M. J. Sailor [35] along with two handbooks, Porous Silicon for Biomedical Applications,

edited by H. A. Santos [36] and Handbook of Porous Silicon, edited by L. T. Canham [37], each providing an in-depth look on the properties of porous silicon.

1.2 Fabrication of porous silicon

Porous silicon can be produced in a multitude of different methods, such as the two initially discovered routes of electrochemical anodization and stain etching. These are accompanied by well over 30 other production routes, such as metal-assisted chemical etching (MACE) [38–43], metallothermic silica reduction [44–48], mechanical compaction [49, 50] and regenerative electroless etching [51–53], chronologically listed in reference [54].

These studies use exclusively electrochemical anodization for the production of PSi; hence the following section focuses only on describing the related fabrication process and formation mechanisms. It should be noted however, that for pharmaceutical applications, the importance of the other methods referred above is significant, considering requirements for cost-effective high volume production [51, 55].

1.2.1 Prerequisites for electrochemical anodization

The most common methods used in fabrication of PSi are electrochemical in nature, of which anodization in galvanostatic conditions is often selected due to its repeatability and versatility in controlling the properties of PSi in great detail. In general, the electrochemical fabrication of PSi is based on fluoride reactions with bulk silicon, and the subsequent selective removal of silicon atoms from the bulk surface.

Typically, the electrolyte is an aqueous HF-based solution, however non-aqueous organic and ammonium fluoride-based etchants have also been used [56, 57]. As the formation of porous layer produces hydrogen, the resulting gas bubbles can prevent the wetting of the hydrophobic silicon surface, locally stopping the anodization. Hence, the surface tension of the electrolyte is typically reduced by adding, *e.g.*, ethanol (EtOH) into the solution which also functions as a diluent. As effective surface tension lowering requires considerable amounts of EtOH, the use of surfactants is also common when high HF-concentrations are required.

The basic requirement for electrochemical anodization of silicon is a suitable etching cell.¹ In its simplest form, this can be any HF-resistant beaker, filled with electrolyte where the electrodes are immersed. In this configuration, the working electrode under anodic polarization is the Si substrate, and the counter-electrode is usually made from HF-resistant metal, such as platinum or from highly degenerate silicon [57]. While the immersion cell is easy to set up and exposes all surfaces of

¹ Commercial versions of etching cells are available currently from a handful of vendors, with the products scaling from laboratory research to industrial scale wafer processing. Such vendors are for example, Redoxme AB (Sweden), AMMT GmbH (Germany) and Lay Concept SAS (France).

the Si substrate to the electrolyte, the main drawback is the inhomogeneity of the forming porous layers. This results from the lateral drop of potential in the substrate, leading to a difference in current densities at the top and bottom and causing an uncontrollable gradient on the porous surfaces [58].

Considerably better configuration is a single tank anodization cell, where the Si substrate lies flat on a metal plate sealed with an O-ring, exposing only one side of the substrate to the electrolyte. The advantages of the cell are the ability to etch homogenous layers and more precise control over the porous layer thickness. A large enough cell can be used to process entire wafers at a time. A crucial aspect in this cell design is uniform back contact for the Si anode. With highly doped Si, a direct contact with the metal plate is enough to produce an ohmic contact. However, Si with low dopant concentration needs either dopant addition or metal layer deposited on the backside to ensure non-rectifying behavior at the metal-semiconductor junction [35].

As deposited metal would affect further processing of the substrate, a double tank cell provides similar advantages as its single tank counterpart, replacing the metallic back contact with an electrolytic one [59]. With high resistivity substrates, dopant addition to the back side is still recommended [58]. The electrolyte-based back contact however ensures high electric field homogeneity of the etched layers, and relatively easy use of either front or back side illumination with *e.g.*, sapphire or acrylate windows.

1.2.2 Electrochemical dissolution of silicon

In ambient conditions, silicon surface is passivated by a thin oxide layer [60]. Immersion into HF containing solution however removes the oxide layer, replacing it with a hydrogen termination [61–64]. While at open circuit conditions in a HF-based electrolyte, the dissolution rate of silicon is negligible, dependent only on the amount of oxidants in the solution. The behavior, however, undergoes a notable change when external bias is applied to the electrochemical system.

The electrochemical behavior of Si in different electrolytes can be described through current-voltage (I - V) curves. Figure 1 shows typical I - V curves for p - and n -type Si in the dark and under illumination with aqueous HF-based electrolyte. In both cases, cathodic polarization of the silicon results in hydrogen generation at the working electrode due to the reduction of water, while the Si remains intact. However, under anodic conditions when holes are available, Si starts to dissolve, in respect to the applied overpotential leading to selective dissolution of the silicon anode. In these conditions, PSi is formed through a divalent reaction accompanied by hydrogen evolution. Increasing the potential gradually changes the I - V behavior from exponential Tafel-like slope into a more linear growth, until reaching a current peak I_{ep} . This transition also moves the balance of the dissolution reaction toward an

indirect tetravalent reaction, indicated by a gradual increase in the effective valence of the reaction, until this takes over above the I_{ep} . After the peak current, the dissolution reaction shifts completely to the tetravalent form, causing electropolishing of the silicon surface and cessation of the hydrogen evolution [57].

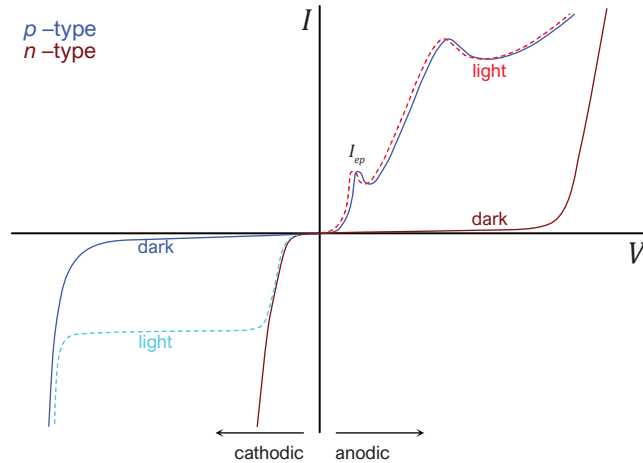


Figure 1. Representative current-voltage (I - V) relationship of p - and n -type Si in dark and under sufficient illumination. The initial current peak, I_{ep} , marks the transition to electropolishing through anodic oxide formation. The actual values for current and voltage are dependent on the Si dopant type, concentration as well as the composition of the electrolyte and the illumination intensity. Adapted from ref. [65].

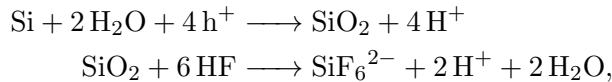
The I - V curve also shows the distinction between the p - and n -type doping, and the requirement for holes as charge carriers for the dissolution reactions. As the carrier supply is not a rate limiting factor for p -type Si, the current can be observed to increase above the critical I_{ep} value in the electropolishing region, eventually showing signs of current oscillations at high anodic overpotentials beyond the second current peak [8, 56, 66–69]. With n -type Si, holes are the minority carriers, and only with highly doped n^+ -type Si a similar I - V behavior can be expected. With low or moderately doped n -type, without sufficient generation of holes through illumination on the working electrode, anodic dissolution will not occur until breakdown conditions at high overpotentials are reached. As the diffusion length of the charge carriers in high purity Si is approximately $500\ \mu\text{m}$, a typical thickness of a Si wafer, the photogenerated holes may be produced either by front- or backside illumination of the Si. While the general I - V behavior of p - and n -type Si under sufficient hole supply is quite similar, the dopant type and concentration affect the required overpotential for the onset of the divalent dissolution. This can be used to provide spatial selectivity in the anodization of the material, with highly doped n^+ and p^+ -types beginning to anodize at lower potentials, while lower doped p and n require higher potentials [15, 65, 70]. Regarding the composition of the electrolyte, with aqueous

HF, changes in the concentration affect mainly the observed value of I_{ep} , with higher concentrations shifting the peak toward higher potentials [70].

The reaction on the Si anode below the critical current I_{ep} can be given by the following equation describing the direct dissolution of Si



where h^+ indicates a hole injection into the Si valence band. Above I_{ep} , the reaction is essentially a two-step process, as shown in equations



with the first step being a tetravalent anodic oxidation of Si followed by chemical dissolution of the oxide by HF, the latter being also the rate limiting step.

Several mechanisms have been presented to describe the dissolution process below I_{ep} [12, 23, 71, 72], one such being the revised Gerischer model [71] shown in simplified form in Figure 2. The reaction mechanism describes the process on the $\langle 100 \rangle$ surface of Si, initiated by the diffusion of a hole, generated either due to anodic polarization or photon absorption, to the surface. The exact behavior of the diffusing hole is not fully understood, with models suggesting it is captured either in the surface Si–H bond [23, 71], the Si–Si back bond [72], or remains delocalized until interacting with a nearby fluoride ion [73]. In all cases, the presence of a hole results in the weakening of the surface Si–H bond, making it susceptible for a nucleophilic attack by an active fluoride species, such as HF (step i, rate-limiting). The first reaction is followed by injection of an electron into the Si conduction band and the formation of Si–F bond (ii). As the bond strength of the silicon fluoride is much higher than Si–H (ca. 6 eV vs. 3.5 eV [62]) the presence of a Si–F bond polarizes the adjacent silicon back bonds, leaving these also susceptible for further attack (iii). The remaining bonds are replaced in rapid succession due to increasing polarization (iv) after which a Si atom can leave the again hydrogen terminated surface as SiHF_3 with the reaction continuing in the solution (v) resulting in silicon hexafluoride and hydrogen. The Si behavior under anodic conditions also reaffirms the observation of a significant activation barrier for the formation of F-termination on bare Si surface instead of H-termination despite the former being more favorable in thermodynamic sense, due its higher bond strength [62, 74].

1.2.3 Formation theories

While the electrochemical reactions taking place at the Si/electrolyte interface can effectively be explained, pore formation has proven to be a challenging concept. A crucial question with the process is not only what leads to the selective, anisotropic

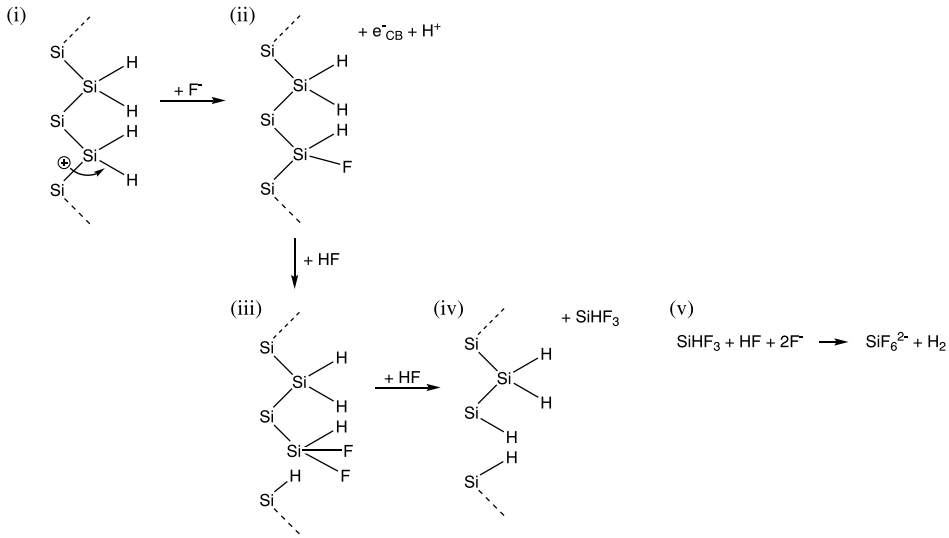


Figure 2. The revised Gerischer reaction mechanism of divalent anodic dissolution of Si in aqueous HF. In all steps, HF is assumed as the reactive species, the other active forms in the electrolyte being HF_2^- and $(\text{HF})_2$. Adapted from refs. [71, 74].

etching in acidic fluoride-based electrolytes below I_{ep} , but also the wall passivation mechanism that allows a porous structure to be formed. Broad range of different models to describe the pore formation have been suggested over the past few decades [23, 70, 75–87]. However, a general theory to bridge all the observed mechanisms has not been discovered yet. Concepts behind several of the models, as well as their scope and limitations are discussed in detail in reference [88]. The main approach toward pore wall passivation can be used to divide the models coarsely to phenomenological and computational models. Here, only few of the most known models in both categories are addressed.

Initial suggestions for the wall passivation were chemical in nature, assuming the accumulation of silicic acid or silicon oxide to hinder the reaction between the silicon and the electrolyte [75, 76]. However, the composition of the porous layer and behavior of Si in HF did not support this assumption [13, 64]. Based on semiconductor physics, the model introduced by Beale *et al.* [77, 89] is considered as the first comprehensive take on explaining the formation of PSi, providing also a framework for later models. The extensive anodization experiments carried out with different types of silicon in combination with earlier observations [16], allowed connecting the observed morphological features to the I - V behavior of Si according to the dopant type and concentration. Initial assumptions in the model are that Si is only dissolved where anodic current can flow and that the silicon-electrolyte interface is considered as a Schottky junction, where the Fermi level is pinned near mid-bandgap. The latter assumptions are based on the rectifying I - V behavior observed on lightly doped Si

and the high resistivity of the obtained porous layer, indicating the walls are fully depleted from charge carriers [77]. During anodization, formation of a depletion layer around the pores focuses the electric field to the pore tips where consequently the field intensification results in localization of the current flow and preferential dissolution. Structural differences in the porous layers would then be controlled by the depletion layer width and the charge transfer across the junction, which in highly doped Si occurs by tunneling and in lightly doped Si by thermionic emission.

The quantum confinement model proposed by Lehmann and Gösele [23] is also based on the concept of charge carrier depletion in the porous structure. With microporous silicon, the observed wall thicknesses are small enough to cause increase in the bandgap energy, transforming the PSi translucent to visible light, and photoluminescent [22]. This leads to quantum confinement of the pore walls, as it becomes increasingly more difficult for the charge carriers to overcome the potential barrier during anodization, causing these regions to become depleted. With the work of Frohnhoff *et al.* [81] the model was extended to account also the observed size variations in the crystallites that form the pore walls. The quantum confinement model can be considered to complement the approach by Beale *et al.*, as it effectively provides a lower limit for the wall thickness, whereas the overlapping depletion layers in Beale model function as the upper limit [90].

The first computational approach to formation of PSi was introduced by Smith *et al.* [78]. The model is based on the diffusion limited aggregation (DLA) algorithm by Witten and Sander [91], which can reproduce patterns that appear in processes such as electrodeposition and crystallization. In the DLA model for porous silicon, the basic assumption is the pore formation being a process limited by the diffusion of holes from the bulk Si to the silicon-electrolyte interface. The diffusion of the holes takes place as a random walk. The random nature of the movement leads to the promotion of pore growth, as the pore tips are more likely contact points as they are better exposed to the meandering holes, with the earlier sections of the pores becoming effectively shadowed. The single controlling parameter in the model is diffusion length, signifying the distance between the hole nucleation site and the interface. Longer diffusion lengths lead to channel-like pores, while shorter lengths result in increasingly branched pores, suggesting connection between the depletion layer width and the diffusion length [65].

While the patterns produced with DLA share similar structures observed in PSi cross-section images in a number of occasions [92], the relative simplicity of the model prevents it taking fully into account several aspects of the anodization, such as the dopant type, or actual charge transfer mechanism [88]. Erlebacher *et al.* [80] included another control parameter to the model, creating a migration envelope around the pore tips at a fixed distance. Upon contact with the envelope the hole movement would turn into biased random walk toward the pore tip, illustrated in Figure 3. This allows the simulation of the electric field intensification around the tips, focusing the

current flow as described in the Beale model. Similar additions to the DLA model were made by He *et al.* [82], John and Singh [93] and Aleksandrov *et al.* [85], improving the simulation capabilities in different anodization conditions.

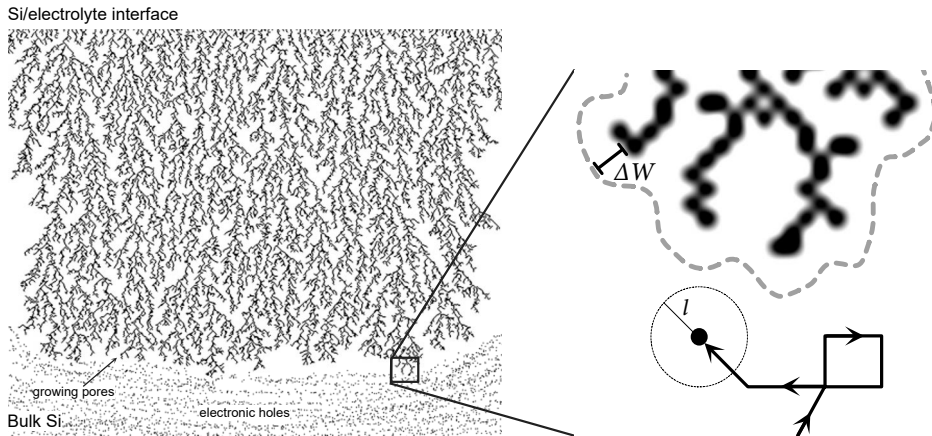


Figure 3. Simplified illustration of pore growth under DLA algorithm. The hole movement is biased toward the Si/electrolyte interface causing growth of branched unidirectional pores. Inclusion of migrational envelope at a fixed distance of ΔW functions as a electric field intensifier around the pore tips, forcing holes to travel directly toward the pore [94]. Modification by John and Singh [93] considers the migrational envelope as the depletion layer, or diffusion length beyond which the holes are launched. Electric field effect is instead considered through a second parameter, drift length l of the meandering hole, where the hole is moved directly to the growing pore front when this is encountered at a radius of l . Illustration adapted from refs. [80, 93].

The current burst model (CBM) presented by Föll *et al.* [95–97] can be considered as the most comprehensive of the formation theories introduced so far for explaining the formation of PSi. The CBM is based on extending a previous model intended to describe the observed oscillating features in the silicon I – V curve at high potentials [67, 86]. The premise of the CBM is that current flow is inhomogeneous. The charge transfer is spatially and temporally localized, proceeding in current bursts. This induces rapid Si dissolution either directly or indirectly, followed by passivation of the surface by reestablishing hydrogen termination. Crucial element in the model is the time scale of each reaction step after the current burst. These are controlled by the anodization conditions, such as electrolyte composition, directing the morphology of the forming pores [97].

1.3 Structural properties of porous silicon

When discussing porous materials, the terminology usually follows the IUPAC² conventions regarding the size of the pores [98, 99], dividing them into three classes

- micropores, for pores with diameter < 2 nm;
- mesopores, for pores with diameter of $2 - 50$ nm;
- macropores, for pores with diameter > 50 nm.

In regards to P*Si*, the classification is quite arbitrary, as the range of pore sizes available through anodization spans from micropores of $1-2$ nm into large macropores that can have diameters in the range of $100 \mu\text{m}$ [100]. With a similar broad range, the porosity of P*Si* can be tuned from fairly low porosities of macroporous Si of only few percent into porosities in excess of 95% with microporous Si, essentially converting the material into aerocrystals as referred by Canham *et al.* [101]. The available specific surface area follows the same pattern where macroporous Si often provides areas of few m^2/g , increasing with mesoporous and microporous Si to several hundreds of m^2/g and even over $1000 \text{m}^2/\text{g}$ [53, 102].

1.3.1 Morphological features of porous silicon

The outcome of the anodization is dependent on various different parameters. Generally, the most important ones are the dopant type and density along with the crystalline direction of the silicon. Similarly, the components related to the involved electrochemistry have a considerable effect, such the composition of the electrolyte, applied potential or current density as well as temperature and level of illumination. On one hand, the number of parameters affecting the P*Si* fabrication appears overwhelming, but the on the other hand, it enables unprecedented control over the structural features of P*Si*, such as the pore size, shape and porosity [103].

While the effects of most of the parameters are not easily predictable due to the limitations of the formation theories, few general observations can be made that apply to some extent. For instance, increasing the anodization current density usually leads to larger pores and faster pore growth rate [104]. Also, as mentioned earlier, assuming an aqueous electrolyte, increasing the HF concentration leads to smaller pores and slower pore growth rate as the I_{ep} is shifted toward higher potentials.

Similar overall trend can be established for the differences in dopant concentrations. For example, lightly doped *n*-type Si usually provides large breakdown pores in the dark and more defined macropores when illuminated, with the pores growing

² International Union of Pure and Applied Chemistry

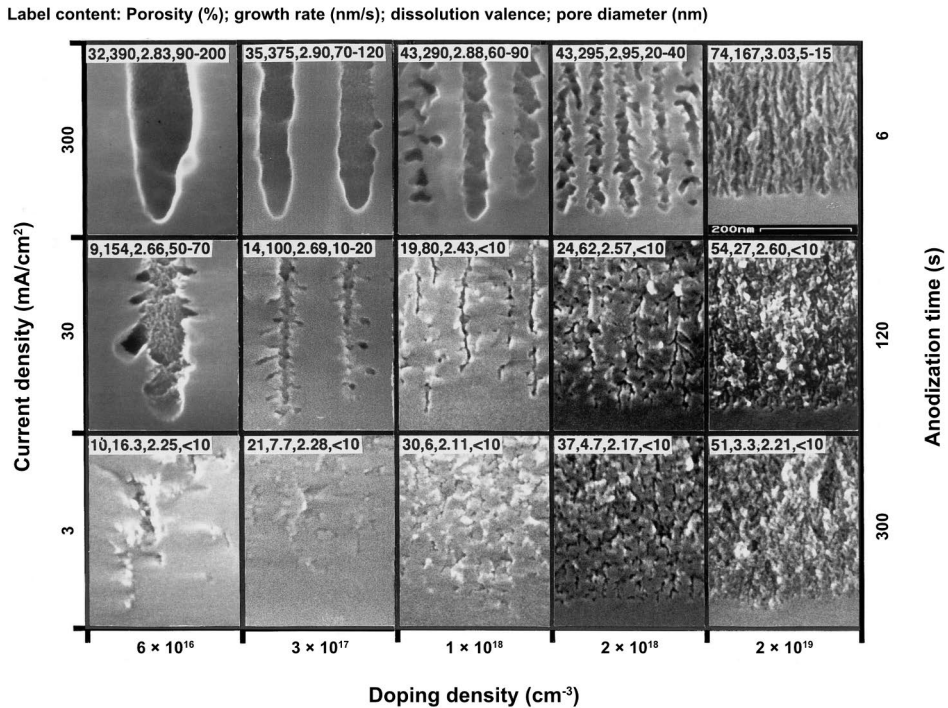


Figure 4. Scanning electron micrographs of electrochemically anodized PSi layers on *n*-type Si(100) substrates. Image adapted with permission from ref. [104].

typically to $\langle 100 \rangle$ direction regardless of the Si orientation. The macropore nucleation can easily be controlled through lithography and backside illumination, allowing also control over the pore shape. Increasing the dopant concentration reduces the pore size, eventually producing well-defined, branching mesopores, as illustrated in Figure 4. With *p*-type Si, the corresponding trend is reversed, with lightly-doped Si usually providing a sponge-like homogenous microporous layers. When increasing the dopant concentration, the pore morphology becomes more anisotropic, forming columnar, fir-tree like branching mesopores perpendicular to the surface, appearing much like their *n*-type counterpart.

Interestingly, with suitable selection of electrolyte composition, *e.g.* aqueous dilute HF-solution or anhydrous organic solvent-HF -mixture and applied current density, the previously described overall trend does not hold. Propst and Kohl [105] showed that large macropores can be anodized on lightly doped *p*-type Si using organic electrolyte mixture. Wehrspohn *et al.* [106] and soon after, Lehmann and Rönnebeck [107] observed macropore formation also using aqueous electrolytes and very low current densities, with the pore walls being covered in micropores, while the gross pore morphology was similar to those obtained with *n*-type Si. With highly-

doped n -type Si, Christophersen *et al.* were able to anodize rectangular macropores instead of the expected mesopores by adding strong oxidizers into the electrolyte [108].

1.3.2 Structural control and modification

Combined with passivation of the pore walls against further anodization, the sensitivity of porous structure to different parameters enables the fabrication of complex multilayers, where the layers have markedly different physical properties. These can be realized either by sequentially altering the dopant concentration in the Si, or simply through altering the fabrication parameters on the fly, such as the anodization current in a predetermined manner [28, 29].

In some applications, further control over the structure is required post-fabrication. For expanding the pore size, chemical etching can be considered as a relatively straightforward method. As the Si surface is prone for oxidation, prolonging the exposure of the porous layer to aqueous HF electrolyte after the anodization enlarges the pores slightly as the small amounts of dissolved oxygen in the electrolyte oxidize the pore walls. The newly formed oxide is immediately removed by the HF, thus gradually thinning the pore walls [22, 73]. This approach can also be realized through deliberate oxidation of the pore walls either chemically [109, 110], or thermally [111]. Rinsing the PSi after the controlled oxidation with HF removes the oxidized surface layers, thinning the pore walls, leading to larger pore sizes and higher porosity. The general pore morphology is not affected, but the roughness of the pore walls can be reduced [111]. This method however requires the pore walls to be thick enough to begin with that the material can withstand the dissolution process, and subsequent removal of the etchant without collapsing due to capillary stress [112].

Another method aimed for post-fabrication structural modification is thermal annealing, applied in Paper I and discussed also in Section 5.1. The restructuring of PSi was noticed by Unagami and Seki when growing epitaxial Si layer on top of the porous surface [113]. As a high surface area material, PSi is especially prone for restructuring through sintering due to its high surface free energy. Structural rearrangement has been observed to start already at moderate temperatures of 350–400 °C [114, 115], coinciding with desorption of the surface hydrogen termination. The process is driven by the minimization of the surface free energy. With suitably high temperatures, the pore surfaces begin to rearrange toward lower surface area. This results in the larger pores and the surface acting as vacancy sinks, with the smaller pores gradually merging into the larger ones, increasing the pore size, thus reducing the available surface area [116, 117]. As the sintering mechanism is mainly due to surface diffusion, the process is sensitive to the PSi surface chemistry. Oxidation or nitridation of the surface before or during the process limits the diffu-

sion of the Si atoms, prompting the use of an inert atmosphere, vacuum or an oxide reducing H_2 atmosphere [114, 118]. At high temperatures over $950\text{ }^\circ\text{C}$, the smallest pores can completely be removed, with the larger pores growing into closed, initially spherical voids that eventually become faceted [117, 119, 120]. Also, the surface and interfaces between layers of differing porosities have been observed to present densified, non-porous layers of few nanometers, effectively sealing the surface or adjacent layers after high temperature annealing as seen in Figure 5 [121–124].

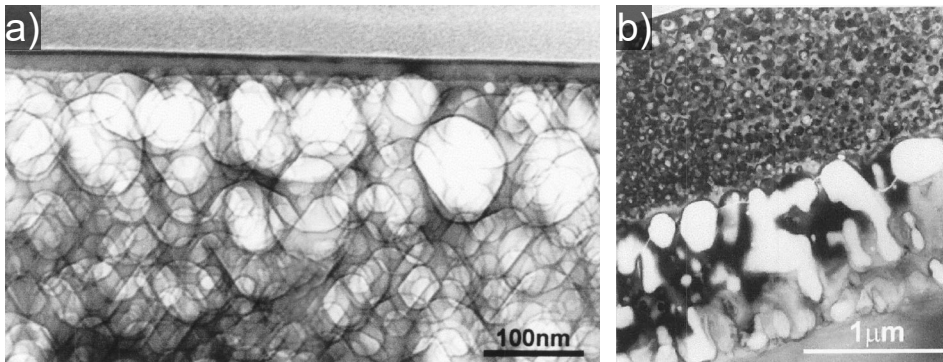


Figure 5. Cross-sectional, bright field TEM (transmission electron microscope) micrographs of a) annealed PSi layer, where the pores have been transformed into faceted voids while the immediate surface has closed, and b) annealed dual layer PSi where shrinking and dissolution of the pores is visible in the upper, lower porosity layer and formation of large voids in the higher porosity layer. Adapted with permission from ref. [117].

1.4 Surface chemistry of porous silicon

As the broad applicability of PSi is based on its large available surface area, the interactions between the pore walls and the surrounding ambient can have a considerable effect on the PSi structure and its stability. For much of the applications of PSi, the surface needs to be chemically stabilized beyond what the native hydride passivation offers. While the native Si–H passivation of PSi surface can be considered moderately stable in ambient conditions, it was discovered early on, that prolonged exposure slowly starts to oxidize the immediate surface, eventually covering the entire surface with a thin oxide layer [6, 13, 125]. Despite this process being overall fairly slow, the initial uptake of oxygen into the silicon hydride structure occurs in the first few hours after fabrication, accompanied by carbon contamination, possibly from small amounts of organic vapor present in ambient air [126].

The development of different surface modifications for PSi has always been strongly application driven, applying methods that have often been adapted from studies conducted on flat Si surfaces [60, 127–131]. Initial efforts aimed to turn PSi structures into effective insulators in integrated circuits [18], while discovery of PL

steered the interest toward stabilizing the luminescent properties [132, 133]. Advancing into sensors and biomedical applications extended the requirement from stability against unwanted degradation of either the host PSi or the guest molecules to incorporate also specific chemical functionality in regards of possible adsorbates [33, 134–137]. Surface modification also enables the control over the aqueous solubility of PSi, as Si can easily be chemically dissolved in alkaline conditions through a nucleophilic attack by OH^- ion, leading to eventual release of an Si atom as silicic acid through a reaction analogous to PSi etching [74, 138]. The main advantage of the hydride covered surface nevertheless lies in the great number of different routes of modification available. Brief discussion on methods based on oxidation, hydrosilylation and thermal carbonization are given in the following sections. More in-depth view on the underlying chemistry of the modifications can be found in several recent reviews [139–145].

1.4.1 Oxidation and Si–O -based modification

Possibly the most common and studied passivation and modification methods for PSi are oxidation based. As the native oxidation of fresh PSi is inevitable, with the oxidation rate affected by the ambient conditions such as humidity, temperature and illumination [125, 126, 146, 147], more controlled methods for passivating the large hydrogen-terminated surface area have been developed. These methods aim to transform the native hydrophobic Si–H_x structures into hydrophilic Si–O–Si and Si–OH-type of chemistry, that can be used to, *e.g.*, limit possible reduction reactions caused by the hydrides [135, 148–150], control the pore morphology through the volume expansion [151] and change the dielectric properties of PSi [59]. Oxidation leaves PSi still susceptible for dissolution through hydrolysis under alkaline conditions. In some applications this may prove as a crucial limitation, but for instance in biological environment, eventual dissolution of the PSi can be beneficial. Oxidation of the material can be achieved using several different routes, all having their distinct features and effects on the overall structure of PSi. Typical methods are electrochemical, chemical and thermal oxidation.

Thermal oxidation of PSi in oxygen or air gained interest in the early attempts to fabricate silicon-on-insulator (SOI)-type structures, due to the relatively rapid oxidation rate of the porous structure compared to bulk Si, allowing selective formation of oxidized areas [18, 59, 152]. This deceptively simple process allows extensive control over the thickness and quality of the forming oxide, affected by several different parameters, such as the oxidation temperature, time, atmosphere and initial morphology of PSi [18, 132, 153–155].

According to temperature, silicon oxidation can be roughly divided into three processes, each requiring a higher temperature while allowing more of the PSi structure to convert into porous SiO₂ [153, 156, 157]. At low temperatures, 210–250°C

and below, the oxidation is quite similar to native oxidation in ambient conditions, with the main difference being higher rate of oxidation. In this region, the Si–Si back bonds of the surface hydrides are more susceptible for reaction with oxygen due to their lower bond strength, selectively forming $-O_y-Si-H_x$ structures [158, 159]. The reaction progresses rapidly for each of the silicon back bonds, as inclusion of one oxygen makes the adjacent Si–Si bonds unstable, and prone to oxidation. Increasing the temperature above 250°C allows also the desorption of the surface hydrides and the formation of Si–O–Si and Si–OH groups, gradually reducing the number of back bond oxidized structures. The low temperature oxidation saturates before the pore walls can be entirely oxidized, as the few nm thick oxide layer prevents the diffusion of the oxidants deeper into the PSi skeleton [153]. This coincides with the onset of structural reorganization of PSi, resulting in coarsening of the porous layer if higher temperatures are applied. However, the thin oxide layer is sufficient to slow down Si surface diffusion, providing protection from sintering of the structure [155]. Overcoming this barrier requires higher temperatures, in the range of 600–800°C, allowing the eventual conversion of the pore walls into SiO₂, with higher temperatures providing faster oxidation. The temperature is also sufficient to remove the remaining hydrides, leaving the surface terminated mainly with siloxane and silanol groups [160]. Increasing the temperature further, to 900–1000°C and above, initiates the densification of the porous oxide, turning the oxidized layer comparable to bulk thermal SiO₂ [155, 156, 161]. The kinetics of the oxidation reaction are also affected whether the process is done in either dry or wet oxygen [152, 155, 162], with the latter showing considerably faster oxidation rates at corresponding temperatures due to the higher solubility of water in SiO₂ compared to oxygen [129].

Electrochemical oxidation can be done in a similar arrangement as the etching of PSi, the electrolyte however being non-fluoride -based, usually aqueous inorganic acid solution such as dilute H₂SO₄ or HNO₃. With pristine hydrogen terminated PSi, under anodic polarization and at low overpotentials, the oxidation is limited by the supply of holes. This causes the preferential oxidation of the bottom of the porous layer. The oxidation proceeds first through the non-depleted areas, followed by the depleted walls, if sufficiently high potential is applied [57, 163]. Eventually, the thickness of the oxide is enough for isolating electrically the porous layer from the substrate, preventing further oxidation. Bsiesy *et al.* showed that initial preoxidation, such as native oxide, causes the anodic oxidation to proceed instead of just the pore tips, from throughout the porous layer if the applied potential is high enough to allow the diffusion of the oxidizing species through the native layer, before the porous layer becomes electrically isolated [163]. Due to the self-limiting nature of the process, anodic oxidation can also be used to thin the silicon walls, creating quantum confined Si crystallites within the oxidized structure, enhancing PL [164].

Another route used to passivate the PSi surface with an oxide is by utilizing different chemical oxidants, such as water, ozone, hydrogen peroxide, nitric acid or

by exposure to *e.g.* gaseous halogens followed by hydrolysis [33, 165–167]. These methods usually produce a thin oxide layer, with a composition and quality determined by the utilized chemical. While oxidation of fresh P_{Si} in water is slow, due to the high hydrophobicity of the non-polar hydrogen termination, Bateman *et al.* showed that inclusion of a suitable surfactant improves the oxidation rate from few days into minutes [168]. With ozone-based oxidation, short treatment durations have been shown to promote the formation of surface Si–OH groups along the oxide, while prolonged treatment reduces the amount of the available silanols [165]. As a simple and straightforward method, chemical oxidation can provide sufficient passivation to limit environmental effects on the P_{Si}.

Secondary functionalization on oxidized P_{Si} can be added utilizing similar modification methods as with silicas due to the resemblance of surface chemistries. The Si–OH groups present on the surface enable tethering of a wide variety of organic molecules using organosilane compounds, such as trialkoxysilanes [33, 169]. In simplified form, the attachment reaction starts with the hydrolysis of the alkoxy group catalyzed by water, followed by condensation with the surface –OH -group, covalently linking the organosilane through siloxane bridge. While silanization is a straightforward method for providing specific distal functional groups for P_{Si}, such as primary amine [134], epoxy [170], or thiol termination [171], trialkoxysilanes tend to often form multilayers through cross-linking if the reaction conditions are not carefully chosen [172, 173], which can be detrimental for porous structures when concerning access to the pores [174]. A more efficient silanization method was recently introduced by Sailor *et al.*, using heterocyclic silanes which can be grafted to the surface Si–OH groups through a ring-opening reaction [175]. A more flexible method in respect of reaction conditions and without multilayer formation was reported by Sweetman *et al.*, where Lewis acid catalyzed hydrosilane grafting to the surface hydroxyls was obtained [176].

Grafting of organic molecules can also be done through Si–OR linking directly on the hydride surface without initial oxidation and without multilayer formation. For instance, alcohols can be covalently bound to the surface through their hydroxyl groups, where the reaction is based on cleavage of the Si–Si back bond [177]. Photoelectrochemical modification of fresh P_{Si} with carboxylic acids has been shown to provide an ester termination on the surface for subsequent modifications [178]. Due to the low coverage and the general susceptibility of the Si–O bond to hydrolysis, the use of these methods has been limited.

1.4.2 Hydrosilylation through Si–C linkage

With the understanding that HF not only removed the native oxide from silicon surfaces, but left it terminated with moderately stable hydrides opened up a broad field of research for oxide-free wet chemical modifications. The ability to create well-

defined monolayers that allowed passivation of a flat Si surface without disordered oxide-layer through direct Si–C bonding was first reported by Linford and Chidsey [131]. The pyrolysis of molten diacyl peroxide resulted in binding the formed alkyl radicals directly to the surface Si–H groups through Si–C bonds. Later Chidsey *et al.* reported that similar results were obtainable by heating the Si substrates immersed in neat 1-alkenes or 1-alkynes with or without diacyl peroxides that functioned as radical initiators. The reactions produced similar monolayers in both cases, as the initiator did not appear to bind to the surface in large extent in the former case [179]. The radical initiated and thermally induced hydrosilylation reactions sparked considerable interest as the results indicated compatibility with bifunctional chemicals, bearing both an unsaturated hydrocarbon and another terminal group which may be derivatized later. The experimental conditions were also relatively mild, necessitating only dry and oxygen-free environment. The use of Si–C linkage also made the surface considerably more stable against unwanted oxidation or degradation in prolonged exposure to acidic and basic conditions.

Hydrosilylation reactions were soon adapted for use with PSi, first reported by Buriak *et al.* using Lewis acid mediated reaction pathway to attach a broad variety of alkynes and alkenes with different distal terminations through Si–C bonds [133, 180]. The hydrosilylation of PSi was found to have only limited effects on the morphology of the material, while the stability against oxidation and hydrolysis was improved considerably. The modified PSi was able to withstand boiling in alkaline solution for several hours and present only gradual oxidation after prolonged immersion into simulated body fluid [133, 181]. This was soon followed by reports of white light induced hydrosilylation on photoluminescent PSi by Stewart and Buriak [182] and direct thermal hydrosilylation by Horrocks *et al.* [183]. More hydrosilylation methods for PSi have also been introduced, such as hydride abstraction-based [184] and transition metal catalyzed reactions [185, 186]. Reactions based on the use of Grignard and organolithium reagents were also reported being able to derivatize the PSi surface through Si–C bonds, with the distinction to hydrosilylation that the hydrocarbon insertion took place in the Si–Si back-bond [187, 188].

The initial mechanism suggested for hydrosilylation was based on the initiator decomposition into alkyl radicals that could abstract hydrogen from the surface Si–H group yielding a Si radical. The Si radical would rapidly react with the unsaturated terminal carbon of an alkene or alkyne molecule, forming a Si–C bond and creating a new radical from the second carbon in the bound alkyl or alkenyl molecule, which in turn could abstract next hydrogen from the surface, propagating a radical chain reaction [179, 189]. The photoassisted reaction on luminescent PSi [182] is suggested to be driven by exciton formation, where the presence of a photogenerated hole near the surface causes the Si–H to function similarly as a Si radical [140]. While the overall reaction mechanism in thermally induced hydrosilylation appears similar to the other presented routes in PSi, the initiation without clear source for surface radicals

is currently debated, as the moderate temperatures utilized ($\sim 150^\circ\text{C}$) are not enough to cleave the Si–H bond. Horrocks *et al.* suggested trace amounts of oxygen in the reaction causing the initial hydrogen abstraction [190], while Coletti *et al.* presented a nonradical concerted pathway for the hydrosilylation [191].

With various hydrosilylation routes available for PSi, multiple new chemical modifications were introduced that enabled facile application specific secondary functionalization. With the emergence of biosensing and other biomedical applications, these often aimed for *e.g.* providing selective immobilization capability for complex biomolecules. Boukherroub *et al.* [192] showed a bifunctional alkene, 10-undecenoic acid, could be thermally hydrosilylated on hydrogen terminated PSi surface, with the reaction leaving the distal carboxylic acid free for further reactions, such as transformation into succinimide ester and using this to immobilize amine-bearing molecules through amide bonding. The improved hydrolytic stability was utilized by Link and Sailor [193], as they showed a multilayer PSi fabrication, etched in two parts with the first anodized multilayer thermally hydrosilylated using a hydrophobic alkene before etching of the second multilayer, which was in turn mildly oxidized after the film lift-off without damaging the hydrosilylated side. Ground to microparticles, the PSi functioned as a “smart dust”, self-assembling and aligning according to surface chemistry on immiscible water/solvent interfaces (Figure 6).

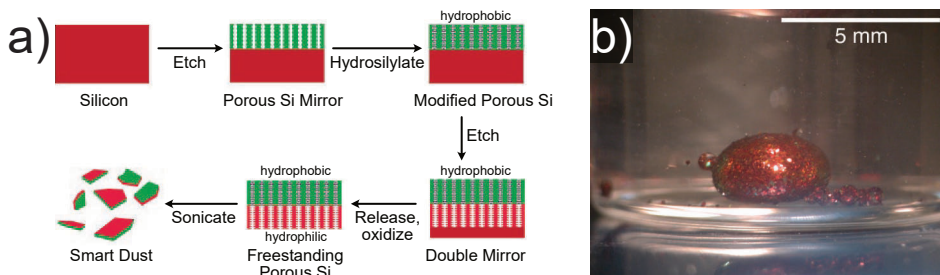


Figure 6. a) Fabrication of multilayer PSi mirror in two stages, with hydrosilylation performed between the etches. After release, the freestanding film is partially oxidized and sonicated into microparticles. b) Photograph of the “smart dust” microparticles self-assembled on the surface of a droplet of dichloromethane in water, presenting the red side of the mirror. Images adapted with permission from ref. [193]. Copyright 2003 National Academy of Sciences, USA.

Taking advantage on the properties and structure of PSi, Gooding’s group have introduced several procedures which allow dual functionalization of PSi films or particles, with the internal and external surfaces both presenting different derivatizations. For instance, Killian *et al.* utilized the hydrophobic nature of hydrosilylated PSi surface, performing a secondary derivatization in an aqueous solution, affecting only the external surface. This was followed by an organic solution that could ingress into the pores and functionalize the internal surfaces [194]. Guan *et al.* showed similar results utilizing alkyne-terminated PSi and grafting differing sec-

ondary modifications using ligand-controlled Cu-catalyzed alkyne-azide cycloaddition (CuAAC) [195] and also using the absorption depths of UV and white light in PSi to induce hydrosilylation either on the exterior or interior of the material [196]. Wu and Sailor presented a method where the pores of mildly preoxidized PSi were filled with an inert organic solvent, immiscible to water-based solutions, enabling selective restoration of the hydride termination using aqueous HF on the external surfaces for hydrosilylation-based modifications [197]. Voelcker *et al.* approached the spatial control of the modification by initially hydrosilylating the PSi, followed by an air plasma treatment that effectively removed the silylated alkyl chains from the external surfaces of the PSi, leaving them with a thin oxide layer, suitable for silanization [198].

Despite the versatility of hydrosilylation-based modifications on PSi, the efficiency of the reaction is limited. The hydrolytic stability in, for example, HF, alkaline conditions and physiological fluids can be considered relatively sufficient, however the reactions taking place on the PSi surface leave considerable amount of the silicon hydrides intact and susceptible for eventual oxidation or degradation. Computational estimates and experimental results suggest that with ideal Si(111) surfaces, the highest coverages are at best around 55 % in well-organized monolayers [199–201], with steric hindrance limiting higher values unless grafting extremely small molecules such as methyl [202] or acetylene groups [200] on Si⟨111⟩ or PSi [203]. Buriak suggests that with PSi, depending on the morphology, the achievable efficiencies with long alkyl chains are similar [204].

1.4.3 Thermal carbonization

Semiconductor industry interest in silicon carbide (SiC) stems from the material properties, such as high mechanical hardness, chemical and thermal stability along with suitability to high power and frequency applications. As the production of SiC-wafers is expensive, alternatives that yield similar properties are actively sought. Extensively studied option is the growth of heteroepitaxial SiC-layers on Si⟨100⟩ and Si⟨111⟩ wafers using hydrocarbon absorption, as a more cost-effective solution. In this field, the use of small unsaturated hydrocarbons such as acetylene and ethylene has received considerable attention, due to the possibility of utilizing only moderate temperatures, below 1000 °C, to form SiC structures. Early studies indicated acetylene being suitable for faster growth of an SiC layer than ethylene [205]. Later studies confirmed this and concluded that chemisorbed acetylene dissociates nearly completely upon heating instead of mainly desorbing like ethylene [206–209]. Upon the hydrocarbon chemisorption and subsequent heating, the Si surface also started rearranging, with the carbon showing tendency to diffuse deeper to the Si structure after acetylene dehydrogenation, starting at ca. 550°C, with complete hydrogen removal at 660°C [210, 211]. Below 600°C, mainly formation of substoichiometric

silicon-carbon alloy was observed, while above 600°C, formation of 3C-SiC crystals started to occur, the carbonization providing a suitable intermediate layer for the SiC epitaxial layer growth [212]. Despite the broad efforts, fabrication of low-defect epitaxial 3C-SiC layers on Si still presents a challenge [213, 214].

PSi already had a role in the early experiments in fabricating SiC layers using gaseous hydrocarbons in conjunction with high temperature annealing [215]. However, in an effort to stabilize the PL using the high chemical and thermal stability of SiC, first attempts to thermally carbonize PSi using acetylene were made by Seo *et al.* [216]. The results were nevertheless inconclusive, showing a slight delay in the quenching of PL with increasing temperature and the material appearing to resist sintering-based collapse due to the partial formation of SiC-like structure. Comprehensive studies on thermal reactions of acetylene with PSi were made by Salonen *et al.* [217–219]. The results established that the pore walls are efficiently passivated with high coverage, due to the small size of acetylene molecule allowing it to diffuse easily into the porous structure. Acetylene also appeared to physically adsorb rather strongly to the surface hydrides even under thermal treatment, thus being available for chemisorption when the PSi hydrogen was desorbing [217]. When the treatment temperature exceeded 400°C, the dehydrogenation of both the PSi and acetylene enabled the formation of a hydrocarbon terminated PSi surface. Utilization of temperatures below 660°C, above which the acetylene hydrogens are completely removed, enables the use of continuous acetylene flow, providing considerably higher coverage without unnecessary formation of pyrolytic carbon products [219]. In a similar fashion with the experiments done on flat Si, above 600°C the hydrocarbon termination gradually starts to transform into non-stoichiometric SiC, with the chemisorbed carbon being embedded into the pore walls, as the temperature is also enough to cause partial sintering of PSi. A considerable transformation in the chemical nature of the PSi surface occurs at slightly higher temperature, ca. 650–730°C, as the hydrocarbon decomposition and the surface diffusion in the pore walls changes the structure from hydrophobic to hydrophilic, shown as a drastic reduction of water contact angle with a PSi layer [220]. This is due to the surface reorganization leaving the immediate pore walls terminated with Si, which upon exposure to ambient conditions forms a thin, hydrophilic oxide layer [221]. The temperature threshold region effectively divides the process into two distinct passivation methods, both having a high surface coverage, but considerably different surface chemistries. The lower temperature region treatment is usually referred as thermal hydrocarbonization (THC), while the higher temperature treatment as thermal carbonization (TC). The latter is often combined with an initial THC-treatment providing a high hydrocarbon coverage that also hinders the sintering of the structure during the high temperature TC-treatment, limiting the effects on the pore morphology [222]. While carbonization results in quenching of the PL, both the THC- and TC-treatments for PSi result in a chemically highly stable surface, capable of resisting *e.g.* HF- and KOH-based

solutions as well as simulated physiological fluids without notable degradation or oxidation [218, 223].

The chemical nature of both carbonization treatments allows also secondary functionalization, combining both a highly stable passivation layer for the PSi itself and the attachment of an application-specific modification. Sciacca *et al.* [224] approached the modification of a PSi surface, thermally hydrocarbonized at 500 °C by adapting a radical initiator based method utilized for diamond surface functionalization to graft a dicarboxylic acid [225]. The initiator, benzoyl peroxide, dissolved with sebacic acid in toluene could abstract a hydrogen from one of the –COOH -groups of the acid, causing its decarbonylation and the formation of an aliphatic radical. The reaction could then proceed either through unsaturated carbon groups on the PSi surface, or initiator generated surface radicals, yielding a carboxylic acid terminated surface. Similar –COOH -functionalization was also introduced by Kovalainen *et al.*, showing that direct reaction with the hydrocarbonized surface and an unsaturated alkene was also possible. By immersing hydrocarbonized PSi into neat undecylenic acid and heating the solution to 120 °C, the alkyl chain covalently bound to the surface, providing a –COOH termination, often referred as UnTHCPSi [226]. This approach is also applied in Paper IV, with thermal addition done using a bifunctional diyne providing an alkyne termination, discussed more in Section 5.4. Figure 7 illustrates the chemical effects observed on THCPSi surface chemistry. The –COOH termination provides also a possibility for selective functionalization, as the material retains its hydrophobic nature. Adapting the method utilized by Kilian *et al.* [194], Alba *et al.* demonstrated successive modifications of the external and internal surfaces of the porous structure using the limited ingress of aqueous solutions into the pores followed by the use of organic solutions for the internal surfaces, introducing distinct tertiary functionalizations with cross-linking chemistry [227].

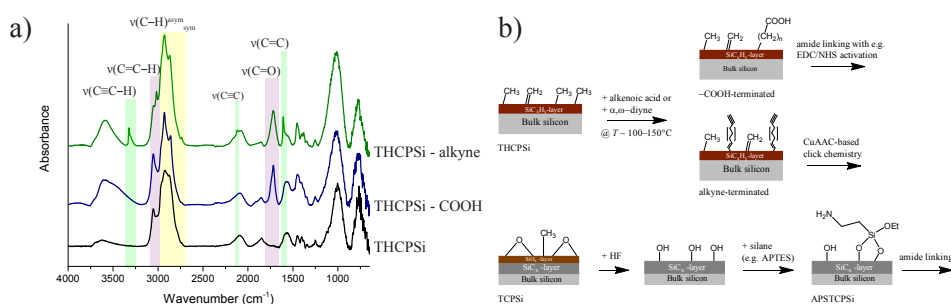


Figure 7. a) Fourier transform infrared (FTIR) spectra of plain, COOH-terminated and alkyne-terminated THCPSi showing the successful attachments of functional groups. b) Typical functionalization routes employed with THCPSi and TCPSi. Figure adapted with permission from ref. [228].

With the SiC-like surface structure provided by TC-treatment, secondary functionalization is relatively easy to accomplish by generating -OH -groups on the surface by rinsing the PSi with HF. In a stark contrast to Si, while the native oxide is also removed, the last oxygen layer remains on the surface providing a hydroxyl termination, instead of hydrides as observed with Si [229, 230]. The hydroxyl layer can then be used for *e.g.* silanization-based modifications as discussed in Section 5.3 and Paper III.

The formation of pyrolytic carbon is usually undesired in surface modification, however with some applications, controlled decomposition of acetylene can be utilized to form graphene layers within the porous structure. Fauchet *et al.* [231] utilized rapid thermal processing at high temperatures with a continuous flow of acetylene to grow thin layers of graphene in the pore walls of a Si-based thin porous nanocrystalline membrane filters. This allowed controlled pore size modification from minute changes to complete pore occlusion, while also enhancing the membrane stability against harsh conditions, such as exposure to alkaline solutions. Formation of a graphene layer on the pore walls of PSi was also studied by Pint *et al.* [232, 233]. The thermally grown carbon layer provided a highly stable and conductive interface for an electrochemical supercapacitor. Another approach for deliberate conformal carbon coating of PSi was presented by the Sailor group [234, 235]. Tsang *et al.* polymerized furfuryl alcohol on preoxidized pore walls followed by heating the polymer-coated PSi up to 700°C in order to pyrolyze the polymer into a protective amorphous carbon layer, able to withstand prolonged contact with a high pH solution [234]. A process based on depolymerization and subsequent thermal hydrosilylation was designed by Wang *et al.* [235]. By infiltrating the pores of freshly etched PSi with dissolved polystyrene, the obtained polymer coating was thermally depolymerized into styrene monomers and other oligomeric radicals able to react with the surface hydrides, covalently binding the carbonaceous coating through Si–C bond formation.

1.5 Applications of porous silicon

The discovery of the room temperature photoluminescence led to considerable interest in PSi and its properties during the 1990s, the material finding applications in a wide field, further broadened by the implications of bioactivity [34]. Research on utilization of PSi in the fabrication either as a sacrificial or a structural part of the application can be found in *e.g.* microelectronics [18, 59, 236], molecular analysis [237–243] and separation [244–246], electrical [247–252] and optical sensors [33, 253–257], not to mention medical and diagnostic applications [258–263] and even microexplosives [27, 264–267]. An excellent survey on the topic can be found in reference [37] along with the corresponding part of the handbook [268] and the numerous references therein. Here, a short overview on a handful of applications

is provided, while omitting the biomedical field which is in turn discussed more in Section 2.4.

With its roots in semiconductor industry, PSi has seen use in the development of SOI structures, such as in FIPOS (Full Isolation by Porous Oxidized Silicon) [59, 269], its functionality demonstrated in fabrication of static random access memory (SRAM) chips in the early 1980s [270]. Another approach in SOI development was taken by Yonehara *et al.* [121, 236, 271–273], paving also way for several other applications. This process combined multiple properties of PSi, such as utilizing formation of stacked low-high porosity layers and their subsequent thermal annealing, causing the closure of surface pores, providing an excellent template for epitaxial Si layer growth. The epitaxial layer is partially oxidized and covalently bonded with a handle wafer. The annealed high porosity layer below functions as a structural weak point due to strain between the porous layers and is easily split from the handle wafer with a highly collimated water jet wedging the layers apart. The handle wafer becomes the SOI wafer after selective etching of the remaining porous layer and surface smoothing by hydrogen annealing, while the original porosified wafer can be reused several times as a template for the epitaxy, reducing production costs. The epitaxial layer transfer (Eltran™) process became the first commercial application of PSi, with Canon Inc. manufacturing the Eltran™ SOI-Epi wafers in the late 1990s and early 2000s.

Layer transfer processes were also adapted to the production of thin film solar cells, again utilizing the porous layer restructuring during thermal annealing for both the active layer fabrication and wafer splitting. Thorough review on the topic was recently published by Sahoo and Kale [124]. With an overall aim of reducing fabrication costs while maintaining high conversion efficiency, epitaxial or restructured porous layer transfer of a thin Si film from a reusable seed Si substrate to more economic substrates is actively developed [119, 274–278], with considerable research effort coming from institutes such as IMEC, ISHF and ISE.³ Currently, commercialization of a thin film Si solar cell is in progress by an ISE spin-off company NexWafe GmbH [279].

Restructuring of PSi under thermal processing has also been applied in the fabrication of structures referred as silicon-on-nothing (SON) layers [280, 281]. Armbruster *et al.* [123] introduced an approach where stacked low and high porosity PSi layers were thermally annealed, with an epitaxial layer deposited on the annealing-sealed surface. The buried high porosity layer in turn rearranges itself during the treatment into a large vacuum cavity as shown in Figure 8. Large scale fabrication and commercialization of these structures was developed by Robert Bosch GmbH as

³ IMEC: Interuniversity Microelectronics Centre, Leuven, Belgium
ISHF: Institut für Solarenergieforschung in Hamelin, Emmerthal, Germany
ISE: Fraunhofer Institute for Solar Energy Systems, Freiburg, Germany

the APSM (Advanced Porous Silicon Membrane) process, utilizing the membranes as piezoresistive pressure sensors [282, 283].

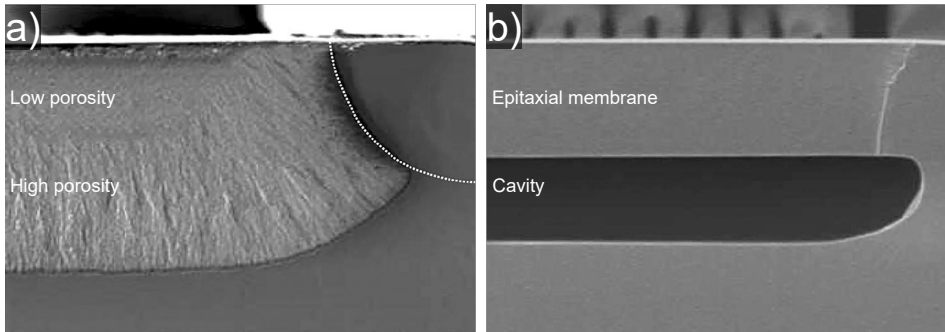


Figure 8. Cross-sectional SEM (scanning electron microscope) micrographs of Bosch APSM process steps. a) Stacked low and high porosity layers are electrochemically anodized on a Si substrate. b) After annealing and epitaxial layer deposition, the high porosity layer has been completely restructured into a cavity on top of which the membrane is grown using the sealed low porosity layer as the template. Adapted with permission from ref. [284].

In the field of energy conversion, aside finding use in layer transfer as described above, PSi has also been studied as a possible anode material in lithium ion batteries, replacing the commonly used graphite [285, 286]. With Si providing ca. 10× higher energy density than graphite, the use of different nanostructured Si-based composites has seen considerable interest. The high porosity ameliorates the tendency of Si to pulverize during charge-discharge cycling due to large volume expansion when alloyed with Li, as it allows the material to essentially expand to its internal pore volume [287]. Since attempts to utilize PSi as a component in Li-ion batteries would require massive amounts of raw material, research efforts often focus on developing methods for economic and facile large-scale production. Suggested methods for PSi production vary from *e.g.* porosification of different silicon grades by MACE [287, 288], to dealloying of AlSi [289], and metallothermic reduction of silicas, produced synthetically [290, 291] or derived from biogenic sources such as bamboo [292] or rice husks [293–295], or from natural minerals, like clinoptilolite [296].

PSi has also been applied to supercapacitor fabrication, aiming for on-chip power delivery in microelectronic devices [297]. The large surface area available in PSi enables high capacitance in electrical double layer capacitors, but also mandates highly stable PSi surface chemistry [298]. Pint *et al.* showed that thermally carbonized, graphene-passivated double layer structure could be constructed having comparable energy density with commercial carbon-based supercapacitors [232, 233]. The carbonized PSi supercapacitor could further be integrated with a dye sensitized solar cell (DSSC) manufactured on the reverse side of the PSi wafer to form a photocapacitor device, which in turn uses another carbonized PSi layer as a counter-electrode in the DSSC [299, 300]. Gardner *et al.* and Grigoras *et al.* fabricated on-chip supercapac-

itors based on thermally carbonized PSi and atomic layer deposition (ALD) -grown titanium nitride coated PSi, suitable for device-integrated energy storage [301–304].

Utilization of PSi as a transducer in different sensor designs is currently one of the most prominent research fields alongside biomedical applications. Interactions between the host PSi and the adsorbed or condensed guest molecules are enhanced due to the large specific surface area available, affording PSi-based sensors high sensitivity and low limits of detection [305]. The versatility in fabrication of the porous structure and surface modification further adds more options to control both the sensitivity and selectivity of the sensors. This also translates to the ability to use PSi in various different types of sensors, such as electrical, electrochemical or optical, each providing multiple modes of transduction [305–307].

Electrical gas sensors, where following the changes in dielectric properties of PSi, such as capacitance and resistance have been successfully demonstrated as humidity sensors, where suitable pore size, and surface chemistry can enable sub-ppm detection limits [220, 247, 308, 309]. Detection of other compounds, such as NO₂ or organic vapors is also possible with very low limits of detection [248, 251, 310]. Device integration has also been shown by Barillaro *et al.*, with field effect transistor-type configurations capable of ppb-level detection, that can be arranged into large sensor arrays as well [255, 311, 312]. Jalkanen *et al.* demonstrated also the possibility of producing printed flexible humidity sensors on paper, where PSi nanoparticle-based ink was used for the sensing element fabrication [252, 313]. Optical gas and liquid sensors where monitoring has been realized through changes in either PL spectra [314–316] or refractive index [136, 317, 318] can also be used to detect organic and inorganic compounds. Combining different electrical and optical features on a single sensor [319–321] or multiple surface chemistries in arrays [322] or stacked reflectors [257, 323], multiparametric sensors with enhanced selectivity can be fabricated.

Most attention in PSi-based sensors has focused on different optical and electrochemical biosensors, where granular control over PSi layer porosity during anodization has enabled the fabrication of various platforms for label-free biomolecule detection, such as rugate filters [324, 325] or microcavities [134, 326]. This flexibility allows assembling stacked reflector structures with differing parameters, providing sensors with internal referencing or size exclusion-based selectivity [327]. The breadth of pore sizes available enables application-specific infiltration of different molecules ranging from, *e.g.*, small drug molecules and peptides to large proteins and DNA [134, 234, 328, 329]. Similar versatility in surface modification has also been an effective tool in providing stability against unwanted dissolution of PSi in aqueous biological solutions, allowing also implantation [330–332]; and in derivatization of the sensor for specific analytes with selected receptors [333, 334]. Sensitivity and limits of detection of PSi-based biosensors has seen considerable improvement in recent years, with Arshavsky-Graham *et al.* [335] com-

bining aptamer-functionalized biosensor with protein concentrating electrophoretic setup for nanomolar level of detection. Further improvements have been shown by, *e.g.*, Barillaro *et al.* [336, 337] presenting an interferogram processing method enabling sub-picomolar levels of detection and Guo *et al.* [338] implementing a stratified TCPSi–THCPSi structure with respective NH₂/COOH dual functionalization for an electrochemical DNA sensor with similar level of detection. Further overviews and detailed examples of PSi-based biosensors can be found from review articles by the Voelcker group [339, 340] and Arshavsky-Graham *et al.* [341], providing also the current status of research in the field.

2 Biomedical use of porous silicon

An ongoing trend in discovery of new drug molecules are the increasing difficulties with the solubility of compounds. Recent estimates suggest that approximately 75 % of new molecular entities suffer from poor solubility [342], placing them in categories II and IV in the Biopharmaceutical Classification System (BCS)⁴ set up by Amidon *et al.* [343]. Another estimate suggests up to 90 % attrition rate of drug candidates during development and clinical trial phases, with the major issues being poor pharmacokinetic properties and toxicity increasing the research costs [344]. Part of the increasing challenges, especially in the small-molecule drug space, is due to the shift to high throughput screening methods and combinatorial chemistry in drug discovery, resulting in candidates with higher molecular weights, lipophilicity or stronger intermolecular bonds, all contributing to lower solubility.

As oral delivery is the most preferred route of administration due to its simplicity and high compliance, compounds with poor aqueous solubility can result in inadequate bioavailability. To address this deficiency, several strategies are available with new methods being actively researched. Such approaches are for example at molecular level, salt formation or modification into a prodrug [342]. At formulation level, much broader toolset becomes available, ranging from drug particle size reduction into micron or submicron range through, *e.g.*, rapid recrystallization processes [345–347], to cyclodextrin complexation [348] or crystal engineering [349], where suitable polymorph or solvate form is formulated, or crystallinity is completely suppressed, leaving the drug in amorphous state. Delivery in amorphous form provides significant advantages in terms of solubility, which in turn can improve drug absorption through generation of supersaturated conditions during dissolution [350]. However, control over the amorphous state has presented another challenge due to the intrinsic thermodynamic instability, that may result in, *e.g.*, spontaneous recrystallization and thus unpredictable bioavailability [351–353]. Nevertheless, for the considerable benefit in solubility, several methods for stabilization of the amorphous state have emerged, such as amorphous solid dispersions, consisting of a drug dispersed into a suitable polymer forming a glass solution [354]. Co-amorphous formulations have

⁴ The BCS classifies drug compounds according to their aqueous solubility and membrane permeability. Class I: high solubility and permeability, Class II: poor solubility and high permeability, Class III: high solubility and poor permeability, Class IV: poor solubility and permeability.

also been introduced, where stabilization is obtained combining the drug with a co-former, that can be for example another drug molecule or an amino acid [355, 356].

Another approach for dissolution enhancement was suggested already in the 1970s by Monkhouse and Lach [357]. Using inorganic high surface area filler material, fumed silica, as an adsorbent for the drug molecules, the particle size of the adsorbed drug was effectively reduced well into submicron level, increasing the dissolution rate considerably compared to the free drug. Konno *et al.* noted that mixing certain drugs with a common mesoporous excipient, magnesium aluminosilicate, used for improving powder flowability, the initially crystalline drug gradually turned amorphous during storage [358, 359]. This resulted in considerably improved dissolution characteristics, showing prolonged supersaturation. The discoveries of ordered mesoporous silicas in the 1990s [360, 361], such as MCM-41 and SBA-15,⁵ and observation of the bioactive nature of PSi brought a resurgence of these approaches. A number of publications from Vallet-Régi *et al.*, Lindén *et al.* and Salonen *et al.* showed the applicability of both PSi and ordered silicas as drug carrier materials, where the mesoporous structure could be adapted to control the dissolution rate through steric effects on diffusion and suppression of crystallinity [362–366] as well as enhance permeation [367].

The versatility in structure and surface chemistry has enabled both PSi and porous silica to function as a carrier material also in the delivery of macromolecular biopharmaceuticals, such as peptides [368, 369], monoclonal antibodies [370, 371] and oligonucleotides [372, 373] which have become more prevalent in modern drug development [374, 375]. The challenges associated to their delivery are not always solubility related, instead the role of the porous carriers extends to protecting the payload from deactivation or degradation during storage and delivery, and enabling control over release kinetics and biodistribution, especially when delivered intravenously [376, 377].

The following sections provide a brief overview on the role of PSi as a drug carrier excipient, addressing the fabrication of micro- and nanoparticles necessary in formulations for different delivery routes, biocompatibility of PSi, as well as methods often employed in loading the drug into mesoporous materials and the effects of physical confinement on the molecular state of the payload. While only anodized PSi was used in this work, several examples are drawn from mesoporous silicas, due to the similarity of the materials in both structure and chemistry.

2.1 Formulation considerations

In both oral and parenteral delivery, depending on the utilized formulation, micro- or nanoparticles may be required. Considering oral delivery, in tablet manufactur-

⁵ MCM-41: Mobil Composition of Matter No. 41; Mobil Corp. (currently ExxonMobil Corp.)
SBA-15: Santa Barbara Amorphous-15; University of California at Santa Barbara, USA.

ing process ensuring powder flow necessitates usually larger microparticles to limit the effect of interparticle cohesion [378]. Microparticles can also be utilized in subcutaneous delivery, especially when the intention is long-term release [379]. In intravenous delivery, particle size and shape play an important role with the surface chemistry in regards of biodistribution and cellular internalization. Different physiological clearance mechanisms, such as sequestration by mononuclear phagocyte system (MPS) can be overcome by proper selection of these parameters. Passive accumulation into tumors by enhanced retention and permeation (EPR) effect through leaky vasculature appears to favor nanoparticles in the size range of 100–200 nm, while larger nanoparticles tend to be filtered by the liver and spleen. Particle shape has been shown to affect their movement in the vasculature under flow, with discoidal particles having the propensity for tumbling motion and drifting toward vascular walls, promoting adhesion [380, 381].

For the fabrication of PSi micro- and nanoparticles, the initial material guides much of the following processing. While outside the scope of this study, porosification of pre-made Si particles using the various methods available, such as stain etching, MACE or regenerative etching sidestep the following processes and their inherent limitations in either control over particle geometry or production volume, but in turn lose some of the versatility brought by anodization. For PSi fabricated by electrochemical anodization, several different methods have been developed and refined to effectively produce particles of size and shape required by the application. Common methods used for comminution are mechanical milling and ultrasonic fragmentation. Due to the role of Si in semiconductor microfabrication, several lithographic approaches have also been adapted, providing extremely fine control over both the size and shape of the final PSi particles. Detailed accounts on several methods can be found in review by Fine *et al.* [382] and pertinent chapters in Handbook of Porous Silicon, by Loni [383] and Sailor [384].

In laboratory setting, ball milling can be considered as the most common method for reducing particle size [385]. Based on rotation around a central axis and often a counterrotation by the grinding jar around its own vertical axis producing a planetary-like motion, the balls within the jar travel on the inside wall and eventually lift off and impact on the opposite site. This provides grinding on the loaded material through friction between the moving balls and the inside wall as well as through crushing of the material during the impact [386]. In the case of PSi, ball milling has been shown to be suitable to reduce the size of PSi films and flakes to microparticles (Figure 10a), ranging from few micrometers to several hundreds, with size separation performed using sieves [365, 387]. Due to the mechanical nature of the grinding, the PSi itself can also cause attrition of the grinding equipment, risking possible sample contamination unless ceramic balls and jar made from, *e.g.*, agate or zirconia are used. Selection of the atmosphere within the grinding jar or using solvent as a milling

medium provides control over the eventual passivation of the new surfaces forming during the process.

Ultrasonic fragmentation, or sonofragmentation, is another common method for particle size engineering. Acoustic cavitation occurring during ultrasonic irradiation in a liquid medium causes the formation of bubbles that subsequently collapse creating shockwaves and microjets. The following interparticle and shockwave collisions are considered to contribute most to the particle fracturing [388, 389]. Sonofragmentation can be used to produce P*Si* microparticles of varying sizes, and it has been shown to work on porous flakes [193, 390], but also on porous layers, still attached to the Si substrate [391, 392].

The fabrication of P*Si* nanoparticles is similarly possible with sonofragmentation [393] and mechanical ball milling (Figure 10b). With the latter, a new method for improving particle fracturing was introduced (Section 5.2, and the associated Paper II). Briefly, the method is based on the assumption that P*Si* becomes more brittle with increasing porosity [394], enabling preferential fragmentation. By applying a multilayer structure on the anodized P*Si* film, layers of higher porosity can be placed at pre-determined intervals, as shown in Figure 9. These regions can function as fracture planes (perforation layers), essentially steering the comminution process. By altering the thickness of the lower porosity layer, limited control over the final nanoparticle size distribution is gained with over fourfold improvement in the yield compared to an approach with a uniform layer using sonofragmentation [395]. Recent results suggest, that high porosity (>80–85 %) P*Si* with uniform structure can also be more efficiently comminuted with either method [53, 396].

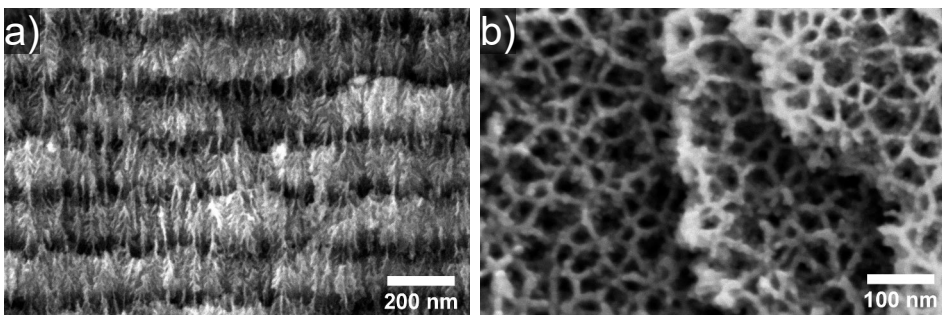


Figure 9. Secondary electron micrograph of a) the cross-section of a P*Si* multilayer film for nanoparticle production with an approximate layer thickness of 130 nm. Figure adapted with permission from ref. [397]. b) Secondary electron micrograph from top of the multilayer film, showing the pore openings and partially broken off layers (unpublished data).

Further improvement in nanoparticle production yield using the multilayer approach has been obtained using high-shear microfluidization. By forcing a suspension containing P*Si* microparticles through narrow channels using high pressure, the velocity of the stream is accelerated greatly, causing considerable shear and impacts

between the particles and the chamber walls. Roberts *et al.* demonstrated the microfluidization method not only improving the nanoparticle yield (24 % vs. 57 %) and size distribution over typical sonofragmentation, but also reducing the duration of the processing from several hours to mere minutes [398].

Methods based on the fragmentation of P*Si* films have limitations on control of the particle size distribution and shape, both having a degree of irregularity, necessitating the use of size selection thorough centrifugation, filtration or sieving. Accurate control over both size and shape can however be achieved through different patterning methods. Small P*Si* microparticles with defined shape could be anodized by utilizing photolithographic patterning to create an etching mask on Si substrate from simply the photoresist resin or from silicon nitride, as demonstrated by Cunin *et al.* [399] and Cohen *et al.* [400], respectively. Lateral dimensions of the particles are determined by the photomask, while the porous structure and layer thickness is controlled with the anodization parameters, allowing selection of the particle aspect ratio. Chiappini *et al.* [401] refined the photopatterning method to facilitate also the fabrication of high porosity microparticles with small macropores without degrading the particle integrity by utilizing multilayer etching for creating transitional structural support layers. For releasing the particles from the substrate through ultrasonication, a final perforation layer was also included. Trench fabrication through the photomask with reactive ion etching (RIE) before anodization was shown to allow further control over the particle shape, enabling the production of accurately defined disk-shaped, discoidal and hemispherical particles of 1–3 μm in diameter, as shown in Figure 10c. Direct photopatterning of particles on an anodized porous layers was demonstrated by Godin *et al.* [402]. Utilizing the thin parasitic layer formed during the initial moments of anodization, low temperature silicon oxide capping was placed on the layer to facilitate the patterning and subsequent RIE processing to fabricate discoidal P*Si* nano- and microparticles (Figure 10d).

As an alternative to photolithography, colloidal lithography is also an effective method for fabricating well-defined P*Si* micro- and nanostructures. By combining MACE and anodization, Alhmoud *et al.* demonstrated a facile method for discoidal nanoparticle production, as shown in Figure 10e [403]. For the porous particle formation with MACE, a shadow mask was created using convective self-assembly of polystyrene nanospheres on a Si substrate before Ag layer deposition. After removal of the nanospheres, the chemical etching process left the masked areas porosified, while the substrate under the metal layer was completely removed. After dissolving the Ag, the porous nanoparticles were released from the substrate with a brief electropolishing anodization. The diameter of the P*Si* nanoparticles was controlled with the size of the nanospheres before metal deposition, while the length was tunable with MACE process duration.

Direct imprinting on an anodized P*Si* layer for nanoparticle fabrication has also been suggested as an alternative for the other lithographic methods (Figure 10f)

[404]. Using a prepatterned, reusable stamp that is hydraulically pressed against the porous layer, the areas surrounding the stamp features are mechanically compacted, while the regions containing the particles retain their structure. The particles can then be released by anodizing a thin high porosity perforation layer to assist in ultrasonication. The size of the particles is controlled with the duration of the initial porous layer anodization and the stamp features, which in turn are prepared using traditional photolithographic and RIE processing.

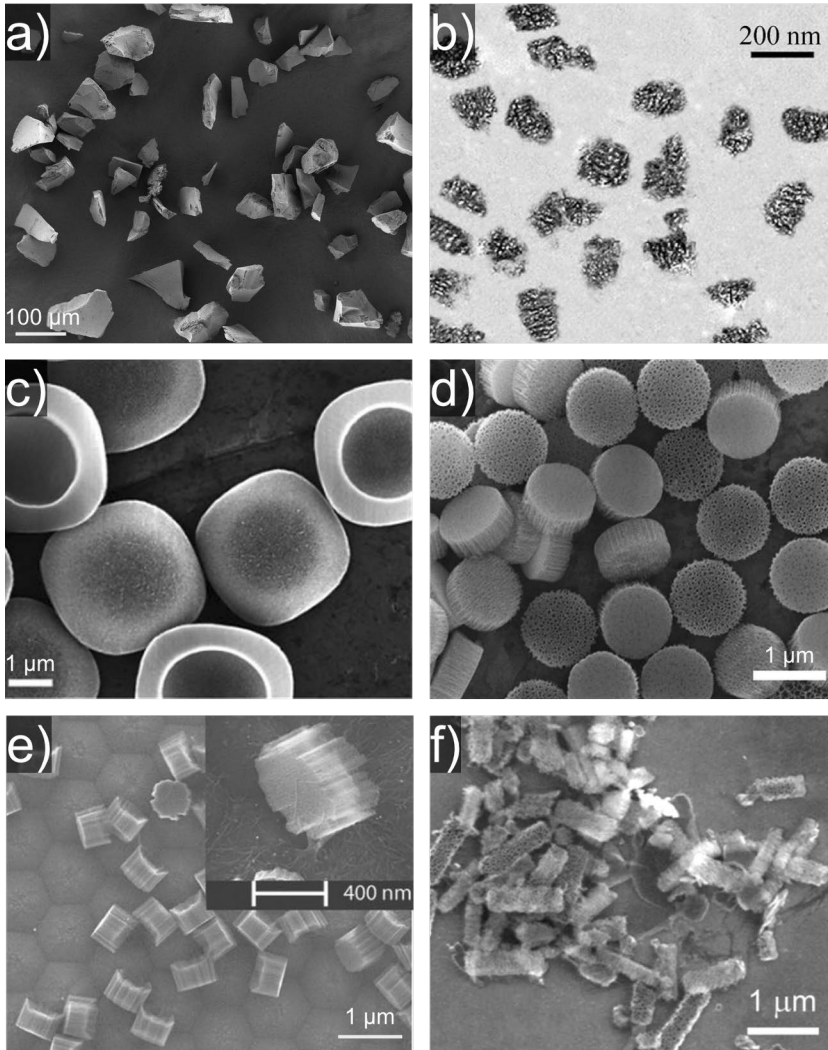


Figure 10. SEM and TEM micrographs of ball-milled PSi a) microparticles (unpublished data) and b) nanoparticles prepared from multilayer films [405], photolithographically patterned and RIE processed c) hemispherical [401] and d) discoidal PSi particles [402], and PSi nanoparticles produced using e) colloidal lithography and MACE [403] and f) direct imprinting [404]. All images adapted with permission from respective publishers.

2.2 Biocompatibility

Considering the use of PSi in drug delivery or other biomedical applications, a crucial aspect is the issue of biocompatibility. The behavior of the material in biological surroundings needs to be evaluated comprehensively, considering, *e.g.*, cytotoxicity and possible chemical reactions caused by the prospective biomaterial and the properties of the degradation products. This includes the immediate environment of the biomaterial, its pH and resident cell types, making estimation of biocompatibility often location-specific. Since introduction of PSi and the ordered mesoporous silicas as capable drug carriers, their role has expanded considerably, prompting various studies regarding their behavior as biomaterials in *in vitro* and *in vivo* settings. Much of this research is summarized in detail in several recent reviews [406–409] and book chapters [410, 411]. Part of the results discussed in Sections 5.2–5.4 and corresponding Papers **II–IV** also touch on the topics below.

An advantage of PSi over other non-Si based biomaterials stems from its degradation behavior. Due to the large available surface area, PSi behaves much like amorphous silicas in aqueous solutions, degrading into orthosilicic acid, $\text{Si}(\text{OH})_4$, through an oxidative hydrolysis process [412], where in a OH^- catalyzed reaction, water produces silanol groups on the PSi surface, weakening the Si–Si back bonds through polarization and consequently leaving these susceptible for further hydrolysis [57, 413]. The water-soluble degradation product, silicic acid, a fairly nontoxic compound, is also the main bioavailable form of Si for humans, and is readily excreted by renal clearance. While the full role of Si in human metabolism is not completely understood, it is suggested that Si is an essential trace element and participating especially in bone and cartilage formation [414, 415]. With the hydrolysis reaction proceeding through the surfaces of PSi into the pore walls, modification of the surface chemistry allows efficient modulation of the degradation rate, where depending also on particle size, the process duration can be tuned from few hours to several weeks [393, 403, 416]. Advantageously, as the surface modifications of PSi are generally only “skin-deep”, the bulk behavior or degradation products are not altered [417]. Due to the hydroxide catalyzed nature of the hydrolysis reaction, the pH of the environment has also a significant effect on the dissolution kinetics as well as to the overall solubility of silicic acid [418, 419].

The surface chemistry along with the particle size have also a role in evaluating PSi cytotoxicity. As briefly mentioned in the previous section, this affects both biodistribution and cellular association of the utilized PSi. The considerable specific surface area inherent to PSi can cause unwanted chemical reactions with, *e.g.*, cellular membranes or other biomolecules, disrupting their functions. With PSi microparticles, it was observed that the presumably conductive carbonized PSi particles appeared to generate more reactive oxygen species (ROS) in *in vitro* testing with Caco-2 intestinal cell line. Prolonged contact with especially microparticles of

< 25 μm size appeared to induce more cellular apoptosis at high particle concentrations, while with larger microparticles and more passive surface modifications, the effects were limited when simulating oral delivery [420]. In a broad study by Shahbazi *et al.* using red blood cells and several immune cell lines along *in vivo* testing with rats, the apparent reactivity of PSi nanoparticles with different surface modifications was demonstrated to have considerable effect on the overall toxicity [421]. Particles bearing carboxylic acid or amine terminations showed consistently higher toxicities through different mechanisms, while non-functionalized, thermally carbonized and oxidized particles presented high biocompatibility.

Further control over the particle behavior and the elicited cytotoxicity can be obtained through different coatings. For instance, one approach to enhance the particle circulation time is to bind a polymer layer of polyethylene glycol (PEG) or dextran to surround the particle. This can be utilized to mask the chemically reactive groups of the particle, possibly reducing cytotoxicity, but also to control the protein corona composition, delaying the clearance of the particles by MPS. Xia *et al.* [422] and Nissinen *et al.* [423] showed considerably improved *in vivo* blood circulation time for PSi nanoparticles in rats after PEG coating, increasing the particle half-life from few minutes to over 4 h. Bimbo *et al.* utilized self-assembling fungal protein, hydrophobin (HFBII) to coat THCPSi nanoparticles, resulting in improved *in vitro* cellular viability and association with Caco-2 and HT-29 cells, relevant to oral drug delivery [424]. Further experiments *in vivo* by Sarparanta *et al.* indicated the HFBII coating alters the biodistribution of the orally dosed nanoparticles in rats, providing the particles mucoadhesive properties and prolonging their transit time in the gastrointestinal tract [425]. With intravenous delivery, the coated and uncoated nanoparticles presented differing protein corona compositions, as well as biodistributions, however the results remain inconclusive on whether this behavior was solely due to the plasma protein adsorption or the hydrophobic nature of the bare THCPSi nanoparticles [426]. Cell membrane derived biomimetic coatings based on isolation from cancer cells and red blood cells have also been demonstrated using PSi nanoparticles for immunotherapy as shown in Figure 11 [427, 428].

2.3 Porous silicon as drug carrier material

Studies utilizing PSi as a drug carrier material showed comparable results to those made with ordered mesoporous silicas, indicating similar versatility, where the porous structure could be used to control the dissolution rate of pharmaceutical molecules through pore size and surface chemistry control [366, 370]. When working with well soluble molecules, diffusion from the pores slowed down the dissolution compared to the free drug, while with poorly soluble compounds, the dissolution rate and solubility were enhanced, also effect of the pH of the dissolution media on the solubility was decreased [365]. The improved characteristics stem from physical confinement

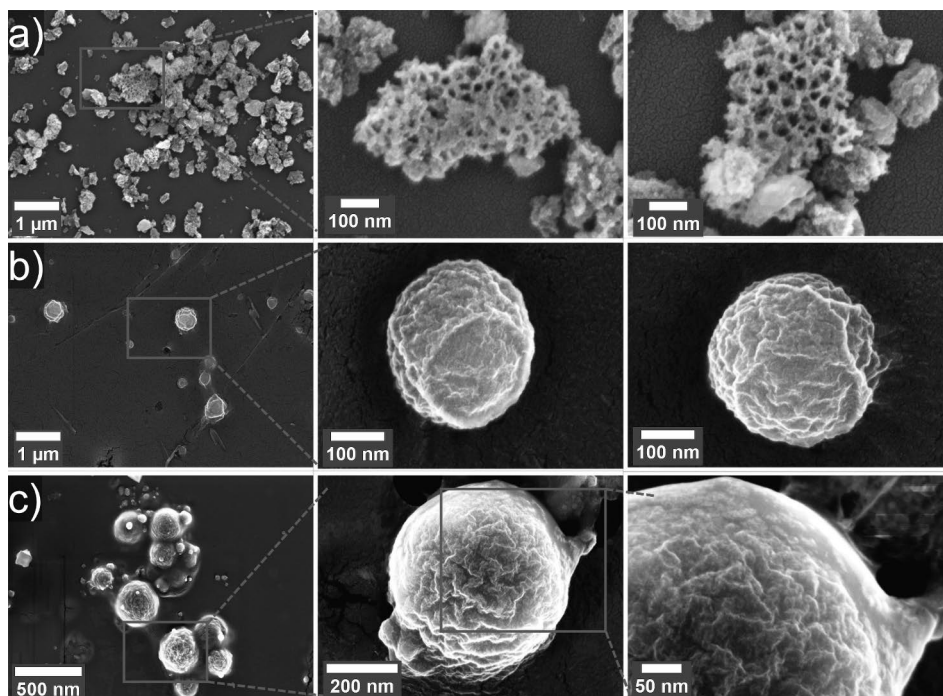


Figure 11. Secondary electron micrographs of TOPSi nanoparticles a) as fabricated, b) coated with acetalated dextran and c) further coated with a cancer cell membrane. Image adapted with permission from ref. [427].

imposed by the porous structure on the adsorbed drug molecules. As the adsorption of the drug is *sine qua non* for obtaining these benefits, multiple methods to load the molecules into the pores have been developed [429, 430].

2.3.1 Drug loading methods and on adsorption from solution

The various methods used for loading PSi and silicas can be divided into several categories, with the simplest division being into solvent-based and solvent-free methods. From these, while less common, the solvent-free methods neatly avoid dealing with possible sources of toxicity from residual solvents. One such approach is directly melting the drug and casting it onto PSi flakes or films, or blending PSi particles with the molten drug. For successful loading, the viscosity of the molten drug should be low enough to allow capillary action to deposit the drug inside the pores [429]. Also, thermal stability of the drug has to be high enough to withstand heating above its melting point without degrading. The utilization of melt method for loading has been successfully shown with various different drug molecules, such as ketoconazole and triclosan with thermally oxidized PSi (TOPSi) [431, 432] and flurbiprofen, ibuprofen and indomethacin using different mesoporous silicas [433–435]. The pres-

ence of pure drug in the mixture presents a challenge in controlling the distribution of the drug, whether it can be completely adsorbed into the pores or if some of the liquid drug remain outside, recrystallizing on the external surfaces of the material.

Another solvent-free method for drug loading is adsorption from vapor phase, where the drug crystals undergo sublimation when in close contact with a porous material, after which the evaporated drug molecules are adsorbed into the pores. As the method appears to require the drug to have relatively high vapor pressure, its application is somewhat rare, the work of Konno *et al.* [358, 359, 436] being one of the few examples. The thermodynamic background of these observations was studied by Qian *et al.* following the adsorption and amorphization of a drug-like compound within mesoporous silica [437]. Hybrid approach utilizing solvent vapors to facilitate the diffusion of the drug molecules presented by Trzeciak *et al.* suggests however the method may be extended for more general use in drug loading [438].

The more common solvent-based loading methods can further be divided into a handful of different types, mainly based on the amount of drug-containing solution used for the adsorbing porous material and the approach for removing the excess solution. In practice, however, the methods are quite similar as they all require the dissolution of the drug compound into a suitable solvent. With poorly soluble small-molecule drugs, this usually necessitates the use of organic solvents [362, 363, 365, 439, 440] or solvent mixtures [441], while with biomolecules, aqueous solutions, often pH-controlled, are utilized to avoid degradation or denaturation [370, 442, 443]. The selection of the solvent also plays further role in the process beyond simply solubilizing the drug. Adsorption from solution is a competitive process, where not only the interactions between the surface and the drug molecules affect the outcome [444], but the interactions between the solution and the surface as well as the solution and the solute molecules have a considerable role. For drug adsorption to occur, whether through physisorption or chemisorption, the adsorbing molecule must be able to displace the solvent. The different interactions in physisorption, such as the ubiquitous van der Waals forces, hydrogen bonding and electrostatic as well as hydrophobic interactions need to be taken into account [445]. For instance, too high affinity between the surface and the solvent molecules may hinder or prevent drug adsorption altogether [439, 446]. Several studies have shown, that, *e.g.*, ibuprofen dissolved in high polarity solvents shows consistently lower obtained payloads compared to adsorption from non-polar liquids with mesoporous silicas [439, 447]. Computational analysis supported the observations, indicating the solvent molecules actively competed with the silanol-terminated adsorption sites, with the high polarity solvents having higher affinity toward the surface than the drug molecules [448]. Similar observations were made by Šoltys *et al.* [449], noting that non-polar solvents appeared generally more effective when tested with different drug molecules.

Interactions between the adsorbate molecules should also be considered. With biomolecules, the ionization of the structure is controlled by the pH of the aqueous

solution. Optimal conditions for the loading would then be having opposite charges on the biomolecule and the adsorbent surface, with electrostatic attraction driving the adsorption [370, 450]. In some cases, however, mutual repulsion of the biomolecules due to the same effect may hinder the adsorption, resulting in lower payloads as shown by Kaasalainen *et al.* with GLP-1 (glucagon-like peptide-1) [443]. It should be noted that for drug release, role of the interactions with the surface is essentially inverted. Weak interactions with the pore walls, such as in the case of hydrophobic drug molecules and hydrophilic silica, and the dissolution rate is mainly limited by the pore size dependent drug diffusion. Conversely, strongly bound drug molecules through, *e.g.*, amide bonds, may require partial erosion of the carrier material to release the drug [451, 452].

From the solvent-based methods, possibly the most common approach is to disperse the porous material in a large amount of drug-containing solution for a specific duration, after which the material is collected through centrifugation or filtration [362, 439, 452, 453]. The durations can vary from few hours to several days, while the solution amount often contains considerably more drug than porous material. In laboratory setting, the procedure often referred as immersion method, provides facile control over the adsorption process through the solvent selection and solution concentration. However, the efficiency of the loading with small molecule drugs is usually quite low, unless methods of reusing the loading solution are sought. For reliable payload estimation, adsorption isotherms are necessary for different solvent and adsorbent surface chemistry combinations. Effects of solution properties on payload and minimization of surface recrystallization are discussed more in Section 5.6 and associated Paper VI.

For avoiding the use of excess drug or solvent, methods derived from catalyst preparation have been adapted for drug loading. The terminology behind these methods has not been properly established in the drug loading setting, with the terms incipient wetness and impregnation often used interchangeably or together to describe two distinct methods. The differences between these methods boil down to how the excess solution is removed, or how much solution is used to begin with.

The term incipient wetness method is more established in catalyst preparation, and refers to using an amount of solution that is enough to fill the pores of the adsorbent. Capillary action rapidly takes the solution into the pores, after which the solvent is allowed to dry, leaving the drug molecules inside the pores [434, 435, 440, 454–457]. Successive wetting of the material can be used to increase the payload [439], especially if solubility of the drug in the solvent is low. However, this may lead to considerable deposition of the drug on the external surfaces to recrystallize. The advantage of the method is nevertheless the predictability of the payload, as essentially all the drug in the solution is utilized.

Similar efficiency in using all the drug available is achieved with a variation of the immersion method. Instead of removing the porous material from the solution,

only the solvent is removed. Easily realized by simply allowing the solvent to evaporate during the loading, the increasing concentration of the drug solution becomes a driving force for the adsorption [447, 458]. Here, too rapid evaporation or too high initial solution concentration may result in excessive recrystallization outside the pores. As an extreme example of solvent evaporation, the use of supercritical CO₂ as a loading solution has also been shown [459–461]. As CO₂ can function as an effective solvent in supercritical state, the loading proceeds much like in immersion method, however, removal of the solvent is very simple and complete, leaving no residual solvents. The systematic study on loading conditions conducted by Ahern *et al.* [460] indicated that only small amounts of crystallized drug were present outside the pores, suggesting the method may be adapted to reduce possible external crystallization.

Both the incipient wetness and evaporation-based immersion method have been shown to scale up beyond laboratory using, *e.g.*, rotary evaporation and spray drying to handle the loading process. Takeuchi *et al.* utilized spray drier to produce indomethacin loaded mesoporous silica particles by spraying the silica containing loading solution into the drier chamber under heated air flow [462]. Further studies comparing indomethacin loading quality in silica particles when these were separated from the loading solution by filtration or evaporation using fluidized bed granulator or rotary evaporator were done by Linnell *et al.* [463]. The results showed significantly higher payloads obtained on the evaporation methods despite considerably lower drug to silica amount, while also avoiding excess surface recrystallization due to solution precipitation. Nagane *et al.* [464] and Hacene *et al.* [465] demonstrated the loading could be done completely in fluidized bed granulator, with the latter combining a subsequent polymer coating step for sustained release. Instead of drying the porous silica from the solution, the particles are initially fluidized and the loading, or coating solution is sprayed onto the particles in the chamber, making the process analogous to the incipient wetness method.

2.3.2 Effects of physical confinement on molecular state

In drug delivery setting with mesoporous materials, the dimensions of the pores approach the size of the adsorbed molecules. The subsequent kinetic and thermodynamic phenomena observed on the molecules are a direct consequence of this imposed physical constraint. When taken into account, these effects on the phase composition of the adsorbed drug enable the use of mesoporous carrier materials not only in drug delivery applications but also in crystal engineering.

Systematic studies by Jackson and McKenna on the effects of nanoscale confinement on phase transition temperatures of small organic molecules showed that while the well-known reduction in crystal melting temperature due to the increased surface-to-volume ratio, when the crystal size is in nanometers was adequately de-

scribed by the Gibbs-Thomson equation, similar predictions could not be made for glass transition temperatures (T_g) or crystallization behavior [466, 467]. Despite being ultimately governed by thermodynamics, the kinetic nature of these state transitions is expressed in some cases as the presence of multiple glass transitions [468], and as shift to either decreased or even increased value of T_g compared to the bulk form [469]. These alterations to the dynamics of the adsorbed molecules appear to be related to the adsorbate-adsorbent interactions, now emphasized due to the high available surface area in confinement.

As the role of mesoporous materials in drug delivery is often to enhance the aqueous solubility of the carrier payload, the main interest generally focuses on stabilizing the confined state within the pores. With nucleation within mesopores observed usually when pore sizes are approximately $10\text{--}20\times$ larger than the guest molecule, stabilization of an amorphous state can occur through steric limitations in smaller pores, as the critical size for nucleation to be energetically favorable cannot be overcome [470, 471]. Different studies have confirmed this indefinite suppression of crystallinity during prolonged storage, barring any adverse reactions between the drug payload and the porous carrier [457, 472, 473], the topic being touched upon also in Section 5.5 and the associated Paper V. Interactions between the pore walls and the immediate surrounding adsorbate molecules have also been shown to have an effect in the crystallization kinetics in small pores, with strong interactions reducing the molecular mobility of the adsorbate considerably, hindering crystallization [474, 475]. This interaction region is sometimes described as a liquid-like layer, and sometimes referred as δ -layer, observed for instance at 1–2 nm thickness in ibuprofen-loaded PSi [453].

When the size of the pores approaches the critical sizes required for nucleation, several interesting observations have been made regarding the physical state of the adsorbed molecules. As partial recrystallization within the confinement becomes accessible, it has been noted that the pore size can be utilized in, *e.g.*, polymorph selection, allowing fabrication of certain crystal forms within the pores. The confined space also affects the Gibbs energy of the adsorbate molecules, showing a dependence on the pore diameter, that may stabilize normally metastable polymorphic forms [476, 477], due to the form being energetically more favorable under the surrounding structural constraints [471]. This enables polymorph screening, bringing otherwise thermodynamically inaccessible forms available for analysis [435, 468, 478, 479], with early reports also suggesting the suitability of PSi for heterogenous nucleation of proteins [480, 481]. Systematic study by Nartowski *et al.* using ^{19}F NMR spectroscopy on flufenamic acid confined in mesoporous silicas of different pore sizes confirmed the strong effect pore size exerts on the molecular state of the adsorbate [473]. The observations indicated that in sufficiently large pores, the adsorbed molecules could reside simultaneously in three distinct states, as confined crystals, amorphous aggregates and in surface interacting liquid-like layer,

represented schematically in Figure 12. Reduction of the pore size below nucleation-favoring limit, instead caused stabilization of the adsorbed drug into amorphous aggregates.

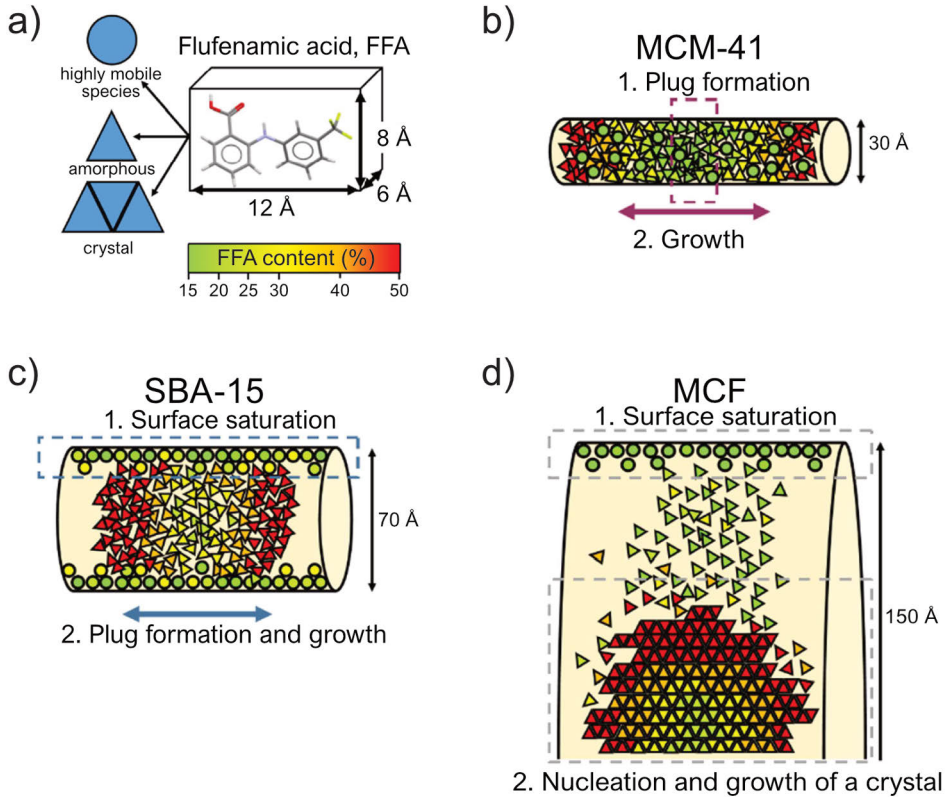


Figure 12. a) Structure of flufenamic acid (FFA) and suggested mechanisms of adsorption and stabilization of amorphous state of FFA in (b) MCM-41 and (c) SBA-15, as well as formation of crystalline FFA in (d) mesocellular foam (MCF). Figure adapted with permission from ref. [473].

2.4 Biomedical and pharmaceutical applications

With the discovery of bioactivity in PSi, along with the interest in similarly structured ordered mesoporous silicas in the late 1990s, the biomedical field has expanded into a broad range of different applications. These range from various forms of delivery of therapeutic agents with PSi-based microparticles [365, 368, 451, 482, 483] and nanoparticles [371, 372, 484, 485] to tissue engineering [486–488], and further, to diagnostic imaging applications through utilization of the intrinsic photoluminescent properties of PSi [393, 489] or through attachment of fluorescent [490] or radioactive labels [221] and beyond. Topical reviews on drug delivery with PSi can be found in references [258, 259, 409, 491], as well as more general approaches for

use of mesoporous materials in the same setting, containing extensive lists of various pharmaceutical molecules utilized and whether *in vitro* and *in vivo* data are presented [492, 493]. Further overviews extending also to diagnostic applications of PSi such as those by Santos *et al.* [409, 494], Voelcker *et al.* [263, 495] and Airaksinen *et al.* [262] along with the chapters in Part III of the book Porous Silicon for Biomedical Applications [36], as well as the pertinent chapters in the Handbook of Porous Silicon [37] and references therein provide the current status of research on the field. Continuing where Section 1.5 branched off, brief examples on a handful of applications for some of the aforementioned subjects are discussed, with emphasis given on the structural or chemical modifications employed.

In the biomedical field, currently one PSi-based application has proceeded through the initial clinical trial phases and appears to reach the market soon. Designed as a brachytherapy device under the market name BrachySil™ by pSivida Corp. for unresectable pancreatic carcinomas, the application is based on the use of partially porosified PSi microparticles containing ^{32}P functioning as β^- -emitter allowing localized intratumoral radiation dose. Produced from atomized, highly phosphorus-doped polycrystalline silicon, the ^{31}P -enriched Si microparticles are size selected and stain etched partially. The natural phosphorous isotope is then transmuted into radioactive ^{32}P with ~ 343 hour half-life using thermal neutrons in $^{31}\text{P}(n, \gamma) ^{32}\text{P}$ reaction [496]. Behaving as a non-leaking source, the microparticles showed promising results in reducing the size of xenografts of hepatocellular and pancreatic carcinomas in mice [497]. Similar results were seen in the first-in-human safety studies indicating the microparticles to function as an effective antitumoral agent [498]. Later Phase II clinical trials under a new market name OncoSil™ and owner OncoSil Medical Ltd. were conducted using a combination of the microparticles and typical chemotherapeutic agents given to patients with advanced unresectable pancreatic cancer, with the results suggesting clinically relevant benefits from the combination therapy [499]. The OncoSil™ particles received a CE mark in 2020⁶, and are currently involved at least in two ongoing clinical trials (NCT05466799 and NCT05131776).

Development of spatiotemporal control mechanisms over the release and targeting of drug payloads from porous materials has received considerable research interest. These extend from various methods of coating PSi with, *e.g.*, polymer or lipid layers to payload entrapment enabling modified release kinetics [500–506], and further to biomolecules grafted on the external surface of PSi or PSi-containing composites for actively targeting the drug release to specific locations through, *e.g.*, receptor mediated uptake and combinations thereof [490, 507–513].

One such approach is to utilize different stimuli-responsive modifications on the PSi, effectively turning the porous carrier material into a gated drug reservoir where

⁶ The British Standards Institution, CE certificates 718878 and 718879

drug release occurs on-demand according to either endogenous stimuli, such as pH [514–516] or temperature [517–520] of the local microenvironment or with exogenous stimuli, *e.g.*, light irradiation [521–524].

As a proof of concept, Wu and Sailor [514] utilized a silane-derivatized oxidized PSi cross-linked with chitosan as pH-responsive gatekeeper for loaded insulin, showing that the behavior of the capping polymer layer under different pH conditions controlled the release of the insulin payload. As the polymer layer swells below the pKa of chitosan, the pores became more accessible, allowing the drug release. At higher pH values, the polymer instead shrunk, closing up the pore entrances.

Shrestha *et al.* [525, 526] presented a construction of a polymer coated PSi nanocomposite for oral delivery of insulin secretion enhancing antidiabetic hormone GLP-1 in synergistic approach with a DPP4 (dipeptidyl peptidase-4) enzyme inhibitor. Using COOH-terminated THCPSi nanoparticles crosslinked with chitosan for improved mucoadhesion, the GLP-1 loaded nanoparticles were coated in aerosol flow reactor with hypromellose acetate succinate, an enteric polymer for pH-responsivity. The enzyme inhibitor in turn was dissolved in the polymer solution, completing the dual peptide-drug delivery system. The nanocomposites indicated low leakage of the peptide at gastric environment in both *in vitro* and *in vivo* studies, and rapid release with the surrounding pH increasing sufficiently high for the enteric polymer to dissolve. The *in vivo* tests also suggested increased pancreatic insulin content after administration of the nanocomposite, showing promise for hypoglycemic regulation.

Introducing a dual capillary electro-spraying approach for fabrication of microcomposites, Roine *et al.* [527, 528] showed a single-step method for coating PSi micro- and nanoparticles with select polymers for oral drug delivery. Atomized droplets with opposite charges sprayed from the capillaries containing immiscible dispersion of drug loaded PSi particles and polymer solution respectively, seek to combine in a rapid fashion neutralizing the charge during the encapsulation process. Demonstrated with enteric polymer Eudragit L100-55 as the encapsulating shell and griseofulvin-loaded TOPSi nanoparticles as the core matrix, the obtained microcomposites showed only limited drug leakage at low pH conditions, while at high pH, the enteric coating dissolved rapidly allowing fast release of the drug. Accelerated stability testing of the microcomposites also indicated the loaded drug to remain in amorphous state, despite tendency of free griseofulvin to rapidly recrystallize during storage. In addition, *in vitro* studies with intestinal epithelial cell cultures showed enhanced permeation of the encapsulated drug over the free form. Kumeria *et al.* [529] demonstrated also the use of enteric polymers from Evonik's Eudragit product line with PSi nanoparticles for site-specific oral delivery. Utilizing PSi as carrier for Immunoglobulin A2 monoclonal antibodies, and combining the protection obtained from both the skeletal silicon and the pH-responsive polymer coating from harsh gastric conditions, the results showed that considerable care must be followed over the

possible interactions between the antibodies and the composite carrier. Comparing the effects the enteric polymers had on the activity of the antibodies, it was surmised that solvents required for dissolving the polymers as well as interactions of the polymer chains during the antibody release had a pronounced activity reducing effect. The results suggested the PSi carrier had also role in protecting the antibodies from the enteric polymers during dissolution.

Microfluidic droplet generation in flow focusing [530, 531] and co-flow geometries [532] were successfully adapted for fabrication of PSi-containing microcomposites suitable for oral delivery as well as nanocomposites for intravenous delivery. With high encapsulation efficiency and monodisperse size distribution, construction of PSi-solid lipid [530, 533] and PSi-polymer [531, 532] composites have been demonstrated. Utilizing a mixture of two hypromellose acetate succinate derivatives, Liu *et al.* presented a pH-responsive multistage system for dual drug delivery [531]. The obtained microcomposites showed pH-dependent drug release in two distinct steps, according to the properties of the selected enteric polymers. Interestingly, the inclusion of PSi in the polymer matrix showed enhanced mechanical degradation of the composites compared to bare polymers, suggesting the possible chemical interactions at the interface between the polymers and the PSi particles having a notable role when designing accurate release profiles.

With certain chemical modifications or payloads, the PSi structure can also be utilized as stimuli-responsive platform for therapeutic effect. Grafting cell-specific antibodies for active targeting on PSi nanoparticles has been shown to enable, *e.g.*, synergistic combination therapy, where co-loaded anticancer drug camptothecin and gold nanoclusters indicated enhanced cytotoxicity *in vitro*. Based on localized heating by the gold nanoclusters under radiofrequency radiation, hyperthermia and release of the chemotherapeutic agent from the internalized PSi nanoparticles were notably more effective in causing cell death than either component individually [534, 535].

Another notable field where PSi has shown promising results is tissue engineering [536]. The tunability in PSi surface chemistry, allowing careful control over the material dissolution rate, as well as the capacity to simultaneously function as drug reservoir, and provide structural support for adhering and proliferating cells, enables the use of PSi as an effective scaffold. These scaffolds can be fabricated both from bare, surface functionalized PSi [488, 537, 538] and PSi-polymer composites [487, 539–541], further highlighting the versatility of PSi.

Scaffolding applications utilizing the resorbable and biomineralization promoting nature of PSi have been of specific interest. Henstock *et al.* showed PSi-polycaprolactone (PCL) composite to release silicic acid considerably more efficiently than an equal amount of the well-known Bioglass 45S5, promoting the formation of calcium phosphate deposits and osteoblast growth [542]. Rosenberg *et al.* [543] developed implantable 3D-printable PCL scaffold containing aminosilanized

PSi conjugated with a bone morphogenic protein. *In vitro* testing suggested the suitability of the printable scaffold for bone repair when native healing is not sufficient to repair the damage. Kaasalainen *et al.* produced lithiated PSi nanowires as scaffolds for periodontal tissue regeneration [544]. The lithiated PSi promoted both bone mineralization and soft tissue formation *in vivo*, showing enhanced performance when compared to lithiated Bioglass or commercial tissue regeneration membrane. Beyond bone repair, *e.g.*, ophthalmic implants based on PSi and PSi-polymer composites have been developed [488, 545, 546]. A conductive cardiac patch fabricated from polyglycerol sebacate was introduced by Ezazi *et al.* [547]. Containing aminosilane-functionalized TCPSi nanoparticles loaded with myocardial regeneration promoting model drug, the patches showed rapid cell attachment and infiltration, indicating suitability for cardiac treatment.

In conjunction with drug delivery and tissue engineering, bioimaging with PSi-based systems has also received broad attention, encompassing multiple imaging modalities, especially in the fields of optical and nuclear imaging, but also in magnetic resonance imaging using entrapped superparamagnetic Fe_3O_4 nanoparticles within PSi micro- and nanoparticles as contrast agent [423, 548] and ultrasound imaging, where PSi nanoparticles can induce acoustic cavitation [549, 550] as well as in photoacoustic imaging where the PSi can function as an enhancer and photostabilizer for a loaded fluorophore [551], or as the contrast agent itself [552].

The structural and chemical properties of PSi play well to its strengths in fluorescence imaging. The intrinsic PL capabilities of PSi can be utilized for *in vivo* imaging, allowing non-invasive observation of biodistribution of, *e.g.*, PSi-based drug delivery system. Being an intrinsic property for the nanostructured silicon, modifications that could alter the behavior of the carrier, influencing the outcome the delivery are unnecessary, thus also avoiding the issue of a fluorescent label molecule detaching from the PSi structure, hindering its tracking. Complex modalities can also be constructed, combining the carrier photoluminescence to the fluorescence of the cargo, allowing co-localization of both components, following the cargo release as well as the eventual degradation of the PSi carrier.

Sailor *et al.* introduced a facile method in activating PL in PSi nanoparticles. Park *et al.* showed that incubation of PSi nanoparticles in deionized water for prolonged duration enabled the formation of an oxide layer on the pore walls, allowing the emergence of PL from the increasingly quantum confined Si crystallites in the walls [393]. The UV excitable PL showed emission in the red – near infrared (NIR) range, well suitable for bioimaging due to the lower tissue absorbance and autofluorescence in this region [553]. The obtained results confirmed that the PL could be used to observe the distribution of drug loaded PSi nanoparticles in living animals and image specific locations such as tumors by allowing the accumulation of the particles in targeted locations. The photostability of the nanoparticles was also noted as markedly better compared to common fluorophores.

Further refinement on the PL activation approach was established by Joo *et al.* [554] by balancing the processes of oxidation of the walls and dissolution of the formed silicon oxides during the aqueous incubation using mild oxidant, sodium tetraborate. The obtained PL emission was noted to be rapid to activate, as well as more efficient, with tunability in the emission wavelength range. Utilizing self-limiting reaction for calcium silicate formation, Kang *et al.* [505] took advantage of the ongoing dissolution of the silicon oxide walls during the incubation through reaction between calcium ions and orthosilicic acid. The precipitated calcium silicate compounds prevented further dissolution and oxidation of the walls, efficiently stabilizing the intrinsic PL of the PSi nanoparticles while also trapping any cargo adsorbed within the pores. Our group adapted regenerative electroless etching for anodized PSi, fabricating a hierarchical nanostructure, allowing controlled thinning of the pore walls and selection of the PL emission color as seen in Figure 13, while retaining the silicon hydride based surface for chemical functionalization of the PSi nanoparticles [53]. Considerable enhancement on the PL quantum yield was presented by Joo *et al.* [555] by reducing the mechanical damage incurred by high porosity PSi during electrolyte removal and drying process in ambient conditions. Application of supercritical drying with CO₂, as shown previously by Canham *et al.* [101], Frohnhoff *et al.* [556] and Loni *et al.* [102] has been demonstrated to enhance PL, as pore collapse due to high capillary stress at the gas-liquid interface inside the pores can be circumvented. The quantum yield of supercritically dried PSi particles was shown to nearly double, when compared to the conventionally air-dried counterpart.

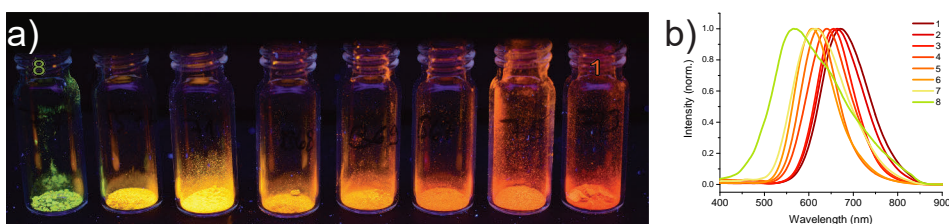


Figure 13. Photograph of luminescent, regeneratively etched PSi samples taken with a DSLR camera using long exposure time under excitation with a hand-held UV lamp at 365 nm. (b) PL spectra of the PSi samples excited at 325 nm. Images adapted with permission from ref. [53]. Copyright 2019 American Chemical Society.

Due to the nature of silicon as an indirect bandgap semiconductor, the long PL emission lifetime of PSi has been reported to be suitable for time-gated fluorescence imaging *in vivo* [557, 558]. As organic fluorophores, including the compounds causing tissue autofluorescence have decay lifetimes in the order of nanoseconds, the microsecond scale half-life of PL emission from PSi nanoparticles allows facile separation of signals at high contrast, with further improvements in the signal-to-noise ratio obtainable by implementing also pulsed excitation.

Applicability of two-photon excitation through NIR radiation has also been shown to function with PSi nanoparticles in imaging setting both *in vitro* and *in vivo* [53, 393, 559]. This allows selective excitation of either the possible fluorophores and the PL, while avoiding tissue autofluorescence. Another advantage in two-photon excitation is deeper penetration of the excitation radiation due to lower tissue absorbance and improved spatial resolution in the imaging.

Beyond imaging, the PL properties of PSi have been reported in, *e.g.*, self-reporting smart bandages for wound healing [560]. Using fluorescence resonance energy transfer (FRET) effect, luminescing PSi nanoparticles initially quenched the fluorescence of the adsorbed drug payload of ciprofloxacin. However, after onset of bacterial infection and subsequent oxidation of the PSi matrix due to alkaline conditions, the FRET effect was gradually diminished allowing the restoration of the drug fluorescence. Observing the fluorescence spectra of the bandage, the progress and nature of the infection could be monitored ratiometrically with the release of the loaded antibiotic. Applying spray nebulization, Zuidema *et al.* fabricated protein carrying PSi-PCL nanofiber composite scaffolds, where the PL of the embedded PSi nanoparticles allowed facile monitoring of the gradual scaffold degradation through time-gated fluorescence imaging [561]. Application of two-photon excitation of PSi for energy transfer to the drug payload in photodynamic therapy has also been demonstrated *in vitro* [562, 563]. Combining active targeting of PSi nanoparticles covalently grafted porphyrin, two-photon excitation was shown to improve considerably the effectiveness of singlet oxygen and reactive oxygen species generation compared to free drug whether excited with either one or two photons.

Nuclear imaging with positron emission tomography (PET) and single photon emission computed tomography (SPECT) have also been applied in various studies regarding biodistribution of PSi nanoparticles in imaging and drug delivery settings. Main advantage in these modalities over the previously described optical methods, is the removal of limitations regarding analysis depth due to tissue absorbance, as well as considerably higher sensitivity [262]. Successful radioactive labeling of PSi necessitates in many cases functionalization of the surface with a chelating group, while avoiding attachment of the radionuclide to other distal groups present, that may result in detachment, and thus erroneous signals during imaging. The short-lived positron emitter, ^{18}F , however, can be directly attached to the surface of chemically passivated PSi, such as thermally carbonized, hydrocarbonized and oxidized PSi. The covalent attachment mechanism is presumed to be substitution of residual silicon hydrides or through nucleophilic attack on the oxygen in Si–O–Si structures [221]. Biodistribution of ^{18}F -labeled bare THCPSi nanoparticles *in vivo* using PET imaging is discussed in Section 5.2 and the associated Paper II.

A combination of SPECT and x-ray computed tomography (CT) was utilized to evaluate the *in vivo* biodistribution of anticancer drug loaded COOH-terminated THCPSi nanoparticles modified with a tumor targeting cyclic peptide iRGD [564].

The gamma-emitting ^{111}In radionuclides for the imaging were chelated to surface grafted DOTA-molecules. The results indicated intravenously administered nanoparticles decorated with targeting peptides showed higher tumor accumulation compared to the PSi nanoparticles without the iRGD modification. However, improved antitumoral effect compared to freely administered drug was not found, as this was rapidly released from the pores, resulting in similar behavior as the free drug. Ferreira *et al.* utilized also ^{111}In -labeling for SPECT/CT to assess targeting and nanoparticle accumulation efficiency into an ischemic heart *in vivo* [565]. Constructing the delivery system around PEGylated COOH-terminated THCPSi nanoparticles that were functionalized with targeting peptide and a DOTA-based chelator for the radionuclide label, the active targeting with atrial natriuretic peptide showed significantly increased cardiac accumulation of the nanoparticles in the endocardial layer compared to the non-targeted counterparts.

3 Aims of the study

As much of the studies conducted on mesoporous PSi applied for drug delivery had focused on the improved dissolution and permeation properties, the behavior of the drug molecules within the mesopores and the approach used for adsorbing the molecules into the confined space had received only limited attention. One of the aims in the studies included here sought to clarify both the physical state of the adsorbed drug molecules within PSi and also systematically explore several key parameters in immersion loading process and their effects on the final payload (Papers **V** and **VI**). Control over the porous structure of PSi through post-fabrication thermal annealing was also studied (Paper **I**), as this was considered as a facile approach for modifying the pore size distribution with some adaptability, with the research done in the group beginning to include also peptides and small proteins as payloads along with the small molecular weight drugs. Possibility to overcome steric hindrances for adsorption in this sense was seen as a desirable outcome, while the method also enabled further studies in the molecular state of the adsorbed payload.

The production method for PSi nanoparticles based on controlled multilayer film etching introduced here (Paper **II**) prompted also a need for further options for surface chemical functionalization. These were studied utilizing the hydrolytically stable hydrocarbonized and carbonized PSi as the initial passivated matrix on which secondary functionalization would be added. The aim was to provide considerable flexibility for biomolecule conjugation while also complementing the existing secondary modification methods (Papers **III** and **IV**).

4 Experimental

Basic details of the fabrication of the PSi and the main analytical methods utilized in the papers are provided in the following section. Detailed information of the reagents and measurement protocols are provided in the articles and the supporting information therein. The research presented was conducted in collaboration with multiple laboratories. The *in vitro* drug dissolution and cellular viability testing were conducted by the Division of Pharmaceutical Chemistry and Technology, University of Helsinki. The radiolabeling and *in vivo* biodistribution experiments were done by the Laboratory of Radiochemistry in Department of Chemistry, University of Helsinki. The Laboratory of Materials Chemistry and Chemical Analysis, University of Turku, using the facilities of the Instrument Centre, carried out the NMR experiments. Also, the facilities and technical support provided by Aalto University Nanomicroscopy Center (Aalto-NMC) is acknowledged for the SEM and TEM access.

4.1 Fabrication and surface modification of porous silicon

In order to provide the multiple concurrent research projects using PSi with the sufficient amounts of material, a cost-effective solution compared to commercial anodic etching cells sold at the time was designed in-house. The selected configuration was a single tank cell for 100 mm Si wafers shown in Figure 14, and manufactured in multiple copies by the mechanical workshop, Protopaja, at University of Turku. Later, a version suitable for 150 mm wafers was also produced.

The fabrication parameters for both microparticles and nanoparticles were both based on the use of boron doped p^+ -type, prime grade Si(100) wafers, having a resistivity of 0.01–0.02 Ωcm . The wafers were sourced from multiple vendors and producers, such as Siegert Wafer GmbH (Germany), Cemat Silicon S.A.⁷ and Okmetic Oy (Finland). The etchant used in the anodization processes was a 1:1 (vol.) solution of hydrofluoric acid (HF, 38%) and ethanol (EtOH, 99.5 %).

For microparticle production, mesoporous freestanding PSi films with uniform pore structure and an approximate thickness of 90–100 μm were anodized and lifted off. The films were then ball milled (Pulverisette 7, Fritsch GmbH, Germany) in an agate grinding jar and fractionated into different size classes using test sieves. Sub-

⁷ currently TopSil GlobalWafers A/S, Denmark

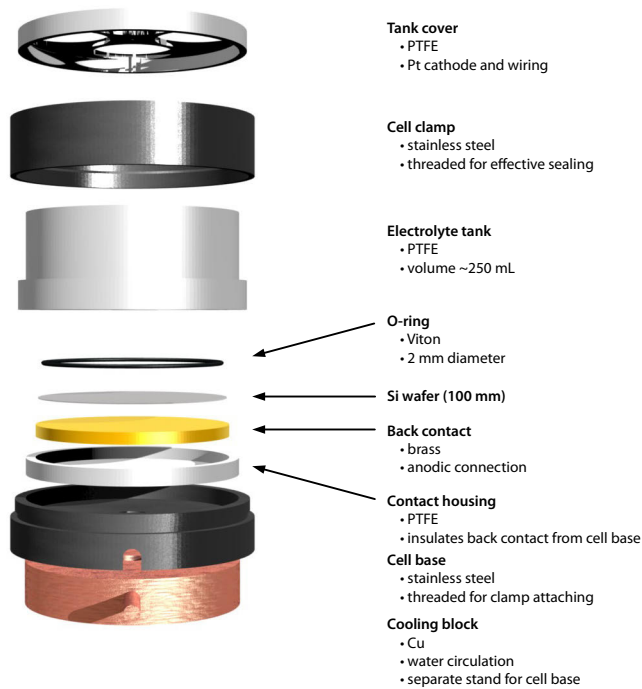


Figure 14. Schematic view of a single tank electrochemical etching cell for PSi anodization used in this work.

sequent surface modifications were done directly for the microparticles, including hydride termination refreshing with an HF rinse.

The production of the nanoparticles was based on etching of multilayer PSi films, where a stack of low and high porosity layers was etched using a purpose-designed etching profile. The multilayer films were etched until the stack thickness was ca. 40–50 μm , after which the film was lifted off. In contrast to the microparticles, the surface modifications were done already for the multilayer films. The treated multilayer films with the high porosity fracture planes were then wet ball milled in zirconia grinding jar using a milling medium suitable for the initial surface modification. This was done to limit the oxidation of the newly exposed surfaces. The obtained particle slurry was then cleaned from the milling solution and redispersed for selection with centrifugation. Visual overview of the both the micro- and nanoparticle fabrication steps is seen in Figure 15.

The primary surface modification used in the papers, were thermal oxidation, hydrocarbonization and carbonization. Thermally oxidized PSi (TOPSi) was produced by heating either the microparticles or the multilayer films at 300 $^{\circ}\text{C}$ in ambient air for at least 2 h, producing a low-temperature oxide surface passivation. Thermally hydrocarbonized PSi (THCPSi) was done by treating as-etched PSi in acetylene. Ini-

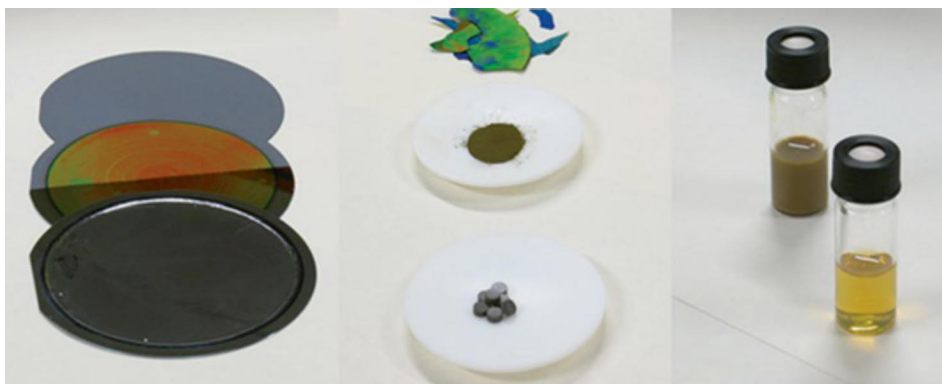


Figure 15. Overview of PSi micro- and nanoparticle fabrication, starting from a Si-wafer, etched with a PSi (multi)layer. The detached porous films can be milled down to fine microparticle powder and compressed into tablets [482], or processed even further, into stable PSi nanoparticle dispersions. Figure taken with permission from ref. [566].

tially, the PSi was dried completely under N_2 flush before introducing C_2H_2 in a 1:1 (vol.) ratio to the gas flow. After 15 minutes of treatment at room temperature, the PSi was heated to $500\text{ }^\circ\text{C}$ for another 15 minutes under the $N_2 + C_2H_2$ flush. Finally, the particles were allowed to cool back to room temperature under N_2 flush. While microparticles were ready for use as-is, the required milling for nanoparticles was done in 1-Decene.

With thermally carbonized PSi (TCPSi), the initial process follows the THCPSi procedure, however instead of exposing the material to ambient, after the cooldown the THCPSi is flushed at room temperature with C_2H_2 for 10 min. Following this step, the THCPSi is annealed at $820\text{ }^\circ\text{C}$ under N_2 flush for 10 min before final cooling back to room temperature.

Secondary modifications for the PSi micro- and nanoparticles were done after the initial passivation phase. In case of aminosilanization with APTES (3-aminopropyl-(triethoxysilane)), the APSTCPSi process was started by rinsing the TCPSi with HF solution, generating a hydroxyl termination on the surfaces. The silanization was carried out by dissolving a suitable amount of APTES in anhydrous toluene and adding the TCPSi into the mixture for 1 h at $25\text{ }^\circ\text{C}$. Finally, the excess silane was removed by washing the obtained APSTCPSi (aminopropylsilane-TCPSi) with fresh toluene and copious amounts of EtOH and dried at $65\text{ }^\circ\text{C}$ for 16 h. With alkyne-THCPSi, the THCPSi multilayer films were immersed into mesitylene containing 10 vol-% of 1,7-Octadiyne for 16 h at $150\text{ }^\circ\text{C}$. Fresh solution was used as the milling media in the grinding process into alkyne-THCPSi nanoparticles.

4.2 Structural characterization

Gas sorption. The physisorption of gas such as N₂ or Ar at their respective boiling points can be used to characterize the structural properties of porous and powdered solids. By following the amount of adsorbed gas in successive admissions as a function of relative pressure, *i.e.*, the ratio of equilibrium pressure and the saturation pressure (p/p_0), an adsorption-desorption isotherm is obtained. The shape of the isotherm can be associated to different types of porous structures, with mesoporous PSi often being classified having a type IV isotherm [567]. The initial slope of the isotherm, often found at p/p_0 range of 0.05–0.2 can be used to determine the specific surface area (SSA) of the sample using the method established by Brunauer, Emmett and Teller (BET) [568]. The total specific pore volume and consequently, the porosity, is often taken as the amount adsorbed at a high relative pressure, such as $p/p_0 = 0.95$ according to the Gurvich rule, if the isotherm has plateaued [99]. In turn, the total pore volume and the SSA can be used to estimate an average pore diameter by assuming the pore shape as cylindrical. Pore size distribution can be evaluated by using, *e.g.*, Barrett, Joyner and Halenda -method (BJH), using either the adsorption or desorption branch of the isotherm as the basis for the calculations [569]. In the included papers I–VI, the gas sorption measurements were done using N₂ as the adsorbate at -196 °C with a TriStar 3000 instrument (Micromeritics Inc., USA). The SSA was calculated using the BET method and the total pore volume taken according to the Gurvich rule. The mesopore size distribution was evaluated using the BJH method on the desorption branch of the isotherm.

Pycnometry. Helium pycnometry is well suited for estimating the true density of porous materials, as helium tends to behave essentially as an ideal gas. As helium can also easily diffuse into mesopores if they are not blocked, pycnometry may be used to evaluate the amount of, *e.g.*, adsorbed drug within the mesopores [365] by comparing the difference in measured true densities of empty and loaded PSi with the equation

$$q = \frac{\rho_{PSi} - \rho_{sample}}{\rho_{PSi} - \rho_{adsorbed}}$$

where q is the amount of adsorbed drug (w_{drug}/w_{sample}) and ρ_{PSi} , ρ_{sample} and $\rho_{adsorbed}$ are the true densities of the empty PSi, the loaded PSi and the adsorbed drug, respectively. Rearranging for $\rho_{adsorbed}$ yields:

$$\rho_{adsorbed} = \frac{q\rho_{PSi} \times \rho_{sample}}{q\rho_{sample} + \rho_{PSi} - \rho_{sample}}$$

In Paper IV the true densities of the samples were measured with AccyPyc 1330 automatic pycnometer (Micromeritics Inc., USA). The density of the loaded drugs was determined using the derived equation above.

Thermal Analysis. Thermal analysis is a set of methods, where physical properties of a sample are monitored as a function of, *e.g.*, temperature or a fixed rate of temperature change. Possibly the most common techniques are differential scanning calorimetry (DSC) and thermogravimetry (TG) [570]. In solid-state analysis of pharmaceutical substances, DSC is especially suitable for monitoring thermal events related to phase transitions, such as crystallization, melting and glass transition. With PSi containing adsorbed drug, DSC analysis can be used to determine whether the sample contains bulk crystalline form of the drug, confined crystallites or disordered, amorphous-like form of the drug. In case of bulk crystalline drug with PSi, the ratio of the observed melting enthalpy to a pure crystalline reference provides the proportion of the drug in the sample (w_{drug}/w_{sample}). In Papers V and VI, the physical state of the adsorbed drugs within the PSi sample were analyzed with Pyris Diamond DSC (PerkinElmer Co., USA) under an inert N₂ atmosphere. In Paper I, DSC was used to monitor the onset of the hydrogen desorption from fresh PSi.

With TG analysis, weight changes in the sample are observed as a function of temperature. These can be utilized to determine the amount of, *e.g.*, volatile compounds such as solvent remnants in drug loaded PSi samples, but also to determine the total amount of adsorbed drug through its complete degradation and evaporation at high temperatures. In Paper IV, TG was used to complement the data obtained with CHN elemental analysis for the polymer surface coating efficiency. In Papers V and VI, TG was used to determine the drug payload. The measurements were done with TGA-7 thermogravimeter (PerkinElmer Co., USA) using a Pt crucible. Despite the surface modifications, PSi is still mainly pure Si, and thus prone to oxidation. In order to avoid unwanted increase in sample mass during the temperature ramp, which could mask the weight loss events, the measurements were conducted under a N₂ flush. It should be noted, that complete loss does not take place with all drug molecules, and this should be verified prior to utilizing this method analytically, as PSi limits the choice of the purge into inert gases only.

Fourier Transform Infrared Spectroscopy (FTIR). Infrared (IR) spectroscopy is a particular technique of vibrational spectroscopy where the interaction of IR radiation with molecular vibrations is monitored. As the mid-IR area (4000–400 cm⁻¹) provides characteristic vibrations of bonds in especially hydrocarbon molecules, FTIR analysis of this region provides information on the molecular structure and chemical state of the samples [571].

Several different sampling and analysis techniques were employed in the included papers. When utilizing attenuated total reflectance (ATR), the sample is pressed against a crystal with a higher refractive index. At the interface, the evanescent wave of the internally reflected radiation extends into the sample and is partially absorbed, providing the spectral information. In Papers II–IV a horizontal ATR accessory (MIRacle, Pike Technologies Inc., USA) with a diamond internal reflec-

tion element was used for free-standing films and PSi nanoparticles. The spectra were measured with either Spectrum BX II (PerkinElmer Inc, USA) or Vertex 70 (Bruker GmbH, Germany) spectrometers equipped with DTGS detectors. In Paper V, the samples were diluted into KBr and the diffusely reflected IR radiation was measured. For the measurements, a diffuse reflectance accessory (Seagull, Harrick Scientific Inc., USA) attached to a Nicolet Nexus 8700 (Thermo Electron Inc., USA) with HgCdTe (MCT) detector was used. In Paper VI, photoacoustic spectroscopy (PAS) was utilized. In PAS, the absorbed IR radiation converts into heat, which in turn diffuses out from the sample into the surrounding gas, causing thermal expansion and providing the photoacoustic signal. The measurements were done using a PA301 photoacoustic detector with an optical cantilever microphone (Gasera Oy, Finland) attached to a Galaxy 6020 (Mattson Instruments Inc, USA) spectrometer. Helium was used as the sample chamber gas.

X-ray Photoelectron Spectroscopy (XPS). More information on the surface chemistry of PSi can be obtained with the use of XPS. XPS is a surface sensitive technique that provides information on the elemental composition and the chemical state of the topmost 5–10 nm of the material. In practice, a sample is irradiated with a beam of soft x-rays, typically with either Al $K\alpha$ or Mg $K\alpha$ radiation, and the photoemitted core level electrons are analyzed [572, 573]. In this work (Paper III), a PHI ESCA 5400 spectrometer (PerkinElmer Co., USA) with a Mg $K\alpha$ X-ray source was used for the collection of the survey and the high-resolution core level spectra.

Organic Elemental Analysis (CHN analysis). The successfulness of the organic derivatizations made to PSi micro- and nanoparticles were evaluated using CHN analysis, where the amounts of the organic-associated elements, carbon, hydrogen and nitrogen, can be directly quantified. The analysis is based on high-temperature combustion of the sample, subsequent chromatographic separation of the evolved gases and their quantification with, *e.g.*, thermal conductivity detector. The analyses conducted for Papers III and IV utilized Vario Micro Cube (Elementar Analysensysteme GmbH, Germany) CHN analyzer for the elemental quantifications.

X-ray Diffraction (XRD). XRD was used to obtain information on the changes in the crystalline structure of PSi and the nanocrystallite size using Scherrer's equation (Paper I). XRD measurements were also used to evaluate the amorphous nature of the adsorbed drugs as well as the melt quenched references in Paper V. In both papers, the measurements were conducted with diffractometers in $\theta/2\theta$ Bragg-Brentano configuration using Cu $K\alpha$ radiation. In Paper I, a Philips PW1820 diffractometer with PW1710 controller and PW1830 generator was utilized (Philips B.V., The Netherlands). In Paper V, an X'Pert Pro diffractometer (Philips/PANalytical B.V., The Netherlands) was used for the experiments.

Nanoparticle size and zeta potential. The average hydrodynamic size and particle size distribution of the P*Si* nanoparticles in Papers **II** and **IV** were determined with dynamic light scattering (DLS). The size analysis was performed with a Zetasizer Nano ZS (Malvern Instruments, UK) instrument. The nanoparticle dispersants were chosen according to their surface chemistry. In Papers **II-IV** the instrument was used for electrophoretic mobility measurements to calculate the zeta (ζ) potential of the micro- and nanoparticles.

Electron microscopy. The porous structure of the P*Si* and the size and shape of the P*Si* micro- and nanoparticles were studied with both scanning electron microscopy (SEM) and transmission electron microscopy (TEM). Secondary electron micrographs of the P*Si* structure and particles were obtained in Papers **II** and **IV** with JSM-6335F and JSM-7500F field emission SEMs (JEOL Ltd., Japan), respectively. In Papers **V** and **VI** the P*Si* samples were analyzed with S-4800 (Hitachi High-Technologies Corp., Japan) and Sigma VP (Carl Zeiss AG, Germany) field emission SEMs, respectively. The TEM micrographs of the nanoparticles and thin sections in Papers **II** and **IV** were obtained with Tecnai 12 (FEI/Thermo Scientific Inc., USA) and JEM-1400 (JEOL Ltd., Japan), respectively.

Solid-state Nuclear Magnetic Resonance Spectroscopy (NMR). NMR spectroscopy was utilized to evaluate the chemical environment of the adsorbed drug molecules in Papers **V** and **VI**, in order to elucidate their solid-state properties, such as molecular mobility and the nature of the physical confinement within the pores. Avance 400 NMR spectrometer (Bruker GmbH, Germany) with a 4 mm MAS (magic angle spinning) probe was used for the solid-state NMR measurements in both papers. In Paper **VI** for the variable temperature measurements, sample temperatures were calibrated for the thermostat setting and the MAS rate using known temperature dependent chemical shift of ^{207}Pb in $\text{Pb}(\text{NO}_3)_2$ [574].

4.3 *In vitro* and *in vivo* experiments

Drug loading. The model drugs used in the Papers, fenofibrate (**III**), griseofulvin (**V**), indomethacin (**V**) and ibuprofen (**VI**), were all loaded into P*Si* microparticles using immersion method. The solvents and immersion durations were chosen according to suitability for each drug. The microparticles were removed from the loading solution by vacuum filtration onto membrane filters, after which the particles were dried either in a regular oven or in a vacuum oven, using a temperature required for removing residual solvents.

Drug dissolution and permeation testing. The drug dissolution experiments in Papers **III** and **V** were conducted using biorelevant release media under sink con-

ditions at 37 °C. The quantity of the drug released and the purity were analyzed with high pressure liquid chromatography (HPLC). Additional supersaturation experiments in Paper V were conducted in a similar fashion, but with a known excess of drug. In Paper VI, the permeability of the drug across the apical to the basolateral chambers in *in vitro* cellular monolayers was followed. The cell lines used for the experiments were Caco-2 human colon carcinoma culture and a co-culture of Caco-2 with mucus-secreting HT-29 goblet-like cells. The amount of the permeated drug was quantified with HPLC. All HPLC measurements conducted were done with Agilent 1260 HPLC (Agilent Technologies Inc., USA) using a UV/Vis spectrophotometer.

Cellular toxicity and association. The cytocompatibility of the PSi micro- and nanoparticles were evaluated with *in vitro* cell cultures using an ATP-based luminescent assay kit (CellTiter-Glo™, Promega Corp., USA), with the luminescence measured with Varioskan Flash fluorometer (Thermo Scientific Inc., USA). The cell lines were selected based on the relevant delivery method. Paper II utilized human Caco-2 cells and RAW264.7 murine macrophage cells and in Paper III Caco-2 and HT-29 cells were used for the cytotoxicity evaluation. In paper IV the nanoparticle toxicity was tested with endothelial EA.hy926 cells and U87 MG brain cells.

Confocal microscopy was utilized to assess the particle association with the cells in Papers II and III. In both cases the particles were initially labeled with FITC (fluorescein isothiocyanate), while Invitrogen CellMask™ plasma membrane stain (Thermo Scientific Inc., USA) was used to visualize the cell membranes. The images in Papers II and III were taken with Leica TCS SP2 and SP5MP confocal microscopes (Leica Microsystems GmbH, Germany), respectively.

In Paper IV, plasma protein adsorption on the PSi nanoparticles was followed with SDS-PAGE (sodium dodecyl sulfate – polyacrylamide gel electrophoresis). For identification, the protein bands were excised from the gel, digested and analyzed with a Sciex QSTAR XL quadrupole time-of-flight mass spectrometer (Applied Biosystems S.A., USA).

Radiolabeling and *in vivo* biodistribution. ¹⁸F used for the radiolabeling of the THCPSi nanoparticles in Paper II was produced in ¹⁸O(p, n) ¹⁸F reaction using ¹⁸O enriched water as the target with 10 MeV protons on IBA Cyclone 10/5 cyclotron (Ion Beam Applications S.A., Belgium). The particle labeling was conducted using a Kryptofix-mediated fluorination reaction. The animal experiments were approved by the National Committee for Animal Experimentation (Hämeenlinna, Finland). The biodistribution studies were conducted with male Wistar Han rats aged 7–10 weeks. The labeled nanoparticles were administered by intragastric gavage for oral administration. Subcutaneous and intravenous injection were used for parenteral delivery.

5 Results and Discussion

The following sections contain a brief overview and some discussion on the main observations of the original papers in conjunction with results obtained from following studies. Here, the focus is mainly on the physicochemical aspects of the different papers, while full results and discussion can be found at the end of this book in the included publications.

5.1 Paper I

Based on earlier studies conducted on thermal annealing of PSi, it appeared that without a surface passivation in place, the rearrangement of the PSi structure would commence in the same temperature range as the surface hydrides begin to desorb. The reduction of the surface free energy drives a change in the pore shape, causing coalescing and eventually closure with increasing annealing temperature as the silicon structure essentially repairs itself by reducing the surface area [116]. At low temperatures, near and slightly above the hydrogen desorption stage, the restructuring effect could be used as an effective post-fabrication tool to enlarge the pores without resorting to material removal, which may quickly result in the complete collapse of the porous network.

By following the changes in the structural parameters of PSi, such as specific surface area and porosity, the earlier observations of the rearrangement beginning along the removal of silicon dihydrides near 400 °C were confirmed. With a strong dependence on the initial porosity, the total pore volume could be maintained up to 700 °C without drastic reduction, using lower porosity samples, as shown in Figure 16. The corresponding specific surface areas however see a rapid decrease regardless of the initial porosity, as the pore walls become smoother with the surface free energy being minimized. The resulting expansion of the pores through merging during the restructuring, increased the average pore diameter with the lower porosity sample from 10 nm to nearly 50 nm. However, the gradual pore coalescing also broadened the pore size distribution considerably.

Further analysis indicated also that combining the annealing with HF immersion in order to refresh the surface hydrides allowed even further expansion of the pore size distribution in certain situations. While the exact mechanism was not conclusively discovered, XRD measurements supported the observation that at 600–700 °C,

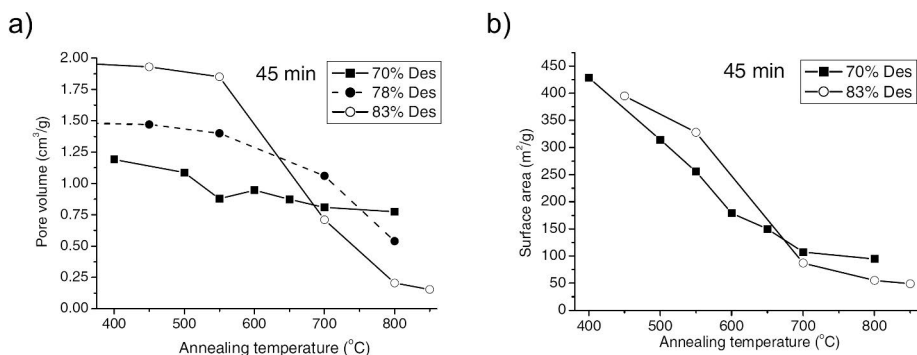


Figure 16. a) Pore volumes and b) specific surface areas of the PSi samples with different initial porosities as a function of annealing temperatures. The annealing time was 45 min. Volumes were calculated from the desorption branches of the isotherms. Figure taken from Paper I.

changes in PSi structure leave the pore walls more susceptible to oxidation, than at lower or higher annealing temperatures, despite retaining partially their crystallinity. As annealing is conducted in inert atmosphere, exposure to ambient air rapidly oxidizes the pore walls, which subsequently can be removed with HF. In this apparent transition region, the average pore diameter could be increased by over 30 % when the surface oxides are removed with hydrofluoric acid.

Overall, thermal annealing allowed the enlargement of mesopores well into the region of smaller macropores, showing the practicality of this post-fabrication modification method. This method was applied for instance to provide a series of samples with progressively increasing pore size for following the behavior of drug molecule crystallization within the pores [453]. Another study utilized the possibility to expand the pores from an initial average of 10–15 nm to 40 nm enabling efficient adsorption of human recombinant insulin into PSi microparticles for oral delivery [575]. The study also confirmed that the thermal annealing can be combined with a subsequent thermal carbonization without refreshing the hydrogen termination of the material with HF immersion between the two steps. Spectroscopic analysis did not show significant differences between the surface chemistries of annealed and non-annealed THCPsi that had also been modified to provide a distal carboxylic acid group for further functionalization.

5.2 Paper II

After systematic evaluation of cytotoxicity of various sizes of microparticles [420], the work was extended to include porous silicon nanoparticles, and also ascertain their biodistribution using several different delivery routes *in vivo*.

For the production of the PSi nanoparticles, we developed a fabrication method where the brittleness of highly porous silicon was used to provide control over how the material is broken down during high energy ball milling. A multilayer PSi film was anodized using an etching profile where a moderate current density etch is followed by a near-electropolishing pulse and a brief pause before repeating the cycle several hundred times. This produced a stack of mesoporous PSi layers with porosity of $\sim 65\%$, loosely connected over a thin separation layer which functions as a fracture plane during the comminution, as was shown in Figure 9 in Section 2.1. The thickness of the lower porosity layers was set by adjusting the anodization time with the lower current density to provide approximately 120–140 nm layers to form the basis of the nanoparticles. The high current pulse was kept brief enough not to cause peeling of the layers during the anodization process. Before starting a new cycle, the etching was paused to allow the concentration of the etchant to level at the bottom of the pores. The etching process was continued until a free-standing film of $\sim 40\ \mu\text{m}$ thick could be lifted off by applying a brief electropolishing period at the end. The multilayer films were initially stabilized by thermal hydrocarbonization followed by the milling. Unwanted oxidation during the formation of new external surface during the fracturing of the THCPSi films was limited by using 1-Decene as a milling medium. Since ball milling is energy intensive process, the increase in temperature within the grinding jar and in the impact areas was assumed to initiate thermal silylation of the alkene chain on the newly exposed surface, maintaining the hydrolytic stability of the nanoparticles. The nanoparticles were separated from the milled dispersion by centrifugation.

The *in vitro* cytotoxicity testing compared nanoparticles separated into few different average sizes, ranging from $\sim 100\ \text{nm}$ to $190\ \text{nm}$ against small THCPSi microparticles. Nanoparticles with an average diameter of $140\ \text{nm}$ were deemed the most optimal for the *in vivo* biodistribution study, as they presented high cellular viability after incubation as well as limited internalization into the tested cells. Since stabilization with thermal hydrocarbonization quenches possible photoluminescence, and fluorescent labeling is, on the other hand, quenched in acidic environment, PET imaging using ^{18}F -labeled THCPSi nanoparticles was employed. With labeled nanoparticles delivered by intragastric gavage, the autoradiographic results showed the nanoparticles to pass through the gastrointestinal tract without crossing the intestinal wall in significant amounts. After an intravenous injection, the ^{18}F -THCPSi nanoparticles were collected in the liver and spleen, indicating rapid clearance of the bare particles from systemic circulation.

Based on the favorable results in toxicity and biodistribution studies with the nanoparticles, the straightforward fabrication method developed for this study remains in use, and is utilized to provide PSi nanoparticles of various surface chemistries to multiple collaborating research groups in, *e.g.*, University of Helsinki, University Medical Center Groningen, Monash University and Harvard University.

The fabrication method has also been adapted by other research groups, as seen elsewhere [576–580].

Succeeding study focusing on the stability of the ^{18}F -label and the possible substitution mechanisms on how the label is introduced [221] confirmed several of the initial observations. The hydrolytic stability of the radiolabel in ^{18}F -THCPSi was very high, with over 90 % of activity still bound to the particles after 4 h immersion into different physiological fluids. With THCPSi, one possible labeling mechanism could be tied to the use of strongly oxidizing agents, such as DMSO (dimethyl sulphoxide) or DMF (dimethylformamide) as solvents for the Kryptofix mediated process at temperatures exceeding 100 °C. XPS analysis on the material after carrier-added labeling indicated slight oxidation of THCPSi surface, where the formed Si–O–Si structures would be susceptible for nucleophilic attack by the fluoride ion.

5.3 Paper III

Thermal carbonization of PSi is recognized as a highly stable passivation method for the reactive, hydrogen terminated, as-etched PSi. However, in biomedical applications a functionalization that provides the ability to, *e.g.*, immobilize peptides or enhance cellular adhesion, is often required. In this vein, we approached the secondary functionalization by taking advantage of the SiC-like surface structure of TCPSi. After immersion into hydrofluoric acid, the native oxides on SiC surfaces are removed, however, instead of leaving the exposed new surface hydride-passivated as with bare Si, it becomes terminated with hydroxyl groups [230], providing a good starting point for silanization-based modifications.

Amine termination was chosen as the target functionalization for TCPSi. For the silane, APTES ((3-Aminopropyl)triethoxysilane) was selected as it has well-known properties. Here, the chain structure provided the name for the functionalized material, aminopropylsilane-TCPSi (APSTCPSi). The complete reaction scheme is shown in Figure 17. The silanization reaction with the HF-generated OH-groups on the TCPSi surface was studied using various surface analytical methods in order to verify the successfulness of the modification, structural changes, and the availability of the amine groups. Gas sorption analysis indicated that the overall reaction did not change the pore structure significantly, with the specific surface area, as well as porosity being comparable to the initial TCPSi, regardless of the concentration of the silane during the process. Chemically, however, the changes are rather notable as indicated by the FTIR and XPS spectra in Figure 18a and Figure 19. The HF-immersion appears to remove the native oxides on the initial TCPSi, as the silicon suboxide-related features in the Si(2p) core level spectra are reduced considerably. This is accompanied by the strengthening of the Si–OH stretch vibration band in the FTIR into a clearly resolved broad peak. The silanization reaction consumes the

surface silanols, while new deformation, overtone and stretching bands that can be assigned to primary amines of the propylsilane chain appear instead. XPS core level spectra of N(1s) also shows the presence of both -NH_2 and its protonated form.

As XPS is extremely surface sensitive, the amount of amine was determined using CHN elemental analysis. With the utilized concentrations of 1, 5 and 10 vol-% of APTES mixed in anhydrous toluene for the silanization reaction (indicated as suffixes -1, -5 and -10), the nitrogen amount varied from 0.38 to 0.6 mmol/g, with the latter two concentrations having practically identical results. These values corresponded to 1–1.6 amine groups/nm², being comparable to post-synthesis grafting of amines into mesoporous silicas. The availability of the amine for bioconjugation reactions was also verified. The test was conducted through biotinylation, which confirmed that the surface was terminated with primary amine groups, that were capable of participating in further functionalization reactions (Figure 18b).

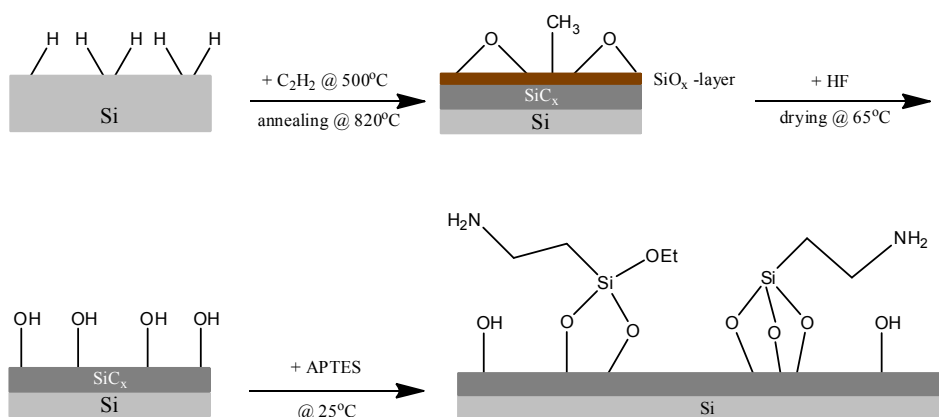


Figure 17. Schematic representation of the thermal carbonization and amine functionalization of PSi with 3-Aminopropyltriethoxysilane. Figure taken from Paper III.

The behavior of the amine-terminated surface chemistry was further tested in aqueous solutions. Acid/base titrations for the TCPSi and APSTCPSi microparticles provided information on how the surface chemistry behaves in different pH conditions. With electrophoretic mobility measurements, the isoelectric points (IEP) were obtained for both plain and the amine-terminated microparticles as shown in Figure 20a. As hydrolytic stability of silanes is known to be rather poor, a method for rapidly testing the quality of the amine termination was designed. By monitoring the surface zeta (ζ)-potential over immersion time in water and in a more physiologically relevant pH 6.8 buffer solution, the stability of the APSTCPSi was evaluated and compared against reference microparticles that were silanized with the same parameters but using thermally oxidized PSi (APSTOPSi) as the initial particles. Figure 20b shows that the oxide-based material loses much of the reactive groups within an hour, while the APSTCPSi appears to undergo slower hydrolysis reaction with the

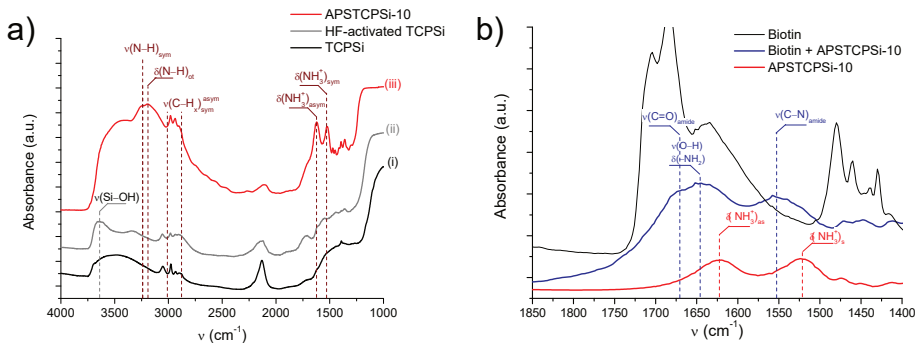


Figure 18. a) FTIR absorbance spectra of TCPSi before (i) and after (ii) HF activation and of APSTCPSi-10 (iii) b) ATR-FTIR absorbance spectra of crystalline biotin, APSTCPSi-10 and biotinylated APSTCPSi-10. Figure taken from Paper III.

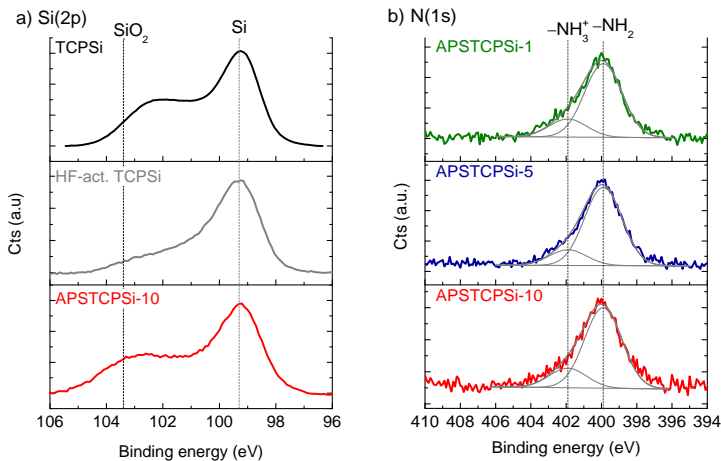


Figure 19. (a) Si(2p) core level spectra of TCPSi, HF-immersed TCPSi, and amino-functionalized APSTCPSi-10. (b) N(1s) core level spectra of the amino-functionalized APSTCPSi samples. Figure taken from Paper III.

ζ -potential remaining comparable to the initial value. This provides a marked advantage for the TCPSi-based particles, especially if prolonged stability is sought, as the underlying carbide structure provides further protection against hydrolysis, while with oxidized PSi, the entire surface is susceptible for rapid dissolution.

The suitability of the surface modification for drug delivery and preliminary cell viability studies were conducted using the APSTCPSi-10 microparticles. Utilizing a poorly soluble lipid regulating agent, fenofibrate, as the model drug, the amine functionalization did not appear to hinder either the drug loading or release, when compared to plain TCPSi. Cellular viability, tested with Caco-2 and HT-29 cells, indicated some toxicity especially with higher particle concentrations when in contact

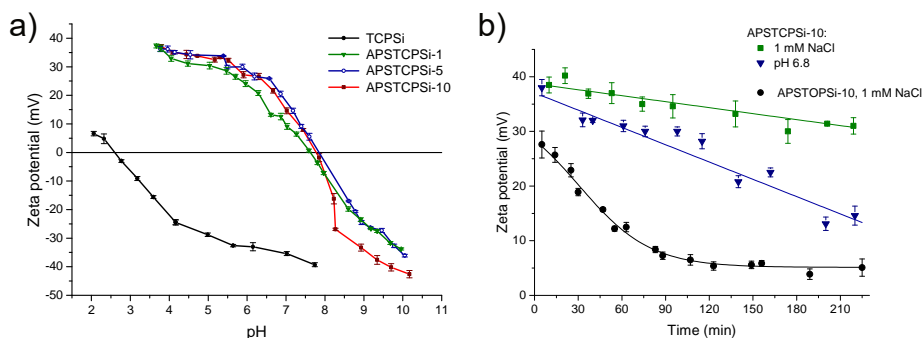


Figure 20. a) Acid-base titration of TCPSi and the APSTCPSi samples. The approximate IEPs are 2.6 and 7.7, respectively, for TCPSi and all the APSTCPSi samples. b) Aqueous stability of the ζ -potentials of APSTCPSi-10 in distilled water and in pH 6.8 phosphate buffer and APSTCPSi-10 in distilled water as a function of time. The solid lines have been fitted to guide the eye. Figure taken from Paper III.

with Caco-2 cells, which could be ascribed for the tendency of the positively charged particles to interact stronger with the cell walls.

In later studies, the functionalization process for APSTCPSi-10 was adapted as the basis for APSTCPSi nanoparticle fabrication. These studies have since provided further information on the broad applicability of the functionalization for, *e.g.*, binding targeting peptides for enhancing cellular uptake or conjugating one type of drug molecule directly to the surface primary amines, while using the remaining pore space for adsorption of a second drug [452, 581]. Toxicological studies in various contexts have confirmed also the positive surface charge to enhance association with cell membranes and subsequently reduce the viability of the cells, possibly through the reactivity of the free primary amine group [421, 581]. However, in immune response studies, the APSTCPSi nanoparticles were noted to cause only negligible immunostimulation, compared to, *e.g.*, oxidized or hydrocarbonized PSi nanoparticles, suggesting the APSTCPSi particles could be suitable for immunosuppressant delivery [582].

5.4 Paper IV

Controlling the behavior of nanoparticles *in vivo* is a crucial requirement for a successful nanoscale drug delivery system. In order to gain further insight on how to modulate the activity of the PSi nanoparticles, a new secondary surface modification for THCPSi was introduced. By adding an alkyne group termination on the pre-stabilized particles, further biofunctionalization could be done relatively simply with click chemistry, using the distal alkynes in copper-catalyzed azide-alkyne cycloaddition (CuAAC) reactions.

While THCPSi is considered hydrolytically stable such as TCPSi, our earlier in-

production of a carboxylic acid -terminated version of THCPsi showed that further functionality could be added chemically [226]. Figure 21 presents of the overview of the stabilization and the subsequent secondary modification process. In a similar fashion as with undecylenic acid, immersing THCPsi into neat or, *e.g.*, mesitylene diluted 1,7-Octadiyne solution and heating it at ca. 150°C for 12-16 h causes covalent attachment of the diyne chain to the THCPsi surfaces. A successful thermal addition can be readily detected by FTIR spectroscopy through the appearance of a new stretching vibration band related to the distal alkyne group at 3320 cm^{-1} and the corresponding C=C stretch at 1605 cm^{-1} indicating the formation of an enyne-like termination on the THCPsi (Figure 22). Unfortunately, reliable determination of the mechanism behind the thermal addition reaction was unsuccessful, and remains a focus for further studies.

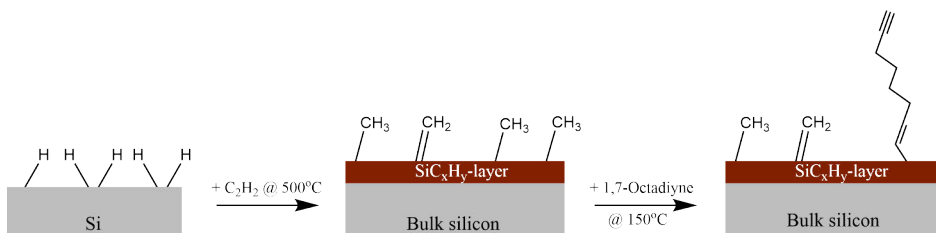


Figure 21. Schematic representation of thermal hydrocarbonization of PSi followed by thermal addition of 1,7-Octadiyne for Alkyne-THCPsi. Figure taken from Paper IV.

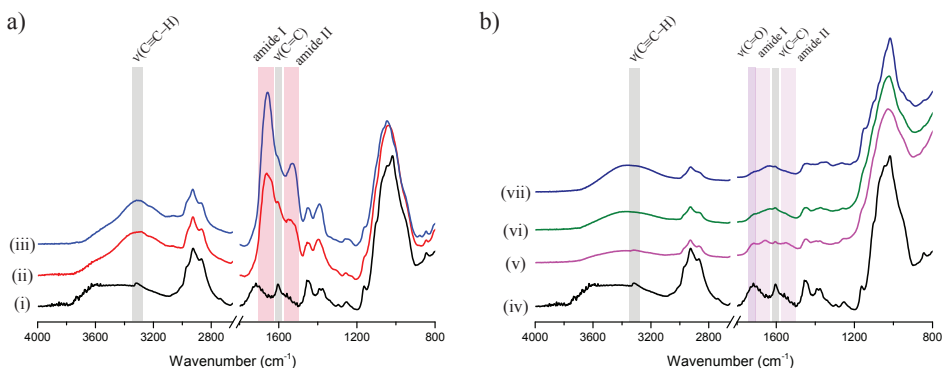


Figure 22. (a and b) FTIR absorbance spectra of Alkyne-THCPsi (i and iv), THCPsi-RGDS (ii), THCPsi-iRGD (iii), THCPsi-PGA (v), THCPsi-Dex6k (vi), and THCPsi-Dex40k (vii) nanoparticles. Figure taken from Paper IV.

In the biofunctionalization experiments, several polymers intended for enhancing cellular uptake and controlling the protein corona formation in plasma with an azide linker were selected and conjugated to alkyne-THCPsi nanoparticles through the click reaction. The addition of the biopolymers was enough to reduce the amount

of available distal alkyne groups below the limits of detection with FTIR, while the amide related bands becoming prominent with the RGD-conjugated nanoparticles. The polymers accounted for 3–6 w-% of the samples according to elemental and thermogravimetric analyses. With the relatively low increase in the particles weight, the size of the nanoparticles increased also only slightly, while the original morphology was retained. Furthermore, the biopolymer-conjugated or the bare nanoparticles did not elicit significant reductions in cellular viability, when incubated with endothelial EA.hy926 or U87 MG brain cells.

The protein corona formation in human plasma was studied with gel electrophoresis from the opsonized proteins. Expectedly, the dextran-modified nanoparticles showed the least association with the plasma proteins, as shown in Figure 23. With the targeting-peptide modified nanoparticles, both RGDS and iRGD appeared to induce considerably more adsorption of the plasma proteins, including fibrinogens and immunoglobulins. Also, the peptide-modified nanoparticles showed adsorption and conversion of the complement C3 protein, which has a considerable role in immune activation.

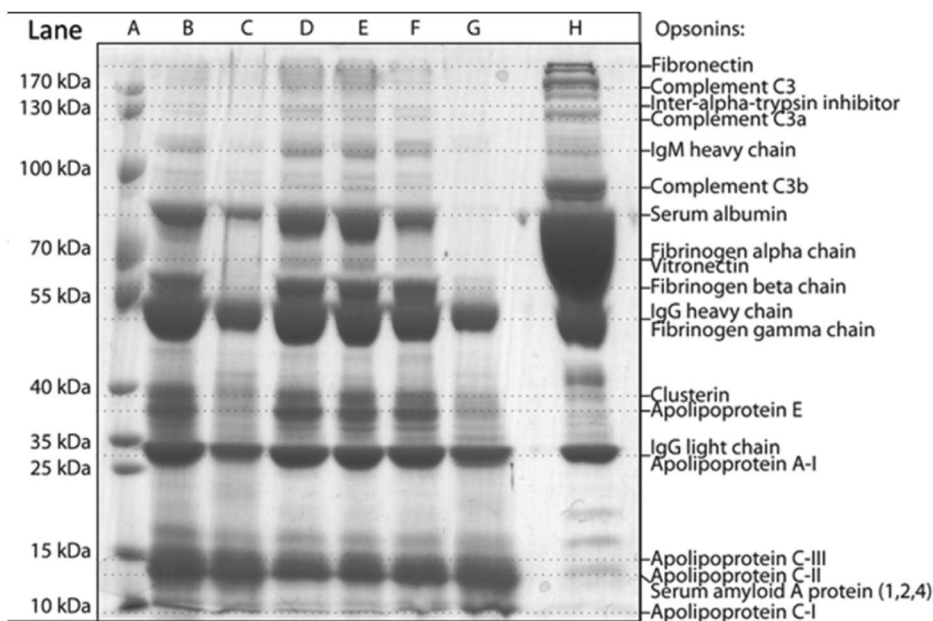


Figure 23. SDS-PAGE separation of the adsorbed plasma proteins on Alkyne-THCPSi nanoparticles (lane B), THCPSi-Dex5k (lane C), THCPSi-RGDS (lane D), THCPSi-iRGD (lane E), THCPSi-PGA (lane F) and THCPSi-Dex40k (lane G). Lane A was the MW marker and lane H was pure human plasma. Figure taken from Paper IV.

5.5 Paper V

The rationale for the study was to acquire more information on the solid-state properties of adsorbed drug molecules confined into mesopores. The drugs selected, indomethacin (IMC) and griseofulvin (GSV) were immersion loaded into THCP*S*i microparticles aiming to provide different payload levels in order to control the quality of the loading process. The physicochemical properties of the confined drugs and the dissolution behavior into biorelevant media were compared to both the common crystalline form as well as to a melt quenched bulk amorphous form.

Thermal analysis and x-ray diffraction are common and straightforward methods to obtain information on the state of the drug molecules in pharmaceutical formulations, however when confined into pores of approximately 10–15 nm in diameter, IMC and GSV both indicate complete suppression of crystallization and subsequent stabilization of the disordered, apparently amorphous state, limiting the information that can be resolved from, *e.g.*, DSC analysis. Interestingly, when preventing the blockage of the pores by the adsorbed drug, the true density of the guest molecules could be obtained with helium pycnometry. Figure 24 shows the progressive reduction of density of IMC and GSV in the different solid states starting from the crystalline form. Melt quenching removes the long-range order of the molecules causing the initial reduction, but a more considerable drop in density is observed in the confined forms where even the short-range order still present in bulk amorphous form is also disrupted. The similarities in the results between the different drug payloads also suggest that possible pore blocking did not significantly influence the results.

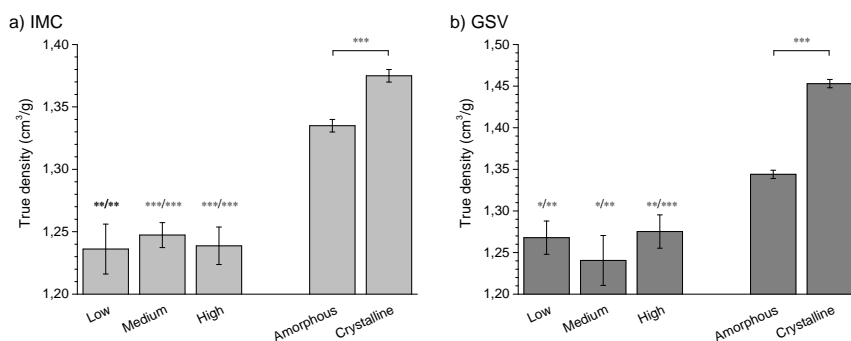


Figure 24. True densities of the THCP*S*i loaded microparticles and bulk forms of IMC (a) and GSV (b). Statistical analysis was made by ANOVA. The level of significance was set at probabilities of **p* < 0.1, ***p* < 0.05, and ****p* < 0.01 between the loaded microparticles and the amorphous/crystalline sample. Errors bars represent the average ± SD (*n* ≥ 3). Figure taken from Paper V.

FTIR and solid-state NMR spectroscopy were employed to obtain further insight to the molecular state of the drugs within the mesopores. As the surface chemistry of the THCP*S*i does not provide active chemical groups capable of participating

through, *e.g.*, hydrogen bonding with the guest molecules, only the physical confinement and interactions between drug molecules could be considered as the source for the observed changes. FTIR analysis indicated the confined state to appear much like the bulk amorphous form, especially with the IMC, where the arrangement of the crystalline γ -form into cyclic dimers provides a distinct absorbance pattern in the carbonyl stretch region. With the removal of the long-range order and apparent reduction in the short range order, some of the dimers are broken, causing broadening of the absorbance peaks, but also formation of shoulder structures confirming the presence of non-hydrogen bonded IMC.

Solid state ^{13}C CP-MAS and ^1H MAS spectra collected from the samples confirmed much of the observations with pycnometry and FTIR, but also provided more information on the immediate surroundings of the drug molecules. Again, the tell-tale signs of the hydrogen bonding disruption in the IMC were most prominent, as can be seen in Figure 25a. However, differences between the bulk amorphous and the confined state were now observed. While some changes could be due to the noise in the NMR signal, new resonance peaks can be observed under the broadening in the chemical shifts caused by the lack of long-range order. The regions related to the IMC carboxyl and carbonyl carbons at 165–185 ppm and the indole related 95–110 ppm area show emergence of small peaks such as those at, *e.g.*, 172 and 174 ppm which could be assigned to a trimer structure of IMC. This may indicate the presence of small clusters of IMC molecules within the pores that are arranged into structures similar to the basic units of both α - and γ -form IMC [583]. The ^1H MAS spectra from both the amorphous and THCPsi confined IMC and GSV provided information on molecular mobility of the drugs. While observations with simpler molecules such as ibuprofen and benzoic acid have yielded high mobilities in mesoporous silicas with transverse relaxation times T_2 in the range of several milliseconds, more complex molecules such as IMC and itraconazole have shown T_2 times of ca. 0.3 ms despite confinement. The bulk amorphous and THCPsi confined IMC showed similar results of T_2 being 0.3 ms, while with GSV the T_2 times were 0.3 and 0.4 ms for the amorphous and confined states, indicating only very limited mobility for adsorbed drug molecules in both cases.

5.6 Paper VI

While ibuprofen is a well-known and broadly applied drug with mesoporous materials, studies with different types of porous silicon have usually focused on the enhanced dissolution and permeation effects. Several aspects of ibuprofen made it, however, an interesting molecule to expand the studies conducted with IMC and GSV, especially regarding the molecular state as ibuprofen was known to be able to crystallize within the same pore size range. To provide more information on possi-

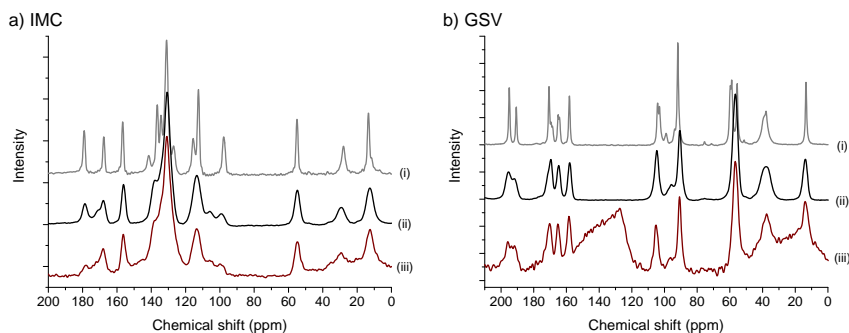


Figure 25. ^{13}C CP-MAS solid state NMR spectra of crystalline (i), amorphous (ii), and THCPsi loaded (iii) IMC (a) and GSV (b) at a MAS rate of $\nu_{\text{MAS}} = 12$ kHz. Figure taken from Paper V.

ble interactions between pore walls of the PSi and the guest molecules, TOPSi with available silanol groups was included alongside the more inert THCPsi.

The solubility of ibuprofen into different types of organic solvents provided an interesting starting point for the study. In order to obtain the highest benefit from the mesoporous carrier material, the adsorption of the drug should be controllable not only payload-wise, but also from the standpoint of excess drug remaining on the external surfaces of the carrier. Uncontrolled recrystallization of the bulk drug around the carrier microparticles could adversely affect the bioavailability of the drug, making the dissolution behavior non-repeatable or necessitating a rinsing step to the loaded material, which may be difficult to realize without releasing some of the confined drug from the pores. With ibuprofen, the externally recrystallized drug can be readily quantified with DSC and also separated from the aforementioned crystallization that takes place within the confinement due to melting point depression according to the Gibbs-Thomson equation. Removing the amount of observed bulk crystalline ibuprofen from the total payload allowed the estimation of the actual payload confined inside the mesopores.

For finding the optimal loading parameters, EtOH, tetrahydrofuran (THF) and chloroform (CHF) were selected as representing solvents that were polar protic, polar aprotic and non-polar, respectively. Immersion loading series were done with both surface chemistries and all three solvents, providing results as shown in Figure 26. With all solvents, the highest confined payloads appear to reside in the range of 800–850 mg/cm^3 , obtained using a loading solution concentration of 400 mg/mL (8:1 drug–PSi ratio). This corresponds with, *e.g.*, the THCPsi, an actual payload of 81–86 % ($w_{\text{drug}}/w_{\text{PSi}}$). After reaching this level, regardless of the solvent, the ibuprofen recrystallizing on the external surface of the microparticles increased rapidly. As the true density of crystalline ibuprofen is approximately 1110 mg/cm^3 and under confinement a reduction of 3–7 % could be expected, the optimal payload can be estimated to fill 75–80 % of the available pore space. Interestingly, THF and CHF

appeared to be more efficient loading media, possibly due to their lower permittivity, but when the drug-PSi ratio was increased, the confined payload started to reduce. This suggests some nucleation may take place even during the immersion that causes the pores to be blocked from further adsorption.

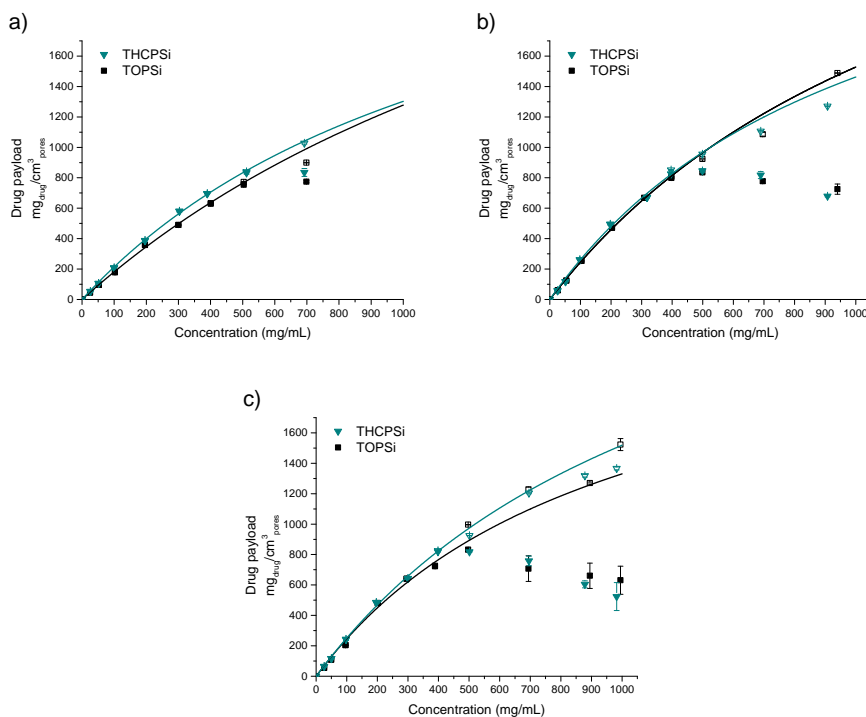


Figure 26. Adsorption of ibuprofen onto TOPSi and THCPsi from (a) EtOH, (b) CHF, and (c) THF. The open symbols show the total amount of ibuprofen adsorbed on the sample, and the solid symbols show the amount of drug confined into the pores. The solid lines were drawn to guide the eye. Figure taken from Paper VI.

Solid-state analysis of the confined ibuprofen was made particularly interesting by the presence of a crystallized phase within the pores. Our earlier thermoanalytical study regarding the state of ibuprofen loaded into PSi suggested that the crystalline drug within the mesopores retains some properties of its bulk counterpart, such as the enthalpy of fusion [453]. In the current study, DSC analysis showed the crystallization within the mesopores starting to take place already at low payloads of 200 mg/cm³. With payloads from 300 mg/cm³ and higher, the confined crystalline portion corresponded for over 50 % of the actual payload, with the remaining molecules either participating in the liquid-like layer between the pore walls and the crystals or dispersed in the remaining pore space [473].

As expected, when comparing the effect of surface chemistry on the adsorbed ibuprofen, the partially silanol-terminated TOPSi pore walls appeared to interact with

the guest molecules providing possible adsorption sites, while disrupting the tendency of ibuprofen of forming cyclic dimers according to both FTIR and ^1H MAS NMR measurements. The presence of two distinct phases was also visible in the room temperature NMR spectra, as the broad baseline bump in the signal, typical for solids, was convoluted with several broad resonance peaks, due to the presence of a mobile phase. A more resolved spectrum was obtained with a higher MAS rate, which effectively increased the sample temperature and partially melted the confined crystalline portion. This can be seen in Figure 27, with the difference between the TOPSi and THCPSi surface chemistries. In THCPSi, the ibuprofen OH-related resonance is visible as a peak at approximately 12 ppm, while with TOPSi, the resonance can be located around 9.4 ppm as a broad band, indicating ongoing interactions between the ibuprofen carboxyl groups and the silanols in the pore walls. The extent of the interaction however appears limited to only the immediate surroundings of the pore walls, not affecting the core regions where crystallization takes place.

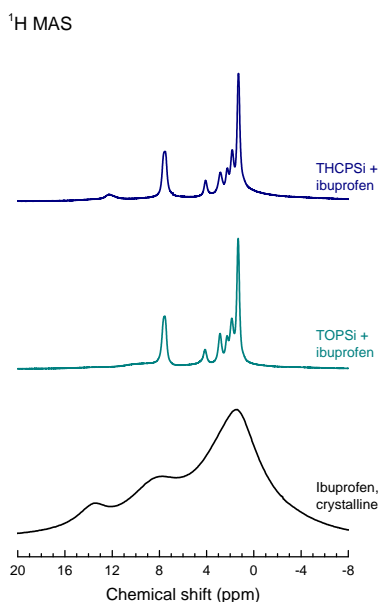


Figure 27. ^1H MAS NMR spectra of bulk crystalline ibuprofen with ibuprofen-loaded TOPSi and THCPSi, obtained using a MAS rate $\nu_{\text{MAS}} = 12$ kHz, with an effective sample temperature of 55°C . Figure taken from Paper VI.

The two confined phases were also observable using a combination of successive ^{13}C CP-MAS and direct MAS measurements, taking advantage of the respective properties of both techniques. The spin polarization transfer used in CP-MAS to enhance the solid-state spectra becomes ineffective if the motion of the molecules is too high in the mobile phase. Conversely, direct MAS measurement with short recycle delay attenuates the crystalline phase contributions due to saturation and line

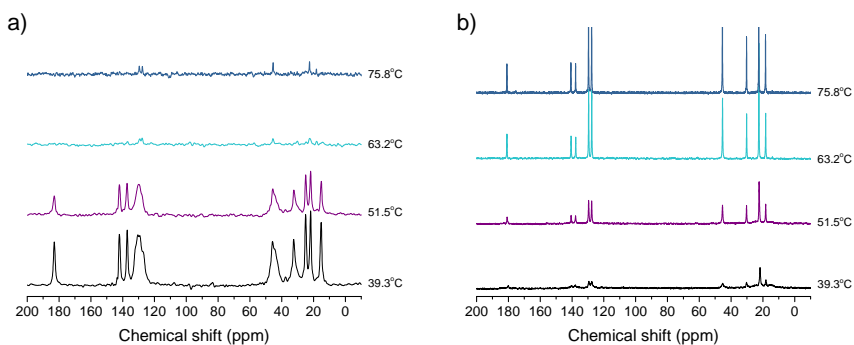


Figure 28. (a) ^{13}C CP-MAS and (b) ^{13}C MAS NMR spectra of ibuprofen confined in TOPSi. The variable temperature spectra were obtained using MAS rates of $\nu_{\text{MAS}} = 10$ kHz, except for the highest temperature where $\nu_{\text{MAS}} = 12$ kHz. Figure taken from Paper VI.

broadening. This enabled nearly selective measurements of both the confined phases. By increasing the measurement temperature, the crystalline phase gradually disappeared, as shown in Figure 28. Using suitable measurement and temperature equilibration durations, the combination of successive CP-MAS and MAS measurements could be extended to provide quantitative information on the confined phases.

6 Conclusions

The studies included in this thesis focus on three aspects of PSi, the first being the structure and post-fabrication control over the porous characteristics and particle size. The second takes a look at the interface between the host PSi structure and adsorbed guest molecules through chemical modification of the PSi surface. The final aspect is the effect of the nanoscale physical confinement imposed by the mesopores on the adsorbate at the molecular level.

Thermal annealing in nitrogen atmosphere provided an effective tool to increase the average pore size post-fabrication in a limited fashion. Thermal processing at temperatures near or slightly above the onset of hydrogen desorption allowed controlled increasing of the pore size without causing considerable pore closure or structural collapse. The benefit of the method is its simplicity and possibility to combine it with a subsequent surface modification step. This enables the adsorption of larger biomolecules than original material would permit, extending the applicability of pre-prepared PSi and an already refined PSi fabrication process.

As the anodization process allows sharp porosity gradients, utilizing the brittleness of a highly porous layer in a multilayer PSi film design enabled etching of pre-determined fracture planes, which eased fabrication of PSi nanoparticles through wet milling. The introduced fabrication process was developed as such that the PSi multilayer film would sustain handling and surface modifications before size reduction. In vitro and in vivo testing of the PSi nanoparticles indicated limited toxicity and rapid clearance from systemic circulation. The fabrication method can be considered as a notable success, as it has been utilized in over 70 publications by our group and adapted for use by other PSi research groups.

The surface modifications introduced here both aimed to provide a secondary functionalization for an already passivated, highly stable PSi. Combining a reactive primary amine group to TCPSi using a simple silanization approach yielded a modification process that allowed the use of the material in further bioconjugation reactions. Also, the silanization onto a SiC-type surface provided considerably enhanced hydrolytic stability for the amine group compared to oxidized PSi. A more flexible secondary functionalization was sought with the grafting of an α,ω -diyne on THCPSi surface. The thermal addition through a possibly silylation-like reaction, verified by the formation of an enyne-structure was confirmed successful as it enabled the use of Cu-catalyzed azide-alkyne cycloaddition for further modification.

This was tested by grafting azide-bearing biopolymers onto the modified THCPSi nanoparticles using the simple click chemistry reaction.

The effect of physical confinement on adsorbed drugs in PSi is usually manifested as improved solubility and permeability. The studies focused on the nature of the molecular disorder of different model drugs. Main observations were the reduced density and enhanced solubility compared to bulk amorphous forms while providing a stabilizing effect on the state. Depending on the selected PSi surface chemistry, the interactions between the pore walls and the adsorbed molecules could be controlled. The effects however were observed to be limited to only the immediate interface region. Adsorption from different solvents with various drug concentrations were also tested. Selection of suitable loading conditions enabled high drug payloads, while limiting or preventing recrystallization of the drug molecule on the external surface of the particles, thus avoiding unnecessary rinsing steps.

These studies underscore the versatility of PSi structure and surface chemistry, both extremely important aspects considering the applicability of PSi in either microscale or nanoscale drug delivery. Confinement and partial crystallization in mesopores offer an interesting avenue for further research, in addition to physically stabilizing an amorphous state but also as a tool in crystal engineering of small molecule drugs.

List of References

- [1] J. Bardeen, W. H. Brattain, The Transistor, A Semi-Conductor Triode, *Physical Review* 74 (1948) 230–231.
- [2] G. L. Pearson, J. Bardeen, Electrical properties of pure silicon and silicon alloys containing boron and phosphorus, *Physical Review* 75 (1949) 865–883.
- [3] M. Tanenbaum, L. B. Valdes, E. Buehler, N. B. Hannay, Silicon *n-p-n* Grown Junction Transistors, *Journal of Applied Physics* 26 (1955) 686–692.
- [4] A. B. Fowler, A Semicentury of Semiconductors, *Physics Today* 46 (1993) 59–62.
- [5] I. M. Ross, Foundation of the silicon age, *Physics Today* 50 (1997) 34–39.
- [6] A. Uhlir, Electrolytic Shaping of Germanium and Silicon, *Bell System Technical Journal* 35 (1956) 333–347.
- [7] A. Uhlir, I. W. Uhlir, Historical perspective on the discovery of porous silicon, *Physica Status Solidi (C)* 2 (2005) 3185–3187.
- [8] D. R. Turner, Electropolishing Silicon in Hydrofluoric Acid Solutions, *Journal of the Electrochemical Society* 105 (1958) 402.
- [9] C. S. Fuller, J. A. Ditzenberger, Diffusion of Donor and Acceptor Elements in Silicon, *Journal of Applied Physics* 27 (1956) 544–553.
- [10] D. R. Turner, On the Mechanism of Chemically Etching Germanium and Silicon, *Journal of the Electrochemical Society* 107 (1960) 810.
- [11] R. Archer, Stain films on silicon, *Journal of Physics and Chemistry of Solids* 14 (1960) 104–110.
- [12] R. Memming, G. Schwandt, Anodic dissolution of silicon in hydrofluoric acid solutions, *Surface Science* 4 (1966) 109–124.
- [13] K. Beckmann, Investigation of the chemical properties of stain films on silicon by means of infrared spectroscopy, *Surface Science* 3 (1965) 314–332.
- [14] R. L. Meek, Electrochemically Thinned N/N⁺ Epitaxial Silicon—Method and Applications, *Journal of the Electrochemical Society* 118 (1971) 1240.
- [15] M. J. J. Theunissen, J. A. Appels, W. H. C. G. Verkuylen, Application of Preferential Electrochemical Etching of Silicon to Semiconductor Device Technology, *Journal of the Electrochemical Society* 117 (1970) 959.
- [16] M. J. J. Theunissen, Etch Channel Formation during Anodic Dissolution of N-Type Silicon in Aqueous Hydrofluoric Acid, *Journal of the Electrochemical Society* 119 (1972) 351.
- [17] Y. Watanabe, T. Sakai, Semiconductor device and method of producing the same. US Patent, 3,640,806, (1970).
- [18] Y. Watanabe, Y. Arita, T. Yokoyama, Y. Igarashi, Formation and Properties of Porous Silicon and Its Application, *Journal of the Electrochemical Society* 122 (1975) 1351.
- [19] Y. Arita, Y. Sunohara, Formation and properties of porous silicon film, *Journal of the Electrochemical Society* 124 (1977) 285–295.
- [20] C. Pickering, M. I. J. Beale, D. J. Robbins, P. J. Pearson, R. Greef, Optical studies of the structure of porous silicon films formed in *p*-type degenerate and non-degenerate silicon, *Journal of Physics C: Solid State Physics* 17 (1984) 6535–6552.
- [21] C. Pickering, M. Beale, D. Robbins, P. Pearson, R. Greef, Optical properties of porous silicon films, *Thin Solid Films* 125 (1985) 157–163.
- [22] L. Canham, Silicon quantum wire array fabrication by electrochemical and chemical dissolution of wafers, *Applied Physics Letters* 57 (1990) 1046–1048.
- [23] V. Lehmann, U. Gösele, Porous silicon formation: A quantum wire effect, *Applied Physics Letters* 58 (1991) 856.
- [24] A. Halimaoui, C. Oules, G. Bomchil, A. Bsiesy, F. Gaspard, R. Herino, M. Ligeon, F. Muller, Electroluminescence in the visible range during anodic oxidation of porous silicon films, *Applied Physics Letters* 59 (1991) 304–306.
- [25] F. Kozlowski, P. Steiner, W. Lang, A model for the electroluminescence of porous *n*-silicon, *Journal of Luminescence* 57 (1993) 163–167.
- [26] P. Steiner, F. Kozlowski, W. Lang, Blue and green electroluminescence from a porous silicon device, *IEEE Electron Device Letters* 14 (1993) 317–319.
- [27] P. McCord, S.-L. L. Yau, A. J. Bard, Chemiluminescence of anodized and etched silicon: evidence for a luminescent siloxene-like layer on porous silicon., *Science* 257 (1992) 68–9.
- [28] M. G. Berger, H. Munder, S. Frohnhoff, M. Thönissen, Optoelektronisches und optisches Bauelement. Deutsches Patentamt, DE 43 19 413 A1, (1993).
- [29] M. Berger, C. Dieker, M. Thonissen, L. Vescan, H. Luth, H. Munder, W. Theiss, M. Wernke, P. Grosse, Porosity superlattices: a new class of Si heterostructures, *Journal of Physics D: Applied Physics* 27 (1994) 1333.
- [30] S. Hilbrich, R. Arens-Fischer, L. Kuepper, W. Theiss, M. G. Berger, M. Krueger, M. Thoenissen, The application of porous silicon interference filters in optical sensors, *Thin Solid Films* 297 (1997) 250–253.

- [31] G. Vincent, Matériau semi-conducteur à porosité variable et son procédé de fabrication. Institut National de la Propriété Industrielle, FR 2 708 630-A1, (1993).
- [32] G. Vincent, Optical properties of porous silicon superlattices, *Applied physics letters* 64 (1994) 2367–2369.
- [33] V. S. Lin, K. Motesharei, K. P. Dancil, M. J. Sailor, M. R. Ghadiri, A porous silicon-based optical interferometric biosensor., *Science* 278 (1997) 840–3.
- [34] L. T. Canham, Bioactive silicon structure fabrication through nanoetching techniques, *Advanced Materials* 7 (1995) 1033–1037.
- [35] M. J. Sailor, *Porous Silicon in Practice*, Wiley, Weinheim, 2011.
- [36] H. A. Santos (Ed.), *Porous Silicon for Biomedical Applications*, 2nd ed., Woodhead Publishing, 2021.
- [37] L. Canham (Ed.), *Handbook of Porous Silicon*, 2nd ed., Springer International Publishing, Cham, 2018.
- [38] C.-L. Lee, K. Tsujino, Y. Kanda, S. Ikeda, M. Matsumura, Pore formation in silicon by wet etching using micrometre-sized metal particles as catalysts, *Journal of Materials Chemistry* 18 (2008) 1015.
- [39] K. W. Kolasinski, Charge Transfer and Nanostructure Formation During Electroless Etching of Silicon, *Journal of Physical Chemistry C* 114 (2010) 22098–22105.
- [40] Z. Huang, N. Geyer, P. Werner, J. de Boor, U. Gösele, Metal-assisted chemical etching of silicon: a review., *Advanced Materials* 23 (2011) 285–308.
- [41] A. Loni, D. Barwick, L. Batchelor, J. Tunbridge, Y. Han, Z. Y. Li, L. T. Canham, Extremely High Surface Area Metallurgical-Grade Porous Silicon Powder Prepared by Metal-Assisted Etching, *Electrochemical and Solid-State Letters* 14 (2011) K25.
- [42] K. W. Kolasinski, W. B. Barclay, Stain Etching of Silicon With and Without the Aid of Metal Catalysts, *ECS Transactions* 50 (2013) 25–30.
- [43] H. Alhmod, D. Brodoceanu, R. Elnathan, T. Kraus, N. H. Voelcker, A MACEing silicon: Towards single-step etching of defined porous nanostructures for biomedicine, *Progress in Materials Science* 116 (2021) 100636.
- [44] H. D. Banerjee, S. Sen, H. N. Acharya, Investigations on the production of silicon from rice husks by the magnesium method, *Materials Science and Engineering* 52 (1982) 173–179.
- [45] Z. Bao, M. R. Weatherspoon, S. Shian, Y. Cai, P. D. Graham, S. M. Allan, G. Ahmad, M. B. Dickerson, B. C. Church, Z. Kang, H. W. Abernathy, C. J. Summers, M. Liu, K. H. Sandhage, Chemical reduction of three-dimensional silica micro-assemblies into microporous silicon replicas., *Nature* 446 (2007) 172–5.
- [46] L. Batchelor, A. Loni, L. T. Canham, M. Hasan, J. L. Coffey, Manufacture of Mesoporous Silicon from Living Plants and Agricultural Waste: An Environmentally Friendly and Scalable Process, *Silicon* 4 (2012) 259–266.
- [47] Y. Lai, J. R. Thompson, M. Dasog, Metallothermic Reduction of Silica Nanoparticles to Porous Silicon for Drug Delivery Using New and Existing Reductants, *Chemistry - A European Journal* 24 (2018) 7913–7920.
- [48] E. K. Richman, C. B. Kang, T. Brezesinski, S. H. Tolbert, Ordered mesoporous silicon through magnesium reduction of polymer templated silica thin films, *Nano Letters* 8 (2008) 3075–3079.
- [49] E. V. Astrova, V. B. Voronkov, A. V. Nashchekin, A. V. Parfeneva, D. A. Lozhkina, M. V. Tomkovich, Y. A. Kukushkina, Formation of Porous Silicon by Nanopowder Sintering, *Semiconductors* 53 (2019) 530–539.
- [50] K. Barraclough, A. Loni, E. Caffull, L. Canham, Cold compaction of silicon powders without a binding agent, *Materials Letters* 61 (2007) 485–487.
- [51] K. W. Kolasinski, N. J. Gimbar, H. Yu, M. Aindow, E. Mäkilä, J. Salonen, Regenerative Electroless Etching of Silicon, *Angewandte Chemie, International Edition* 56 (2017) 624–627.
- [52] K. W. Kolasinski, J. Salonen, E. Mäkilä, Regenerative Electroless Etching. US Patent, 10,590,562, (2018).
- [53] E. Mäkilä, A.-M. Anton Willmore, H. Yu, M. Irri, M. Aindow, T. Teesalu, L. T. Canham, K. W. Kolasinski, J. Salonen, Hierarchical Nanostructuring of Porous Silicon with Electrochemical and Regenerative Electroless Etching, *ACS Nano* 13 (2019) 13056–13064.
- [54] L. Canham, Routes of formation for porous silicon, in: L. T. Canham (Ed.), *Handbook of Porous Silicon*, 1st ed., Springer International Publishing, Cham, 2018, pp. 3–11.
- [55] L. T. Canham, Nanoscale semiconducting silicon as a nutritional food additive, *Nanotechnology* 18 (2007) 185704.
- [56] H. Föll, M. Christophersen, J. Carstensen, G. Hasse, Formation and application of porous silicon, *Materials Science and Engineering: R: Reports* 39 (2002) 93–141.
- [57] V. Lehmann, *Electrochemistry of Silicon: Instrumentation, Science, Materials and Applications*, Wiley-VCH Verlag GmbH, Weinheim, 2002.
- [58] O. Bisi, S. Ossicini, L. Pavesi, Porous silicon: a quantum sponge structure for silicon based optoelectronics, *Surface Science Reports* 38 (2000) 1–126.
- [59] K. Imai, H. Unno, FIPOS (Full Isolation by Porous Oxidized Silicon) technology and its application to LSI's, *IEEE Transactions on Electron Devices* 31 (1984) 297–302.

- [60] D. Graf, M. Grundner, R. Schulz, L. Muhlhoff, Oxidation of HF-treated Si wafer surfaces in air, *Journal of Applied Physics* 68 (1990) 5155–5161.
- [61] G. S. Higashi, Y. J. Chabal, G. W. Trucks, K. Raghavachari, Ideal hydrogen termination of the Si (111) surface, *Applied Physics Letters* 56 (1990) 656.
- [62] G. Trucks, K. Raghavachari, G. Higashi, Y. Chabal, Mechanism of HF etching of silicon surfaces: A theoretical understanding of hydrogen passivation, *Physical Review Letters* 65 (1990) 504–507.
- [63] H. Ubara, T. Imura, A. Hiraki, Formation of Si-H bonds on the surface of microcrystalline silicon covered with SiO_x by HF treatment, *Solid State Communications* 50 (1984) 673–675.
- [64] E. Yablonovitch, D. Allara, C. Chang, T. Gmitter, T. Bright, Unusually Low Surface-Recombination Velocity on Silicon and Germanium Surfaces, *Physical Review Letters* 57 (1986) 249–252.
- [65] R. L. Smith, S. D. Collins, Porous silicon formation mechanisms, *Journal of Applied Physics* 71 (1992) R1.
- [66] C. da Fonseca, F. Ozanam, J.-N. Chazalviel, In situ infrared characterisation of the interfacial oxide during the anodic dissolution of a silicon electrode in fluoride electrolytes, *Surface Science* 365 (1996) 1–14.
- [67] J. Carstensen, R. Prange, G. Popkurov, H. Föll, A model for current oscillations in the Si-HF system based on a quantitative analysis of current transients, *Applied Physics A: Materials Science & Processing* 67 (1998) 459–467.
- [68] J.-N. Chazalviel, C. da Fonseca, F. Ozanam, In Situ Infrared Study of the Oscillating Anodic Dissolution of Silicon in Fluoride Electrolytes, *Journal of the Electrochemical Society* 145 (1998) 964.
- [69] J. Grzanna, H. Jungblut, H. J. Lewerenz, Model for electrochemical oscillations at the Si—electrolyte contact: Part II. Simulations and experimental results, *Journal of Electroanalytical Chemistry* 486 (2000) 190–203.
- [70] X. G. Zhang, S. D. Collins, R. L. Smith, Porous Silicon Formation and Electropolishing of Silicon by Anodic Polarization in HF Solution, *Journal of the Electrochemical Society* 136 (1989) 1561–1565.
- [71] H. Gerischer, P. Allongue, V. Costa Kieling, The Mechanism of the Anodic Oxidation of Silicon in Acidic Fluoride Solutions Revisited, *Berichte der Bunsengesellschaft für Physikalische Chemie* 97 (1993) 753–757.
- [72] E. S. Kooij, D. Vanmaekelbergh, Catalysis and Pore Initiation in the Anodic Dissolution of Silicon in HF, *Journal of the Electrochemical Society* 144 (1997) 1296.
- [73] K. W. Kolasinski, The mechanism of Si etching in fluoride solutions, *Physical Chemistry Chemical Physics* 5 (2003) 1270–1278.
- [74] K. W. Kolasinski, Etching of silicon in fluoride solutions, *Surface Science* 603 (2009) 1904–1911.
- [75] T. Unagami, Formation Mechanism of Porous Silicon Layer by Anodization in HF Solution, *Journal of the Electrochemical Society* 127 (1980) 476.
- [76] V. Parkhutik, L. Glinenko, V. Labunov, Kinetics and mechanism of porous layer growth during n-type silicon anodization in HF solution, *Surface Technology* 20 (1983) 265–277.
- [77] M. Beale, J. Benjamin, M. Uren, N. Chew, A. Cullis, An experimental and theoretical study of the formation and microstructure of porous silicon, *Journal of Crystal Growth* 73 (1985) 622–636.
- [78] R. L. Smith, S. F. Chuang, S. D. Collins, A theoretical model of the formation morphologies of porous silicon, *Journal of Electronic Materials* 17 (1988) 533–541.
- [79] V. Lehmann, H. Föll, Formation Mechanism and Properties of Electrochemically Etched Trenches in n-Type Silicon, *Journal of the Electrochemical Society* 137 (1990) 653.
- [80] J. Erlebacher, K. Sieradzki, P. C. Searson, Computer simulations of pore growth in silicon, *Journal of Applied Physics* 76 (1994) 182.
- [81] S. Frohnhoff, M. Marso, M. G. Berger, M. Thönissen, H. Lüth, H. Münder, An Extended Quantum Model for Porous Silicon Formation, *Journal of the Electrochemical Society* 142 (1995) 615.
- [82] Z. He, Y. Huang, R. Kwor, A modified computer model for the formation of porous silicon, *Thin Solid Films* 265 (1995) 96–100.
- [83] Y. Kang, J. Jorné, Dissolution Mechanism for p-Si during Porous Silicon Formation, *Journal of the Electrochemical Society* 144 (1997) 3104.
- [84] A. Valance, Theoretical model for early stages of porous silicon formation from *n*- and *p*-type silicon substrates, *Physical Review B* 55 (1997) 9706–9715.
- [85] L. Aleksandrov, P. Novikov, Morphology of porous silicon structures formed by anodization of heavily and lightly doped silicon, *Thin Solid Films* 330 (1998) 102–107.
- [86] J. Carstensen, R. Prange, H. Föll, A Model for Current-Voltage Oscillations at the Silicon Electrode and Comparison with Experimental Results, *Journal of the Electrochemical Society* 146 (1999) 1134.
- [87] R. B. Wehrspohn, F. Ozanam, J.-N. Chazalviel, Nano- and Macropore Formation in p-Type Silicon, *Journal of the Electrochemical Society* 146 (1999) 3309.
- [88] X. G. Zhang, *Electrochemistry of Silicon and its Oxide*, Kluwer Academic Publishers, New York, NY, 2001.

- [89] M. I. J. Beale, N. G. Chew, M. J. Uren, A. G. Cullis, J. D. Benjamin, Microstructure and formation mechanism of porous silicon, *Applied Physics Letters* 46 (1985) 86.
- [90] G. C. John, V. A. Singh, Porous silicon: theoretical studies, *Physics Reports* 263 (1995) 93–151.
- [91] T. A. Witten, L. M. Sander, Diffusion-Limited Aggregation, a Kinetic Critical Phenomenon, *Phys. Rev. Lett.* 47 (1981) 1400.
- [92] R. Smith, S.-F. Chuang, S. Collins, Porous silicon morphologies and formation mechanism, *Sensors and Actuators A: Physical* 23 (1990) 825–829.
- [93] G. C. John, V. A. Singh, Two-scale model for aggregation and etching, *Physical Review E* 53 (1996) 3920–3924.
- [94] J. Erlebacher, P. Searson, K. Sieradzki, Computer simulations of dense-branching patterns, *Physical Review Letters* 71 (1993) 3311–3314.
- [95] J. Carstensen, M. Christophersen, H. Föll, Pore formation mechanisms for the Si-HF system, *Materials Science and Engineering B* 69 (2000) 23–28.
- [96] E. Foca, J. Carstensen, H. Föll, Modelling electrochemical current and potential oscillations at the Si electrode, *Journal of Electroanalytical Chemistry* 603 (2007) 175–202.
- [97] H. Föll, J. Carstensen, Pattern Formation during Anodic Etching of Semiconductors, *Journal of the Electrochemical Society* 158 (2011) D357.
- [98] K. S. W. Sing, D. H. Everett, R. A. W. Haul, L. Moscou, R. A. Pierotti, J. Rouquerol, T. Siemieniewska, Reporting physisorption data for gas/solid systems, *Pure and Applied Chemistry* 57 (1985) 603–619.
- [99] M. Thommes, K. Kaneko, A. V. Neimark, J. P. Olivier, F. Rodriguez-Reinoso, J. Rouquerol, K. S. Sing, Physisorption of gases, with special reference to the evaluation of surface area and pore size distribution (IUPAC Technical Report), *Pure and Applied Chemistry* 87 (2015) 1051–1069.
- [100] P. Kleimann, J. Linnros, S. Petersson, Formation of wide and deep pores in silicon by electrochemical etching, *Materials Science and Engineering B* 69 (2000) 29–33.
- [101] L. T. Canham, A. G. Cullis, C. Pickering, O. D. Dosser, T. I. Cox, T. P. Lynch, Luminescent anodized silicon aerocrystal networks prepared by supercritical drying, *Nature* 368 (1994) 133–135.
- [102] A. Loni, L. T. Canham, T. Defforge, G. Gautier, Supercritically-Dried Porous Silicon Powders with Surface Areas Exceeding 1000 m²/g, *ECS Journal of Solid State Science and Technology* 4 (2015) P289–P292.
- [103] X. G. Zhang, Morphology and Formation Mechanisms of Porous Silicon, *Journal of the Electrochemical Society* 151 (2004) C69.
- [104] V. Lehmann, R. Stengl, A. Luigart, On the morphology and the electrochemical formation mechanism of mesoporous silicon, *Materials Science and Engineering: B* 69-70 (2000) 11–22.
- [105] E. K. Propst, P. A. Kohl, The Electrochemical Oxidation of Silicon and Formation of Porous Silicon in Acetonitrile, *Journal of the Electrochemical Society* 141 (1994) 1006.
- [106] R. B. Wehrspohn, J.-N. Chazalviel, F. Ozanam, Macropore Formation in Highly Resistive p-Type Crystalline Silicon, *Journal of the Electrochemical Society* 145 (1998) 2958.
- [107] V. Lehmann, S. Rönnebeck, The Physics of Macropore Formation in Low-Doped p-Type Silicon, *Journal of the Electrochemical Society* 146 (1999) 2968.
- [108] M. Christophersen, J. Carstensen, H. Föll, Macropore Formation on Highly Doped n-Type Silicon, *Physica Status Solidi (A): Applications and Materials Science* 182 (2000) 45–50.
- [109] E. J. Anglin, M. P. Schwartz, V. P. Ng, L. A. Perelman, M. J. Sailor, Engineering the chemistry and nanostructure of porous silicon Fabry-Pérot films for loading and release of a steroid, *Langmuir* 20 (2004) 11264–11269.
- [110] A. M. Tinsley-Bown, L. T. Canham, M. Hollings, M. H. Anderson, C. L. Reeves, T. I. Cox, S. Nicklin, D. J. Squirrell, E. Perkins, A. Hutchinson, M. J. Sailor, A. Wun, Tuning the pore size and surface chemistry of porous silicon for immunoassays, *Physica Status Solidi (A): Applications and Materials Science* 182 (2000) 547–553.
- [111] E. Secret, C.-C. Wu, A. Chaix, A. Galarneau, P. Gonzalez, D. Cot, M. J. Sailor, J. Jestin, J.-M. Zanotti, F. Cunin, B. Coasne, Control of the Pore Texture in Nanoporous Silicon via Chemical Dissolution, *Langmuir* 31 (2015) 8121–8128.
- [112] A. Loni, T. Defforge, E. Caffull, G. Gautier, L. Canham, Porous silicon fabrication by anodisation: Progress towards the realisation of layers and powders with high surface area and micropore content, *Microporous and Mesoporous Materials* 213 (2015) 10–13.
- [113] T. Unagami, M. Seki, Structure of Porous Silicon Layer and Heat-Treatment Effect, *Journal of the Electrochemical Society* 125 (1978) 1339.
- [114] R. Herino, A. Perio, K. Barla, G. Bomchil, Microstructure of porous silicon and its evolution with temperature, *Materials Letters* 2 (1984) 519–523.
- [115] Y. H. Ogata, N. Yoshimi, R. Yasuda, T. Tsuboi, T. Sakka, A. Otsuki, Structural change in p-type porous silicon by thermal annealing, *Journal of Applied Physics* 90 (2001) 6487–6492.
- [116] V. Labunov, V. Bondarenko, I. Glinenko, A. Dorofeev, L. Tabulina, Heat treatment effect on porous silicon, *Thin Solid Films* 137 (1986) 123–134.
- [117] N. Ott, M. Nerdling, G. Müller, R. Brendel, H. P. Strunk, Evolution of the microstructure during annealing of porous silicon multilayers, *Journal of Applied Physics* 95 (2004) 497–503.

- [118] G. Müller, M. Nerdling, N. Ott, H. P. Strunk, R. Brendel, Sintering of porous silicon, *Physica Status Solidi (A): Applications and Materials Science* 197 (2003) 83–87.
- [119] V. Depauw, O. Richard, H. Bender, I. Gordon, G. Beaucarne, J. Poortmans, R. Mertens, J. P. Celis, Study of pore reorganisation during annealing of macroporous silicon structures for solar cell application, *Thin Solid Films* 516 (2008) 6934–6938.
- [120] N. Milenkovic, M. Drießen, C. Weiss, S. Janz, Porous silicon reorganization: Influence on the structure, surface roughness and strain, *Journal of Crystal Growth* 432 (2015) 139–145.
- [121] N. Sato, K. Sakaguchi, K. Yamagata, Y. Fujiyama, T. Yonehara, Epitaxial Growth on Porous Si for a New Bond and Etchback Silicon-on-Insulator, *Journal of the Electrochemical Society* 142 (1995) 3116.
- [122] G. Müller, R. Brendel, Simulated annealing of porous silicon, *Physica Status Solidi (A): Applications and Materials Science* 182 (2000) 313–318.
- [123] S. Armbruster, F. Schafer, G. Lammel, H. Artmann, C. Schelling, H. Benzel, S. Finkbeiner, F. Larmer, R. Ruther, O. Paul, A novel micromachining process for the fabrication of monocrystalline Si-membranes using porous silicon, in: *Transducers '03. 12th International Conference on Solid-State Sensors, Actuators and Microsystems. Digest of Technical Papers, volume 1, IEEE, 2003, pp. 246–249.*
- [124] M. K. Sahoo, P. Kale, Restructured porous silicon for solar photovoltaic: A review, *Microporous and Mesoporous Materials* 289 (2019) 109619.
- [125] E. Petrova, K. Bogoslovskaya, L. Balagurov, G. Kochoradze, Room temperature oxidation of porous silicon in air, *Materials Science and Engineering B* 69 (2000) 152–156.
- [126] L. Canham, M. Houlton, W. Leong, C. Pickering, J. Keen, Atmospheric impregnation of porous silicon at room temperature, *Journal of Applied Physics* 70 (1991) 422–431.
- [127] M. M. Atalla, E. Tannenbaum, E. J. Scheibner, Stabilization of Silicon Surfaces by Thermally Grown Oxides, *Bell System Technical Journal* 38 (1959) 749–783.
- [128] Y. Chung, W. Siekhaus, G. Somorjai, Studies of acetylene and oxygen adsorption on silicon surfaces by low energy electron loss spectroscopy, *Surface Science* 58 (1976) 341–348.
- [129] B. E. Deal, A. S. Grove, General relationship for the thermal oxidation of silicon, *Journal of Applied Physics* 36 (1965) 3770–3778.
- [130] J. Kraitchman, J. Oroshnik, Anodic Oxide Growth Behavior on Silicon, *Journal of the Electrochemical Society* 114 (1967) 405.
- [131] M. R. Linford, C. E. D. Chidsey, Alkyl monolayers covalently bonded to silicon surfaces, *Journal of the American Chemical Society* 115 (1993) 12631–12632.
- [132] V. Petrova-Koch, T. Muschik, A. Kux, B. K. Meyer, F. Koch, V. Lehmann, Rapid-thermal-oxidized porous Si - The superior photoluminescent Si, *Applied Physics Letters* 61 (1992) 943–945.
- [133] J. M. Buriak, M. P. Stewart, T. W. Geders, M. J. Allen, H. C. Choi, J. Smith, D. Raftery, L. T. Canham, Lewis Acid Mediated Hydrosilylation on Porous Silicon Surfaces, *Journal of the American Chemical Society* 121 (1999) 11491–11502.
- [134] H. Ouyang, M. Christophersen, R. Viard, B. L. Miller, P. M. Fauchet, Macroporous Silicon Microcavities for Macromolecule Detection, *Advanced Functional Materials* 15 (2005) 1851–1859.
- [135] J. Riikonen, M. Salomäki, J. van Wonderen, M. Kemell, W. Xu, O. Korhonen, M. Ritala, F. MacMillan, J. Salonen, V.-P. Lehto, Surface chemistry, reactivity, and pore structure of porous silicon oxidized by various methods., *Langmuir* 28 (2012) 10573–83.
- [136] T. Jalkanen, E. Mäkilä, Y.-I. Suzuki, T. Urata, K. Fukami, T. Sakka, J. Salonen, Y. H. Ogata, Studies on Chemical Modification of Porous Silicon-Based Graded-Index Optical Microcavities for Improved Stability Under Alkaline Conditions, *Advanced Functional Materials* 22 (2012) 3890–3898.
- [137] O. Keinänen, E. M. Mäkilä, R. Lindgren, H. Virtanen, H. Liljenbäck, V. Oikonen, M. Sarparanta, C. Molthoff, A. D. Windhorst, A. Roivainen, J. J. Salonen, A. J. Airaksinen, Pretargeted PET Imaging of *trans*-Cyclooctene-Modified Porous Silicon Nanoparticles, *ACS Omega* 2 (2017) 62–69.
- [138] J. J. Kelly, H. G. Philipsen, Anisotropy in the wet-etching of semiconductors, *Current Opinion in Solid State and Materials Science* 9 (2005) 84–90.
- [139] J. M. Buriak, Organometallic chemistry on silicon and germanium surfaces., *Chemical Reviews* 102 (2002) 1271–308.
- [140] J. M. Buriak, Illuminating Silicon Surface Hydrosilylation: An Unexpected Plurality of Mechanisms, *Chemistry of Materials* 26 (2014) 763–772.
- [141] S. Ciampi, J. B. Harper, J. J. Gooding, Wet chemical routes to the assembly of organic monolayers on silicon surfaces via the formation of Si-C bonds: surface preparation, passivation and functionalization., *Chemical Society Reviews* 39 (2010) 2158–83.
- [142] J. J. Gooding, Y. Zhu, Modifying porous silicon with self-assembled monolayers for biomedical applications, in: H. A. Santos (Ed.), *Porous Silicon for Biomedical Applications*, Woodhead Publishing, 2014, pp. 81–103.
- [143] K. W. Kolasinski, Photochemical and non-thermal chemical modification of porous silicon

- for biomedical applications, in: H. A. Santos (Ed.), *Porous Silicon for Biomedical Applications*, Woodhead Publishing, 2014, pp. 52–80.
- [144] J. Salonen, E. Mäkilä, Thermal stabilization of porous silicon for biomedical applications, in: H. A. Santos (Ed.), *Porous Silicon for Biomedical Applications*, Elsevier, 2014, pp. 21–34.
- [145] J. Salonen, E. Mäkilä, Thermally Carbonized Porous Silicon and Its Recent Applications, *Advanced Materials* 30 (2018) 1703819.
- [146] J. Salonen, V. Lehto, E. Laine, The room temperature oxidation of porous silicon, *Applied Surface Science* 120 (1997) 191–198.
- [147] J. Salonen, V. Lehto, M. Björkqvist, E. Laine, A role of illumination during etching to porous silicon oxidation, *Applied Physics Letters* 75 (1999) 826.
- [148] T. F. Harper, M. J. Sailor, Using Porous Silicon as a Hydrogenation Agent: Derivatization of the Surface of Luminescent Nanocrystalline Silicon with Benzoquinone, *Journal of the American Chemical Society* 119 (1997) 6943–6944.
- [149] T. Laaksonen, H. Santos, H. Vihola, J. Salonen, J. Riikonen, T. Heikkilä, L. Peltonen, N. Kumar, D. Y. Murzin, V. P. Lehto, J. Hirvonen, Failure of MTT as a toxicity testing agent for mesoporous silicon microparticles, *Chemical Research in Toxicology* 20 (2007) 1913–1918.
- [150] E. C. Wu, J. S. Andrew, A. Buyanin, J. M. Kinsella, M. J. Sailor, Suitability of porous silicon microparticles for the long-term delivery of redox-active therapeutics., *Chemical Communications* 47 (2011) 5699–701.
- [151] N. L. Fry, G. R. Boss, M. J. Sailor, Oxidation-Induced Trapping of Drugs in Porous Silicon Microparticles, *Chemistry of Materials* 26 (2014) 2758–2764.
- [152] T. Unagami, Oxidation of porous silicon and properties of its oxide film, *Japanese Journal of Applied Physics* 19 (1980) 231–241.
- [153] A. E. Pap, K. Kordás, T. F. George, S. Leppävuori, Thermal Oxidation of Porous Silicon: Study on Reaction Kinetics, *Journal of Physical Chemistry B* 108 (2004) 12744–12747.
- [154] J. Salonen, V. Lehto, E. Laine, Thermal oxidation of free-standing porous silicon films, *Applied Physics Letters* 70 (1997) 637.
- [155] J. Yon, K. Barla, R. Herino, G. Bomchil, The kinetics and mechanism of oxide layer formation from porous silicon formed on p-Si substrates, *Journal of Applied Physics* 62 (1987) 1042–1048.
- [156] G. Bomchil, A. Halimaoui, R. Herino, Porous silicon: The material and its applications in silicon-on-insulator technologies, *Applied Surface Science* 41 (1989) 604–613.
- [157] T. Nakamura, T. Ogawa, N. Hosoya, S. Adachi, Effects of thermal oxidation on the photoluminescence properties of porous silicon, *Journal of Luminescence* 130 (2010) 682–687.
- [158] Y. Kato, T. Ito, A. Hiraki, Low temperature oxidation of crystalline porous silicon, *Applied Surface Science* 41-42 (1989) 614–618.
- [159] D. B. Mawhinney, J. A. Glass, J. T. Yates, FTIR Study of the Oxidation of Porous Silicon, *Journal of Physical Chemistry B* 101 (1997) 1202–1206.
- [160] J. Yan, S. Shih, K. H. Jung, D. L. Kwong, M. Kovar, J. M. White, B. E. Gnade, L. Magel, Study of thermal oxidation and nitrogen annealing of luminescent porous silicon, *Applied Physics Letters* 64 (1994) 1374–1376.
- [161] Z. Y. Wu, S. Hall, J. M. Keen, Electrical Properties of Thermally Oxidized Porous Silicon, *Journal of the Electrochemical Society* 143 (1996) 2972.
- [162] Y. H. Ogata, T. Tsuboi, T. Sakka, S. Naito, Oxidation of porous silicon in dry and wet environments under mild temperature conditions, *Journal of Porous Materials* 7 (2000) 63–66.
- [163] A. Bsiesy, F. Gaspard, R. Herino, M. Ligeon, F. Muller, Anodic Oxidation of Porous Silicon Layers Formed on Lightly p-Doped Substrates, *Journal of the Electrochemical Society* 138 (1991) 3450.
- [164] A. Bsiesy, J. Vial, F. Gaspard, R. Herino, M. Ligeon, F. Muller, R. Romestain, A. Wasiela, A. Halimaoui, G. Bomchil, Photoluminescence of high porosity and of electrochemically oxidized porous silicon layers, *Surface Science* 254 (1991) 195–200.
- [165] A. Janshoff, K.-P. S. Dancil, C. Steinem, D. P. Greiner, V. S.-Y. Lin, C. Gurtner, K. Moteshareei, M. J. Sailor, M. R. Ghadiri, Macroporous p-Type Silicon Fabry-Perot Layers. Fabrication, Characterization, and Applications in Biosensing, *Journal of the American Chemical Society* 120 (1998) 12108–12116.
- [166] J. M. Lauerhaas, M. J. Sailor, Chemical modification of the photoluminescence quenching of porous silicon, *Science* 261 (1993) 1567–1568.
- [167] J. H. Song, M. J. Sailor, Chemical Modification of Crystalline Porous Silicon Surfaces, *Comments on Inorganic Chemistry* 21 (1999) 69–84.
- [168] J. E. Bateman, R. D. Eagling, B. R. Horrocks, A. Houlton, D. R. Worrall, Role for organic molecules in the oxidation of porous silicon, *Chemical Communications* (1997) 2275–2276.
- [169] R. Anderson, R. Muller, C. Tobias, Chemical Surface Modification of Porous Silicon, *Journal of the Electrochemical Society* 140 (1993) 1393.
- [170] S. Chan, Y. Li, L. J. Rothberg, B. L. Miller, P. M. Fauchet, Nanoscale silicon microcavities for biosensing, *Materials Science and Engineering: C* 15 (2001) 277–282.
- [171] K.-P. S. Dancil, D. P. Greiner, M. J. Sailor, A Porous Silicon Optical Biosensor: Detection of Reversible Binding of IgG to a Protein A-Modified Surface, *Journal of the American Chemical Society* 121 (1999) 7925–7930.

- [172] J. A. Howarter, J. P. Youngblood, Optimization of silica silanization by 3-aminopropyltriethoxysilane., *Langmuir* 22 (2006) 11142–7.
- [173] K. A. Kilian, T. Böcking, J. J. Gooding, The importance of surface chemistry in mesoporous materials: lessons from porous silicon biosensors., *Chemical Communications* (2009) 630–40.
- [174] H. Ritter, D. Brühwiler, Accessibility of Amino Groups in Postsynthetically Modified Mesoporous Silica, *Journal of Physical Chemistry C* 113 (2009) 10667–10674.
- [175] D. Kim, J. M. Zuidema, J. Kang, Y. Pan, L. Wu, D. Warther, B. Arkles, M. J. Sailor, Facile Surface Modification of Hydroxylated Silicon Nanostructures Using Heterocyclic Silanes, *Journal of the American Chemical Society* 138 (2016) 15106–15109.
- [176] M. J. Sweetman, S. J. P. McInnes, R. B. Vasani, T. Guinan, A. Blencowe, N. H. Voelcker, Rapid, metal-free hydrosilanisation chemistry for porous silicon surface modification., *Chemical Communications* 51 (2015) 10640–3.
- [177] N. Y. Kim, P. E. Laibinis, Thermal derivatization of porous silicon with alcohols, *Journal of the American Chemical Society* 119 (1997) 2297–2298.
- [178] E. J. Lee, T. W. Bitner, J. S. Ha, M. J. Shane, M. J. Sailor, Light-Induced Reactions of Porous and Single-Crystal Si Surfaces with Carboxylic Acids, *Journal of the American Chemical Society* 118 (1996) 5375–5382.
- [179] M. R. Linford, P. Fenter, P. M. Eisenberger, C. E. D. Chidsey, Alkyl Monolayers on Silicon Prepared from 1-Alkenes and Hydrogen-Terminated Silicon, *Journal of the American Chemical Society* 117 (1995) 3145–3155.
- [180] J. M. Buriak, M. J. Allen, Lewis Acid Mediated Functionalization of Porous Silicon with Substituted Alkenes and Alkynes, *Journal of the American Chemical Society* 120 (1998) 1339–1340.
- [181] L. T. Canham, C. L. Reeves, J. P. Newey, M. R. Houlton, T. I. Cox, J. M. Buriak, M. P. Stewart, Derivatized mesoporous silicon with dramatically improved stability in simulated human blood plasma, *Advanced Materials* 11 (1999) 1505–1507.
- [182] M. P. Stewart, J. M. Buriak, Photopatterned Hydrosilylation on Porous Silicon, *Angewandte Chemie, International Edition* 37 (1998) 3257–3260.
- [183] J. E. Bateman, R. D. Eagling, D. R. Worrall, B. R. Horrocks, A. Houlton, Alkylation of Porous Silicon by Direct Reaction with Alkenes and Alkynes, *Angewandte Chemie, International Edition* 37 (1998) 2683–2685.
- [184] J. M. Schmeltzer, L. A. Porter, M. P. Stewart, J. M. Buriak, Hydride, abstraction initiated hydrosilylation of terminal alkenes and alkynes on porous silicon, *Langmuir* 18 (2002) 2971–2974.
- [185] J. M. Holland, M. P. Stewart, M. J. Allen, J. M. Buriak, Metal Mediated Reactions on Porous Silicon Surfaces, *Journal of Solid State Chemistry* 147 (1999) 251–258.
- [186] M. S. Yoon, K. H. Ahn, R. W. Cheung, H. Sohn, J. R. Link, F. Cunin, M. J. Sailor, Covalent crosslinking of 1-D photonic crystals of microporous Si by hydrosilylation and ring-opening metathesis polymerization, *Chemical Communications* (2003) 680–681.
- [187] N. Y. Kim, P. E. Laibinis, Derivatization of porous silicon by grignard reagents at room temperature, *Journal of the American Chemical Society* 120 (1998) 4516–4517.
- [188] J. H. Song, M. J. Sailor, Functionalization of Nanocrystalline Porous Silicon Surfaces with Aryllithium Reagents: Formation of Silicon-Carbon Bonds by Cleavage of Silicon-Silicon Bonds, *Journal of the American Chemical Society* 120 (1998) 2376–2381.
- [189] R. L. Cicero, C. E. D. Chidsey, G. P. Lopinski, D. D. M. Wayner, R. A. Wolkow, Olefin Additions on H-Si(111): Evidence for a Surface Chain Reaction Initiated at Isolated Dangling Bonds, *Langmuir* 18 (2002) 305–307.
- [190] L. C. P. M. de Smet, H. Zuilhof, E. J. R. Sudhölter, L. H. Lie, A. Houlton, B. R. Horrocks, Mechanism of the hydrosilylation reaction of alkenes at porous silicon: experimental and computational deuterium labeling studies., *Journal of Physical Chemistry B* 109 (2005) 12020–31.
- [191] C. Coletti, A. Marrone, G. Giorgi, A. Scamellotti, G. Cerofolini, N. Re, Nonradical mechanisms for the uncatalyzed thermal functionalization of silicon surfaces by alkenes and alkynes: a density functional study., *Langmuir* 22 (2006) 9949–56.
- [192] R. Boukherroub, J. Wojtyk, D. Wayner, D. Lockwood, Thermal Hydrosilylation of Undecylenic Acid with Porous Silicon, *Journal of the Electrochemical Society* 149 (2002) H69–H63.
- [193] J. R. Link, M. J. Sailor, Smart dust: self-assembling, self-orienting photonic crystals of porous Si., *Proceedings of the National Academy of Sciences* 100 (2003) 10607–10.
- [194] K. A. Kilian, T. Böcking, K. Gaus, J. J. Gooding, Introducing distinctly different chemical functionalities onto the internal and external surfaces of mesoporous materials., *Angewandte Chemie, International Edition* 47 (2008) 2697–9.
- [195] B. Guan, S. Ciampi, G. Le Saux, K. Gaus, P. J. Reece, J. J. Gooding, Different functionalization of the internal and external surfaces in mesoporous materials for biosensing applications using “click” chemistry., *Langmuir* 27 (2011) 328–34.
- [196] B. Guan, S. Ciampi, E. Luais, M. James, P. J. Reece, J. J. Gooding, Depth-resolved chemical modification of porous silicon by wavelength-tuned irradiation., *Langmuir* 28 (2012) 15444–9.

- [197] C. C. Wu, M. J. Sailor, Selective functionalization of the internal and the external surfaces of mesoporous silicon by liquid masking, *ACS Nano* 7 (2013) 3158–3167.
- [198] D. X. Zhang, C. Yoshikawa, N. G. Welch, P. Pasic, H. Thissen, N. H. Voelcker, Spatially Controlled Surface Modification of Porous Silicon for Sustained Drug Delivery Applications, *Scientific Reports* 9 (2019) 1–11.
- [199] B. Gelloz, H. Sano, R. Boukherroub, D. D. M. Wayner, D. J. Lockwood, N. Koshida, Stable electroluminescence from passivated nanocrystalline porous silicon using undecylenic acid, *Physica Status Solidi (C)* 2 (2005) 3273–3277.
- [200] R. D. Rohde, H. D. Agnew, W. Yeo, R. C. Bailey, J. R. Heath, A non-oxidative approach toward chemically and electrochemically functionalizing Si(111), *Journal of the American Chemical Society* 128 (2006) 9518–25.
- [201] L. Scheres, B. Rijkssen, M. Giesbers, H. Zuilhof, Molecular modeling of alkyl and alkenyl monolayers on hydrogen-terminated Si(111), *Langmuir* 27 (2011) 972–80.
- [202] A. Bansal, X. Li, S. I. Yi, W. H. Weinberg, N. S. Lewis, Spectroscopic Studies of the Modification of Crystalline Si(111) Surfaces with Covalently-Attached Alkyl Chains Using a Chlorination/Alkylation Method, *Journal of Physical Chemistry B* 105 (2001) 10266–10277.
- [203] I. Lees, H. Lin, C. Canaria, C. Gurtner, M. Sailor, G. Miskelly, Chemical stability of porous silicon surfaces electrochemically modified with functional alkyl species, *Langmuir* 19 (2003) 9812–9817.
- [204] L. A. Huck, J. M. Buriak, Toward a mechanistic understanding of exciton-mediated hydrosilylation on nanocrystalline silicon., *Journal of the American Chemical Society* 134 (2012) 489–97.
- [205] I. H. Khan, R. N. Summergrad, The growth of single-crystal films of cubic silicon carbide on silicon, *Applied Physics Letters* 11 (1967) 12–13.
- [206] J. Yoshinobu, H. Tsuda, M. Onchi, M. Nishijima, Rehybridization of acetylene on the Si(111)(7×7) surface - a vibrational study, *Chemical Physics Letters* 130 (1986) 170–174.
- [207] L. Clemen, R. Wallace, P. Taylor, Adsorption and thermal behavior of ethylene on Si(100)-(2×1), *Surface Science* 268 (1992) 205–216.
- [208] C. Cheng, P. Taylor, R. Wallace, H. Gutleben, L. Clemen, M. Colaianni, P. Chen, W. Weinberg, W. Choyke, J. Yates Jr, Hydrocarbon surface chemistry on Si(100), *Thin Solid Films* 225 (1993) 196–202.
- [209] W. Widdra, C. Huang, S. Yi, W. Weinberg, Coadsorption of hydrogen with ethylene and acetylene on Si(100)-(2×1), *Journal of Chemical Physics* 105 (1996) 5605–5617.
- [210] G. Dufour, F. Rochet, F. Stedile, C. Poncey, M. De Crescenzi, R. Gunnella, M. Froment, SiC formation by reaction of Si (001) with acetylene: Electronic structure and growth mode, *Physical Review B* 56 (1997) 4266–4282.
- [211] M. De Crescenzi, M. Marucci, R. Gunnella, P. Castrucci, M. Casalboni, G. Dufour, F. Rochet, Si_{1-x}C_x formation by reaction of Si(111) with acetylene: growth mode, electronic structure and luminescence investigation, *Surface Science* 426 (1999) 277–289.
- [212] M. De Crescenzi, R. Bernadini, M. Cardella, R. Gunnella, P. Castrucci, R. Pizzoferrato, M. Casalboni, Structural and electronic investigation of Si(001) surface after acetylene interaction, *Surface Science* 521 (2002) 57–68.
- [213] T. Kimoto, J. A. Cooper, Epitaxial Growth of Silicon Carbide, in: T. Kimoto, J. A. Cooper (Eds.), *Fundamentals of Silicon Carbide Technology*, Wiley Interscience, 2014, pp. 75–124.
- [214] M. Zimbone, M. Mauceri, G. Litrico, E. G. Barbagiovanni, C. Bongiorno, F. La Via, Protrusions reduction in 3C-SiC thin film on Si, *Journal of Crystal Growth* 498 (2018) 248–257.
- [215] J. L. Deines, S.-M. Ku, M. R. Poponiak, P. J. Tsang, Process for forming monocrystalline silicon carbide on silicon substrates. US Patent, 4,028,149, (1976).
- [216] Y. J. Seo, H. J. Cheon, D. J. Choi, Enhancement of the thermal stability of photoluminescence by the carbonization of porous silicon, *Journal of Materials Science Letters* 17 (1998) 313–315.
- [217] J. Salonen, V. Lehto, M. Björkqvist, E. Laine, L. Niinistö, Studies of thermally-carbonized porous silicon surfaces, *Physica Status Solidi (A): Applications and Materials Science* 182 (2000) 123–126.
- [218] J. Salonen, E. Laine, L. Niinistö, Thermal carbonization of porous silicon surface by acetylene, *Journal of Applied Physics* 91 (2002) 456.
- [219] J. Salonen, M. Björkqvist, E. Laine, L. Niinistö, Stabilization of porous silicon surface by thermal decomposition of acetylene, *Applied Surface Science* 225 (2004) 389–394.
- [220] M. Björkqvist, J. Paski, J. Salonen, V. Lehto, Studies on hysteresis reduction in thermally carbonized porous silicon humidity sensor, *Sensors Journal, IEEE* 6 (2006) 542–547.
- [221] M. Sarparanta, E. Mäkilä, T. Heikkilä, J. Salonen, E. Kukk, V.-P. Lehto, H. A. Santos, J. Hirvonen, A. J. Airaksinen, ¹⁸F-labeled modified porous silicon particles for investigation of drug delivery carrier distribution in vivo with positron emission tomography., *Molecular Pharmaceutics* 8 (2011) 1799–1806.
- [222] J. Tuura, M. Björkqvist, J. Salonen, V. Lehto, Long-Term Stability of Thermally-Carbonized Porous Silicon Humidity Sensor, *Materials Research Society Symposium Proceedings* 876E (2005) R8.8.1–6.
- [223] M. Björkqvist, J. Salonen, E. Laine, L. Niinistö, Comparison of stabilizing treatments on porous

- silicon for sensor applications, *Physica Status Solidi (A): Applications and Materials Science* 197 (2003) 374–377.
- [224] B. Sciacca, S. D. Alvarez, F. Geobaldo, M. J. Sailor, Bioconjugate functionalization of thermally carbonized porous silicon using a radical coupling reaction., *Dalton Transactions* 39 (2010) 10847–53.
- [225] S. Ida, T. Tsubota, S. Tanii, M. Nagata, Y. Matsumoto, Chemical modification of the diamond surface using benzoyl peroxide and dicarboxylic acids, *Langmuir* 19 (2003) 9693–9698.
- [226] M. Kovalainen, J. Mönkäre, E. Mäkilä, J. Salonen, V.-P. Lehto, K.-H. Herzig, K. Järvinen, Mesoporous silicon (PSi) for sustained peptide delivery: effect of PSi microparticle surface chemistry on peptide YY3-36 release., *Pharmaceutical Research* 29 (2012) 837–46.
- [227] M. Alba, M. Robin, D. Menzies, T. R. Gengenbach, B. Prieto-Simon, N. H. Voelcker, Differential functionalisation of the internal and external surfaces of carbon-stabilised nanoporous silicon, *Chemical Communications* 55 (2019) 8001–8004.
- [228] J. Salonen, M. Kaasalainen, O.-P. Rauhala, L. Lassila, M. Hakamies, T. Jalkanen, R. Hahn, P. Schmuki, E. Mäkilä, Thermal Carbonization of Porous Silicon: The Current Status and Recent Applications, *ECS Transactions* 69 (2015) 167–176.
- [229] L. Muehlhoff, M. J. Bozack, W. J. Choyke, J. T. Yates, Comparative oxidation studies of SiC(000 $\bar{1}$) and SiC(0001) surfaces, *Journal of Applied Physics* 60 (1986) 2558–2563.
- [230] S. Dhar, O. Seitz, M. D. Halls, S. Choi, Y. J. Chabal, L. C. Feldman, Chemical properties of oxidized silicon carbide surfaces upon etching in hydrofluoric acid., *Journal of the American Chemical Society* 131 (2009) 16808–13.
- [231] D. Z. Fang, C. C. Striemer, T. R. Gaborski, J. L. McGrath, P. M. Fauchet, Pore Size Control of Ultrathin Silicon Membranes by Rapid Thermal Carbonization, *Nano Letters* 10 (2010) 3904–3908.
- [232] L. Oakes, A. Westover, J. W. Mares, S. Chatterjee, W. R. Erwin, R. Bardhan, S. M. Weiss, C. L. Pint, Surface engineered porous silicon for stable, high performance electrochemical supercapacitors, *Scientific Reports* 3 (2013) 3020.
- [233] S. Chatterjee, R. Carter, L. Oakes, W. R. Erwin, R. Bardhan, C. L. Pint, Electrochemical and Corrosion Stability of Nanostructured Silicon by Graphene Coatings: Toward High Power Porous Silicon Supercapacitors, *Journal of Physical Chemistry C* 118 (2014) 10893–10902.
- [234] C. K. Tsang, T. L. Kelly, M. J. Sailor, Y. Y. Li, Highly stable porous silicon-carbon composites as label-free optical biosensors, *ACS Nano* 6 (2012) 10546–10554.
- [235] J. Wang, J. Joo, R. M. Kennard, S.-W. Lee, M. J. Sailor, Thermolytic Grafting of Polystyrene to Porous Silicon, *Chemistry of Materials* 28 (2016) 79–89.
- [236] T. Yonehara, K. Sakaguchi, ELTRAN; Novel SOI Wafer Technology., *JSAP International* 70 (2001) 10–16.
- [237] J. Wei, J. Buriak, G. Siuzdak, Desorption–ionization mass spectrometry on porous silicon, *Nature* 399 (1999) 243–246.
- [238] Z. Shen, J. J. Thomas, C. Averbuj, K. M. Broo, M. Engelhard, J. E. Crowell, M. G. Finn, G. Siuzdak, Porous silicon as a versatile platform for laser desorption/ionization mass spectrometry, *Analytical Chemistry* 73 (2001) 612–619.
- [239] N. Shenar, S. Cantel, J. Martinez, C. Enjalbal, Comparison of inert supports in laser desorption/ionization mass spectrometry of peptides: Pencil lead, porous silica gel, DIOS-chip and NALDI™ target, *Rapid Communications in Mass Spectrometry* 23 (2009) 2371–2379.
- [240] J. Tan, W.-J. Zhao, J.-K. Yu, S. Ma, M. J. Sailor, J.-M. Wu, Capture, Enrichment, and Mass Spectrometric Detection of Low-Molecular-Weight Biomarkers with Nanoporous Silicon Microparticles, *Advanced Healthcare Materials* 1 (2012) 742–750.
- [241] J. Sun, D. Cui, F. Guan, X. Chen, L. Zhang, High resolution microfabricated gas chromatography column with porous silicon acting as support, *Sensors and Actuators B: Chemical* 201 (2014) 19–24.
- [242] T. Guinan, C. Della Vedova, H. Kobus, N. H. Voelcker, Mass spectrometry imaging of fingerprint sweat on nanostructured silicon., *Chemical Communications* 51 (2014) 6088–6091.
- [243] T. Guinan, M. Ronci, R. Vasani, H. Kobus, N. Voelcker, Comparison of the performance of different silicon-based SALDI substrates for illicit drug detection, *Talanta* 132 (2015) 494–502.
- [244] R. M. Tiggelaar, V. Verdoold, H. Eghbali, G. Desmet, J. G. E. Gardeniers, Characterization of porous silicon integrated in liquid chromatography chips., *Lab on a Chip* 9 (2009) 456–63.
- [245] Z. Wang, H.-J. Wu, D. Fine, J. Schmulen, Y. Hu, B. Godin, J. X. J. Zhang, X. Liu, Ciliated micropillars for the microfluidic-based isolation of nanoscale lipid vesicles., *Lab on a Chip* (2013).
- [246] Y. He, T. Leïchlé, Fabrication of lateral porous silicon membranes for planar microfluidics by means of ion implantation, *Sensors and Actuators B: Chemical* 239 (2017) 628–634.
- [247] P. J. Burkhardt, M. R. Poponiak, Porous silicon dioxide moisture sensor and method for manufacture of a moisture sensor. US Patent, 4,057,823, (1976).
- [248] R. C. Anderson, R. S. Muller, C. W. Tobias, Investigations of porous silicon for vapor sensing, *Sensors and Actuators A: Physical* 23 (1990) 835–839.

- [249] I. Schechter, M. Ben-Chorin, A. Kux, Gas Sensing Properties of Porous Silicon, *Analytical Chemistry* 67 (1995) 3727–3732.
- [250] M. Björkqvist, J. Salonen, E. Laine, Humidity behavior of thermally carbonized porous silicon, *Applied Surface Science* 222 (2004) 269–274.
- [251] M. Björkqvist, J. Salonen, J. Tuura, T. Jalkanen, V.-P. Lehto, Detecting amine vapours with thermally carbonized porous silicon gas sensor, *Physica Status Solidi (C)* 6 (2009) 1769–1772.
- [252] T. Jalkanen, E. Mäkilä, A. Määttänen, J. Tuura, M. Kaasalainen, V.-P. Lehto, P. Ihalainen, J. Peltonen, J. Salonen, Porous silicon micro- and nanoparticles for printed humidity sensors, *Applied Physics Letters* 101 (2012) 263110.
- [253] C. Pacholski, M. Sartor, M. J. Sailor, F. Cunin, G. M. Miskelly, Biosensing using porous silicon double-layer interferometers: reflective interferometric Fourier transform spectroscopy., *Journal of the American Chemical Society* 127 (2005) 11636–45.
- [254] J. Saarinen, S. Weiss, P. Fauchet, J. E. Sipe, Optical sensor based on resonant porous silicon structures., *Optics Express* 13 (2005) 3754–64.
- [255] G. Barillaro, P. Bruschi, F. Pieri, L. M. Strambini, CMOS-compatible fabrication of porous silicon gas sensors and their readout electronics on the same chip, *Physica Status Solidi (A): Applications and Materials Science* 204 (2007) 1423–1428.
- [256] B. H. King, A. M. Ruminski, J. L. Snyder, M. J. Sailor, Optical-fiber-mounted porous silicon photonic crystals for sensing organic vapor breakthrough in activated carbon, *Advanced Materials* 19 (2007) 4530–4534.
- [257] A. M. Ruminski, M. M. Moore, M. J. Sailor, Humidity-Compensating Sensor for Volatile Organic Compounds Using Stacked Porous Silicon Photonic Crystals, *Advanced Functional Materials* 18 (2008) 3418–3426.
- [258] E. J. Anglin, L. Cheng, W. R. Freeman, M. J. Sailor, Porous silicon in drug delivery devices and materials., *Advanced Drug Delivery Reviews* 60 (2008) 1266–77.
- [259] J. Salonen, A. M. Kaukonen, J. Hirvonen, V.-P. Lehto, Mesoporous silicon in drug delivery applications., *Journal of Pharmaceutical Sciences* 97 (2008) 632–53.
- [260] L. M. Bonanno, E. Segal, Nanostructured porous silicon-polymer-based hybrids: from biosensing to drug delivery., *Nanomedicine* 6 (2011) 1755–70.
- [261] H. A. Santos, L. M. Bimbo, V.-P. Lehto, A. J. Airaksinen, J. Salonen, J. Hirvonen, Multifunctional Porous Silicon for Therapeutic Drug Delivery and Imaging, *Current Drug Discovery Technologies* 8 (2011) 228–249.
- [262] D. S. Karaman, M. P. Sarparanta, J. M. Rosenholm, A. J. Airaksinen, Multimodality Imaging of Silica and Silicon Materials In Vivo, *Advanced Materials* 30 (2018) 1703651.
- [263] T. Tieu, M. Alba, R. Elnathan, A. Cifuentes-Rius, N. H. Voelcker, Advances in Porous Silicon-Based Nanomaterials for Diagnostic and Therapeutic Applications, *Advanced Therapeutics* 2 (2019) 1800095.
- [264] F. V. Mikulec, J. D. Kirtland, M. J. Sailor, Explosive nanocrystalline porous silicon and its use in atomic emission spectroscopy, *Advanced Materials* 14 (2002) 38–41.
- [265] D. Clément, J. Diener, E. Gross, N. Künzner, V. Y. Timoshenko, D. Kovalev, Highly explosive nanosilicon-based composite materials, *Physica Status Solidi (A): Applications and Materials Science* 202 (2005) 1357–1364.
- [266] M. du Plessis, Nanoporous silicon explosive devices, *Materials Science and Engineering: B* 147 (2008) 226–229.
- [267] M. du Plessis, A decade of porous silicon as nano-explosive material, *Propellants, Explosives, Pyrotechnics* 39 (2014) 348–364.
- [268] L. Canham, Porous silicon application survey, in: L. T. Canham (Ed.), *Handbook of Porous Silicon: Second Edition*, 2nd ed., Springer International Publishing, Cham, 2018, pp. 1089–1097.
- [269] K. Imai, H. Unno, H. Takaoka, Crystalline quality of silicon layer formed by FIPOS technology, *Journal of Crystal Growth* 63 (1983) 547–553.
- [270] T. Mano, T. Baba, S. Sirotoshi, K. Imai, FIPOS CMOS 16K-Bit Static RAM, in: 1982 Symposium on VLSI Technology, IEEE, Oiso, 1982, pp. 12–13.
- [271] K. Sakaguchi, N. Sato, K. Yamagata, Y. Fujiyama, T. Yonehara, Extremely High Selective Etching of Porous Si for Single Etch-Stop Bond-and-Etch-Back SOI, in: *International Conference on Solid State Devices and Materials*, Yokohama, 1994, pp. 259–261.
- [272] N. Sato, T. Yonehara, Hydrogen annealed silicon-on-insulator, *Applied Physics Letters* 65 (1994) 1924–1926.
- [273] K. Sakaguchi, T. Yonehara, SOI wafers based on epitaxial technology, *Solid State Technology* 43 (2000) 88.
- [274] J. H. Petermann, D. Zielke, J. Schmidt, F. Haase, E. G. Rojas, R. Brendel, 19%-efficient and 43 μm -thick crystalline Si solar cell from layer transfer using porous silicon, *Progress in Photovoltaics: Research and Applications* 20 (2012) 1–5.
- [275] S. Kajari-Schröder, J. Käsewieter, J. Hensen, R. Brendel, Lift-off of free-standing layers in the kerfless porous silicon process, *Energy Procedia* 38 (2013) 919–925.
- [276] E. Matte, K. Van Nieuwenhuysen, V. Depauw, J. Govaerts, I. Gordon, Layer transfer process assisted by laser scribing for thin film solar cells based on epitaxial foils, *Physica Status So-*

- lidi (A): Applications and Materials Science 210 (2013) 682–686.
- [277] N. Milenkovic, M. Drießen, E. Gust, S. Janz, S. Reber, Reorganization of porous silicon: Effect on epitaxial layer quality and detachment, *Energy Procedia* 55 (2014) 552–558.
- [278] H. S. Radhakrishnan, R. Martini, V. Depauw, K. Van Nieuwenhuysen, M. Debucquoy, J. Govaerts, I. Gordon, R. Mertens, J. Poortmans, Improving the quality of epitaxial foils produced using a porous silicon-based layer transfer process for high-efficiency thin-film crystalline silicon solar cells, *IEEE Journal of Photovoltaics* 4 (2014) 70–77.
- [279] A. Ivanov, R. Sorgenfrei, E. Gust, P. Barth, K. V. Nieuwenhuysen, S. Kühnhold-Pospischil, S. Riepe, S. Janz, Optimization of Inline Processes for the Production of Freestanding Epitaxially Grown Thin Films for Solar Cells, *Proceedings of the 35th European Photovoltaic Solar Energy Conference and Exhibition* (2018) 309–313.
- [280] T. Sato, N. Aoki, I. Mizushima, Y. Tsunashima, New substrate engineering for the formation of Empty Space in Silicon (ESS) induced by silicon surface migration, *Technical Digest - International Electron Devices Meeting* (1999) 517–520.
- [281] I. Mizushima, T. Sato, S. Taniguchi, Y. Tsunashima, Empty-space-in-silicon technique for fabricating a silicon-on-nothing structure, *Applied Physics Letters* 77 (2000) 3290–3292.
- [282] B. Adam, T. Brandt, R. Henn, S. Reiss, M. Lang, C. Ohl, A New Micromechanical Pressure Sensor for Automotive Airbag Applications, in: J. Vallendorf, W. Gessner (Eds.), *Advanced Microsystems for Automotive Applications 2008*, Springer Berlin Heidelberg, Berlin, Heidelberg, 2008, pp. 259–284.
- [283] M. Boehringer, H. Artmann, K. Witt, Porous Silicon in a Semiconductor Manufacturing Environment, *Journal of Microelectromechanical Systems* 21 (2012) 1375–1381.
- [284] A. C. Fischer, F. Forsberg, M. Lapis, S. J. Bleiker, G. Stemme, N. Roxhed, F. Niklaus, Integrating MEMS and ICs, *Microsystems and Nanoengineering* 1 (2015).
- [285] J. Entwistle, A. Rennie, S. Patwardhan, A review of magnesiothermic reduction of silica to porous silicon for lithium-ion battery applications and beyond, *Journal of Materials Chemistry A* 6 (2018) 18344–18356.
- [286] N.-L. Wu, S.-S. Huang, Porous Silicon and Li-Ion Batteries, in: L. T. Canham (Ed.), *Handbook of Porous Silicon: Second Edition*, 2nd ed., Springer International Publishing, Cham, 2018, pp. 1501–1516.
- [287] Y. Jin, S. Zhang, B. Zhu, Y. Tan, X. Hu, L. Zong, J. Zhu, Simultaneous Purification and Perforation of Low-Grade Si Sources for Lithium-Ion Battery Anode, *Nano Letters* 15 (2015) 7742–7747.
- [288] M. Ge, Y. Lu, P. Ercius, J. Rong, X. Fang, M. Mecklenburg, C. Zhou, Large-scale fabrication, 3D tomography, and lithium-ion battery application of porous silicon, *Nano Letters* 14 (2014) 261–268.
- [289] Z. Jiang, C. Li, S. Hao, K. Zhu, P. Zhang, An easy way for preparing high performance porous silicon powder by acid etching Al-Si alloy powder for lithium ion battery, *Electrochimica Acta* 115 (2014) 393–398.
- [290] D. Vrankovic, M. Graczyk-Zajac, C. Kalcher, J. Rohrer, M. Becker, C. Stabler, G. Trykowski, K. Albe, R. Riedel, Highly Porous Silicon Embedded in a Ceramic Matrix: A Stable High-Capacity Electrode for Li-Ion Batteries, *ACS Nano* 11 (2017) 11409–11416.
- [291] H. Jia, X. Li, J. Song, X. Zhang, L. Luo, Y. He, B. Li, Y. Cai, S. Hu, X. Xiao, C. Wang, K. M. Rosso, R. Yi, R. Patel, J. G. Zhang, Hierarchical porous silicon structures with extraordinary mechanical strength as high-performance lithium-ion battery anodes, *Nature Communications* 11 (2020) 1–9.
- [292] C. Zhang, X. Cai, W. Chen, S. Yang, D. Xu, Y. Fang, X. Yu, 3D Porous Silicon/N-Doped Carbon Composite Derived from Bamboo Charcoal as High-Performance Anode Material for Lithium-Ion Batteries, *ACS Sustainable Chemistry & Engineering* 6 (2018) 9930–9939.
- [293] D. S. Jung, M.-H. Ryou, Y. J. Sung, S. B. Park, J. W. Choi, Recycling rice husks for high-capacity lithium battery anodes, *Proceedings of the National Academy of Sciences* 110 (2013) 12229–12234.
- [294] W. C. Cho, H. J. Kim, H. I. Lee, M. W. Seo, H. W. Ra, S. J. Yoon, T. Y. Mun, Y. K. Kim, J. H. Kim, B. H. Kim, J. W. Kook, C. Y. Yoo, J. G. Lee, J. W. Choi, 5L-Scale Magnesio-Milling Reduction of Nanostructured SiO₂ for High Capacity Silicon Anodes in Lithium-Ion Batteries, *Nano Letters* 16 (2016) 7261–7269.
- [295] J. Cui, Y. Cui, S. Li, H. Sun, Z. Wen, J. Sun, Microsized Porous SiO_x@C Composites Synthesized through Aluminothermic Reduction from Rice Husks and Used as Anode for Lithium-Ion Batteries, *ACS Applied Materials & Interfaces* 8 (2016) 30239–30247.
- [296] R. Miao, J. Yang, Y. Wu, J. Wang, Y. Nuli, W. Lu, Nanoporous silicon from low-cost natural clinoptilolite for lithium storage, *RSC Advances* 5 (2015) 56772–56779.
- [297] K. Grigoros, J. Ahopelto, M. Prunnila, Porous silicon supercapacitors, in: L. T. Canham (Ed.), *Handbook of Porous Silicon: Second Edition*, 2nd ed., Springer International Publishing, Cham, 2018, pp. 1517–1529.
- [298] S. E. Rowlands, R. J. Latham, W. S. Schlindwein, Supercapacitor devices using porous silicon electrodes, *Ionics* 5 (1999) 144–149.

- [299] W. R. Erwin, L. Oakes, S. Chatterjee, H. F. Zarick, C. L. Pint, R. Bardhan, Engineered porous silicon counter electrodes for high efficiency dye-sensitized solar cells., *ACS Applied Materials & Interfaces* 6 (2014) 9904–10.
- [300] A. P. Cohn, W. R. Erwin, K. Share, L. Oakes, A. S. Westover, R. E. Carter, R. Bardhan, C. L. Pint, All Silicon Electrode Photocapacitor for Integrated Energy Storage and Conversion, *Nano Letters* 15 (2015) 2727–2731.
- [301] D. Gardner, C. Holzwarth, Y. Liu, S. Clendenning, W. Jin, B. Moon, C. Pint, Z. Chen, E. Hannah, R. Chen, C. Wang, C. Chen, E. Mäkilä, J. Gustafson, Integrated on-chip energy storage using porous-silicon electrochemical capacitors, in: 2014 IEEE International Electron Devices Meeting, February, IEEE, 2014, pp. 8.2.1–8.2.4.
- [302] K. Grigoros, J. Keskinen, L. Grönberg, J. Ahopelto, M. Prunnila, Coated Porous Si for High Performance On-Chip Supercapacitors, *Journal of Physics: Conference Series* 557 (2014) 012058.
- [303] D. S. Gardner, C. W. Holzwarth, Y. Liu, S. B. Clendenning, W. Jin, B.-K. Moon, C. Pint, Z. Chen, E. C. Hannah, C. Chen, C. Wang, E. Mäkilä, R. Chen, T. Aldridge, J. L. Gustafson, Integrated on-chip energy storage using passivated nanoporous-silicon electrochemical capacitors, *Nano Energy* 25 (2016) 68–79.
- [304] K. Grigoros, J. Keskinen, L. Grönberg, E. Yli-Rantala, S. Laakso, H. Välimäki, P. Kauranen, J. Ahopelto, M. Prunnila, Conformal titanium nitride in a porous silicon matrix: A nanomaterial for in-chip supercapacitors, *Nano Energy* 26 (2016) 340–345.
- [305] G. Barillaro, Porous silicon gas sensing, in: L. T. Canham (Ed.), *Handbook of Porous Silicon: Second Edition*, 2nd ed., Springer International Publishing, Cham, 2018, pp. 1251–1262.
- [306] A. A. Ensafi, M. M. Abarghoui, N. Ahmadi, Porous silicon electrochemical biosensors: Basic principles and detection strategies, in: L. T. Canham (Ed.), *Handbook of Porous Silicon: Second Edition*, 2nd ed., Springer International Publishing, Cham, 2018, pp. 1275–1291.
- [307] G. Shtenberg, E. Segal, Porous silicon optical biosensors, in: L. T. Canham (Ed.), *Handbook of Porous Silicon: Second Edition*, 2nd ed., Springer International Publishing, Cham, 2018, pp. 1263–1273.
- [308] Z. M. Rittersma, A. Splinter, A. Bödecker, W. Bennecke, Novel surface-micromachined capacitive porous silicon humidity sensor, *Sensors and Actuators, B: Chemical* 68 (2000) 210–217.
- [309] J. Salonen, J. Tuura, M. Björkqvist, V. P. Lehto, Sub-ppm trace moisture detection with a simple thermally carbonized porous silicon sensor, *Sensors and Actuators, B: Chemical* 114 (2006) 423–426.
- [310] S. Belhousse, H. Cheraga, N. Gabouze, R. Out-amzabet, Fabrication and characterisation of a new sensing device based on hydrocarbon groups (CH_x) coated porous silicon, *Sensors and Actuators, B: Chemical* 100 (2004) 250–255.
- [311] G. Barillaro, A. Nannini, F. Pieri, APSFET: A new, porous silicon-based gas sensing device, *Sensors and Actuators, B: Chemical* 93 (2003) 263–270.
- [312] M. Sainato, L. M. Strambini, S. Rella, E. Mazzotta, G. Barillaro, Sub-Parts Per Million NO₂ Chemi-Transistor Sensors Based on Composite Porous Silicon/Gold Nanostructures Prepared by Metal-Assisted Etching, *ACS Applied Materials & Interfaces* 7 (2015) 7136–7145.
- [313] T. Jalkanen, A. Määttä, E. Mäkilä, J. Tuura, M. Kaasalainen, V.-P. Lehto, P. Ihalainen, J. Peltonen, J. Salonen, Fabrication of Porous Silicon Based Humidity Sensing Elements on Paper, *Journal of Sensors* 2015 (2015) 1–10.
- [314] J. M. Lauerhaas, G. M. Credo, J. L. Heinrich, M. J. Sailor, Reversible luminescence quenching of porous silicon by solvents, *Journal of the American Chemical Society* 114 (1992) 1911–1912.
- [315] M. Ben-Chorin, A. Kux, I. Schechter, Adsorbate effects on photoluminescence and electrical conductivity of porous silicon, *Applied Physics Letters* 64 (1994) 481–483.
- [316] J. Harper, M. J. Sailor, Detection of nitric oxide and nitrogen dioxide with photoluminescent porous silicon., *Analytical chemistry* 68 (1996) 3713–7.
- [317] R. B. Björklund, S. Zangoie, H. Arwin, Color changes in thin porous silicon films caused by vapor exposure, *Applied Physics Letters* 69 (1996) 3001–3003.
- [318] T. Gao, J. Gao, M. J. Sailor, Tuning the response and stability of thin film mesoporous silicon vapor sensors by surface modification, *Langmuir* 18 (2002) 9953–9957.
- [319] S. E. Létant, S. Content, T. T. Tan, F. Zenhausern, M. J. Sailor, Integration of porous silicon chips in an electronic artificial nose, *Sensors and Actuators, B: Chemical* 69 (2000) 193–198.
- [320] C. Baratto, G. Faglia, G. Sberveglieri, Z. Gaburro, L. Pancheri, C. Oton, L. Pavesi, Multiparametric porous silicon sensors, *Sensors* 2 (2002) 121–126.
- [321] T. Jalkanen, J. Tuura, E. Mäkilä, J. Salonen, Electro-optical porous silicon gas sensor with enhanced selectivity, *Sensors and Actuators B: Chemical* 147 (2010) 100–104.
- [322] M. J. Sweetman, N. H. Voelcker, Chemically patterned porous silicon photonic crystals towards internally referenced organic vapour sensors, *RSC Advances* 2 (2012) 4620–4622.
- [323] T. Jalkanen, V. Torres-Costa, E. Mäkilä, M. Kaasalainen, R. Koda, T. Sakka, Y. H. Ogata,

- J. Salonen, Selective Optical Response of Hydrolytically Stable Stratified Si Rugate Mirrors to Liquid Infiltration, *ACS Applied Materials & Interfaces* 6 (2014) 2884–2892.
- [324] K. A. Kilian, T. Böcking, K. Gaus, M. Gal, J. J. Gooding, Peptide-modified optical filters for detecting protease activity, *ACS Nano* 1 (2007) 355–361.
- [325] R. Chhasatia, M. J. Sweetman, B. Prieto-Simon, N. H. Voelcker, Performance optimisation of porous silicon rugate filter biosensor for the detection of insulin, *Sensors and Actuators, B: Chemical* 273 (2018) 1313–1322.
- [326] Y. Zhao, G. Gaur, S. T. Retterer, P. E. Laibinis, S. M. Weiss, Flow-through porous silicon membranes for real-time label-free biosensing, *Analytical Chemistry* 88 (2016) 10940–10948.
- [327] C. Pacholski, C. Yu, G. M. Miskelly, D. Godin, M. J. Sailor, Reflective Interferometric Fourier Transform Spectroscopy: A Self-Compensating Label-Free Immunosensor Using Double-Layers of Porous SiO₂, *Journal of the American Chemical Society* 128 (2006) 4250–4252.
- [328] B. Sciacca, E. Secret, S. Pace, P. Gonzalez, F. Geobaldo, F. Quignard, F. Cunin, Chitosan-functionalized porous silicon optical transducer for the detection of carboxylic acid-containing drugs in water, *Journal of Materials Chemistry* 21 (2011) 2294–2302.
- [329] R. Layouni, M. H. Choudhury, P. E. Laibinis, S. M. Weiss, Thermally Carbonized Porous Silicon for Robust Label-Free DNA Optical Sensing, *ACS Applied Bio Materials* 3 (2020) 622–627.
- [330] K. A. Kilian, T. Böcking, S. Ilyas, K. Gaus, W. Jessup, M. Gal, J. J. Gooding, Forming Antifouling Organic Multilayers on Porous Silicon Rugate Filters Towards In Vivo/Ex Vivo Biophotonic Devices, *Advanced Functional Materials* 17 (2007) 2884–2890.
- [331] L. N. Acquaroli, T. Kuchel, N. H. Voelcker, Towards implantable porous silicon biosensors, *RSC Advances* 4 (2014) 34768.
- [332] W. Y. Tong, M. J. Sweetman, E. R. Marzouk, C. Fraser, T. Kuchel, N. H. Voelcker, Towards a subcutaneous optical biosensor based on thermally hydrocarbonised porous silicon, *Biomaterials* 74 (2016) 217–230.
- [333] G. Rong, A. Najmaie, J. E. Sipe, S. M. Weiss, Nanoscale porous silicon waveguide for label-free DNA sensing, *Biosensors and Bioelectronics* 23 (2008) 1572–1576.
- [334] F. S. H. Krismastuti, A. Cavallaro, B. Prieto-Simon, N. H. Voelcker, Toward multiplexing detection of wound healing biomarkers on porous silicon resonant microcavities, *Advanced Science* 3 (2015) 1–8.
- [335] S. Arshavsky-Graham, N. Massad-Ivanir, F. Paratore, T. Scheper, M. Bercovici, E. Segal, On Chip Protein Pre-Concentration for Enhancing the Sensitivity of Porous Silicon Biosensors, *ACS Sensors* 2 (2017) 1767–1773.
- [336] S. Mariani, L. M. Strambini, G. Barillaro, Femtomole Detection of Proteins Using a Label-Free Nanostructured Porous Silicon Interferometer for Perspective Ultrasensitive Biosensing, *Analytical Chemistry* 88 (2016) 8502–8509.
- [337] S. Mariani, V. Robbiano, L. M. Strambini, A. Debrassi, G. Egri, L. Dähne, G. Barillaro, Layer-by-layer biofunctionalization of nanostructured porous silicon for high-sensitivity and high-selectivity label-free affinity biosensing, *Nature Communications* 9 (2018).
- [338] K. Guo, M. Alba, G. P. Chin, Z. Tong, B. Guan, M. J. Sailor, N. H. Voelcker, B. Prieto-Simón, Designing Electrochemical Biosensing Platforms Using Layered Carbon-Stabilized Porous Silicon Nanostructures, *ACS Applied Materials & Interfaces* 14 (2022) 15565–15575.
- [339] A. Jane, R. Dronov, A. Hodges, N. H. Voelcker, Porous silicon biosensors on the advance., *Trends in Biotechnology* 27 (2009) 230–9.
- [340] S. N. Jenie, S. E. Plush, N. H. Voelcker, Recent Advances on Luminescent Enhancement-Based Porous Silicon Biosensors, *Pharmaceutical Research* 33 (2016) 2314–2336.
- [341] S. Arshavsky-Graham, N. Massad-Ivanir, E. Segal, S. Weiss, Porous Silicon-Based Photonic Biosensors: Current Status and Emerging Applications, *Analytical Chemistry* 91 (2019) 441–467.
- [342] L. Di, P. V. Fish, T. Mano, Bridging solubility between drug discovery and development, *Drug Discovery Today* 17 (2012) 486–495.
- [343] G. L. Amidon, H. Lennernäs, V. P. Shah, J. R. Crison, A theoretical basis for a biopharmaceutical drug classification: the correlation of in vitro drug product dissolution and in vivo bioavailability., *Pharmaceutical Research* 12 (1995) 413–20.
- [344] C. Y. Jia, J. Y. Li, G. F. Hao, G. F. Yang, A drug-likeness toolbox facilitates ADMET study in drug discovery, *Drug Discovery Today* 25 (2020) 248–258.
- [345] N. Rasenack, B. W. Müller, Dissolution rate enhancement by in situ micronization of poorly water-soluble drugs., *Pharmaceutical Research* 19 (2002) 1894–900.
- [346] M. Turk, P. Hils, B. Helfgen, K. Schaber, H. Martin, M. Wahl, Micronization of pharmaceutical substances by the Rapid Expansion of Supercritical Solutions (RESS): a promising method to improve bioavailability of poorly soluble pharmaceutical agents, *Journal of Supercritical Fluids* 22 (2002) 75–84.
- [347] J. Pessi, I. Lassila, A. Meriläinen, H. Rääkkönen, E. Hægström, J. Yliruusi, Controlled Expansion of Supercritical Solution: A Robust Method to Produce Pure Drug Nanoparticles With Narrow Size-Distribution, *Journal of Pharmaceutical Sciences* 105 (2016) 2293–2297.

- [348] M. E. Brewster, T. Loftsson, Cyclodextrins as pharmaceutical solubilizers., *Advanced Drug Delivery Reviews* 59 (2007) 645–66.
- [349] N. Blagden, M. de Matas, P. T. Gavan, P. York, Crystal engineering of active pharmaceutical ingredients to improve solubility and dissolution rates., *Advanced Drug Delivery Reviews* 59 (2007) 617–30.
- [350] D. D. Sun, P. I. Lee, Evolution of Supersaturation of Amorphous Pharmaceuticals: The Effect of Rate of Supersaturation Generation, *Molecular Pharmaceutics* 10 (2013) 4330–4346.
- [351] B. C. Hancock, G. Zografi, Characteristics and significance of the amorphous state in pharmaceutical systems., *Journal of Pharmaceutical Sciences* 86 (1997) 1–12.
- [352] B. C. Hancock, M. Parks, What is the true solubility advantage for amorphous pharmaceuticals?, *Pharmaceutical Research* 17 (2000) 397–404.
- [353] J. Bevernage, J. Brouwers, M. E. Brewster, P. Augustijns, Evaluation of gastrointestinal drug supersaturation and precipitation: Strategies and issues., *International Journal of Pharmaceutics* 453 (2013) 25–35.
- [354] D. E. Alonzo, Y. Gao, D. Zhou, H. Mo, G. G. Zhang, L. S. Taylor, Dissolution and Precipitation Behavior of Amorphous Solid Dispersions, *Journal of Pharmaceutical Sciences* 100 (2011) 3316–3331.
- [355] K. Löbmann, H. Grohganz, R. Laitinen, C. Strachan, T. Rades, Amino acids as co-amorphous stabilizers for poorly water soluble drugs – Part I: Preparation, stability and dissolution enhancement, *European Journal of Pharmaceutics and Biopharmaceutics* 85 (2013) 873–881.
- [356] R. Laitinen, K. Löbmann, H. Grohganz, P. Priemel, C. J. Strachan, T. Rades, Supersaturating drug delivery systems: The potential of co-amorphous drug formulations, *International Journal of Pharmaceutics* 532 (2017) 1–12.
- [357] D. C. Monkhouse, J. L. Lach, Use of adsorbents in enhancement of drug dissolution II, *Journal of Pharmaceutical Sciences* 61 (1972) 1435–1441.
- [358] T. Konno, K. Kinuno, K. Kataoka, Physical and chemical changes of medicinals in mixtures with adsorbents in the solid state. I. Effect of vapor pressure of the medicinals on changes in crystalline properties., *Chemical & Pharmaceutical Bulletin* 34 (1986) 301–307.
- [359] T. Konno, K. Kinuno, Physical and chemical changes of medicinals in mixtures with adsorbents in the solid state. II. Application of reduced pressure treatment for the improvement of dissolution of flufenamic acid., *Chemical & Pharmaceutical Bulletin* 37 (1989) 2481.
- [360] C. T. Kresge, M. E. Leonowicz, W. J. Roth, J. C. Vartuli, J. S. Beck, Ordered mesoporous molecular sieves synthesized by a liquid-crystal template mechanism, *Nature* 359 (1992) 710–712.
- [361] D. Zhao, J. Feng, Q. Huo, N. Melosh, G. H. Fredrickson, B. F. Chmelka, G. D. Stucky, Triblock Copolymer Syntheses of Mesoporous Silica with Periodic 50 to 300 Angstrom Pores, *Science* 279 (1998) 548–552.
- [362] M. Vallet-Regí, A. Rámila, R. P. del Real, J. Pérez-Pariente, A New Property of MCM-41: Drug Delivery System, *Chemistry of Materials* 13 (2001) 308–311.
- [363] J. Andersson, J. Rosenholm, S. Areva, M. Lindén, Influences of Material Characteristics on Ibuprofen Drug Loading and Release Profiles from Ordered Micro- and Mesoporous Silica Matrices, *Chemistry of Materials* 16 (2004) 4160–4167.
- [364] P. Horcajada, A. Rámila, J. Pérez-Pariente, M. Vallet-Regí, Influence of pore size of MCM-41 matrices on drug delivery rate, *Microporous and Mesoporous Materials* 68 (2004) 105–109.
- [365] J. Salonen, L. Laitinen, A. M. Kaukonen, J. Tuura, M. Björkqvist, T. Heikkilä, K. Vähä-Heikkilä, J. Hirvonen, V.-P. Lehto, Mesoporous silicon microparticles for oral drug delivery: loading and release of five model drugs., *Journal of Controlled Release* 108 (2005) 362–74.
- [366] T. Linnell, J. Riikonen, J. Salonen, A. M. Kaukonen, L. Laitinen, J. Hirvonen, V.-P. Lehto, Surface chemistry and pore size affect carrier properties of mesoporous silicon microparticles., *International Journal of Pharmaceutics* 343 (2007) 141–7.
- [367] A. M. Kaukonen, L. Laitinen, J. Salonen, J. Tuura, T. Heikkilä, T. Linnell, J. Hirvonen, V.-P. Lehto, Enhanced in vitro permeation of furosemide loaded into thermally carbonized mesoporous silicon (TCPSi) microparticles., *European Journal of Pharmaceutics and Biopharmaceutics* 66 (2007) 348–56.
- [368] A. B. Foraker, R. J. Walczak, M. H. Cohen, T. A. Boiarski, C. F. Grove, P. W. Swaan, Microfabricated porous silicon particles enhance paracellular delivery of insulin across intestinal Caco-2 cell monolayers., *Pharmaceutical Research* 20 (2003) 110–6.
- [369] M. Kilpeläinen, J. Riikonen, M. A. Vlasova, A. Huotari, V. P. Lehto, J. Salonen, K. H. Herzig, K. Järvinen, In vivo delivery of a peptide, ghrelin antagonist, with mesoporous silicon microparticles., *Journal of Controlled Release* 137 (2009) 166–70.
- [370] J. S. Andrew, E. J. Anglin, E. C. Wu, M. Y. Chen, L. Cheng, W. R. Freeman, M. J. Sailor, Sustained Release of a Monoclonal Antibody from Electrochemically Prepared Mesoporous Silicon Oxide., *Advanced Functional Materials* 20 (2010) 4168–4174.
- [371] L. Gu, L. E. Ruff, Z. Qin, M. Corr, S. M. Hedrick, M. J. Sailor, Multivalent porous silicon nanoparticles enhance the immune activation potency of

- agonistic CD40 antibody., *Advanced Materials* 24 (2012) 3981–7.
- [372] T. Tanaka, L. S. Mangala, P. E. Vivas-Mejia, R. Nieves-Alicea, A. P. Mann, E. Mora, H.-D. Han, M. M. K. Shahzad, X. Liu, R. Bhavane, J. Gu, J. R. Fakhoury, C. Chiappini, C. Lu, K. Matsuo, B. Godin, R. L. Stone, A. M. Nick, G. Lopez-Berestein, A. K. Sood, M. Ferrari, Sustained small interfering RNA delivery by mesoporous silicon particles., *Cancer Research* 70 (2010) 3687–96.
- [373] C. T. Turner, M. Hasanzadeh Kafshgari, E. Melville, B. Delalat, F. Harding, E. Mäkilä, J. J. Salonen, A. J. Cowin, N. H. Voelcker, Delivery of Flightless I siRNA from Porous Silicon Nanoparticles Improves Wound Healing in Mice, *ACS Biomaterials Science & Engineering* 2 (2016) 2339–2346.
- [374] A. C. Anselmo, S. Mitragotri, Nanoparticles in the clinic, *Bioengineering & Translational Medicine* 1 (2016) 10–29.
- [375] G. Walsh, Biopharmaceutical benchmarks 2018, *Nature Biotechnology* 36 (2018) 1136–1145.
- [376] S. Mitragotri, J. Lahann, Materials for drug delivery: Innovative solutions to address complex biological hurdles, *Advanced Materials* 24 (2012) 3717–3723.
- [377] N. Habibi, D. F. Quevedo, J. V. Gregory, J. Lahann, Emerging methods in therapeutics using multifunctional nanoparticles, *WIREs Nanomedicine and Nanobiotechnology* 12 (2020) 1–22.
- [378] S. Chattoraj, C. C. Sun, Crystal and Particle Engineering Strategies for Improving Powder Compression and Flow Properties to Enable Continuous Tablet Manufacturing by Direct Compression, *Journal of Pharmaceutical Sciences* 107 (2018) 968–974.
- [379] S. Mitragotri, P. A. Burke, R. Langer, Overcoming the challenges in administering biopharmaceuticals: Formulation and delivery strategies, *Nature Reviews Drug Discovery* 13 (2014) 655–672.
- [380] P. Decuzzi, B. Godin, T. Tanaka, S.-Y. Lee, C. Chiappini, X. Liu, M. Ferrari, Size and shape effects in the biodistribution of intravascularly injected particles., *Journal of Controlled Release* 141 (2010) 320–7.
- [381] E. Blanco, H. Shen, M. Ferrari, Principles of nanoparticle design for overcoming biological barriers to drug delivery, *Nature Biotechnology* 33 (2015) 941–951.
- [382] D. Fine, A. Grattoni, R. Goodall, S. S. Bansal, C. Chiappini, S. Hosali, A. L. van de Ven, S. Srinivasan, X. Liu, B. Godin, L. Brousseau, I. K. Yazdi, J. Fernandez-Moure, E. Tasciotti, H.-J. Wu, Y. Hu, S. Klemm, M. Ferrari, Silicon micro- and nanofabrication for medicine., *Advanced Healthcare Materials* 2 (2013) 632–66.
- [383] A. Loni, Milling of porous silicon microparticles, in: L. T. Canham (Ed.), *Handbook of Porous Silicon: Second Edition*, 2nd ed., Springer International Publishing, Cham, 2018, pp. 1051–1060.
- [384] M. J. Sailor, Porous silicon nanoparticles, in: L. T. Canham (Ed.), *Handbook of Porous Silicon: Second Edition*, 2nd ed., Springer International Publishing, Cham, 2018, pp. 215–225.
- [385] C. Barry Carter, M. Grant Norton, *Ceramic Materials: Science and Engineering*, 2007.
- [386] C. Suryanarayana, Mechanical alloying and milling, *Progress in Materials Science* 46 (2001) 1–184.
- [387] M. Kovalainen, R. Kamakura, J. Riikonen, M. Finnilä, T. Nissinen, J. Rantanen, M. Niemelä, P. Perämäki, M. Mäkinen, K. H. Herzig, V. P. Lehto, Biodegradation of inorganic drug delivery systems in subcutaneous conditions, *European Journal of Pharmaceutics and Biopharmaceutics* 122 (2018) 113–125.
- [388] J. R. Sander, B. W. Zeiger, K. S. Suslick, Sonocrystallization and sonofragmentation, *Ultrasonics Sonochemistry* 21 (2014) 1908–1915.
- [389] J. Jordens, T. Appermont, B. Gielen, T. Van Geven, L. Braeken, Sonofragmentation: Effect of Ultrasound Frequency and Power on Particle Breakage, *Crystal Growth and Design* 16 (2016) 6167–6177.
- [390] S. Meade, M. Yoon, K. Ahn, M. Sailor, Porous silicon photonic crystals as encoded microcarriers, *Advanced Materials* 16 (2004) 1811–1814.
- [391] J. L. Heinrich, C. L. Curtis, G. M. Credo, M. J. Sailor, K. L. Kavanagh, M. J. Sailor, Luminescent colloidal silicon suspensions from porous silicon., *Science* 255 (1992) 66–8.
- [392] U. Jakobsson, E. Mäkilä, A. J. Airaksinen, O. Alanen, A. Etilä, U. Köster, S. Ranjan, J. Salonen, H. A. Santos, K. Helariutta, Porous Silicon as a Platform for Radiation Theranostics Together with a Novel RIB-Based Radiolanthanoid, *Contrast Media & Molecular Imaging* 2019 (2019) 1–9.
- [393] J.-H. Park, L. Gu, G. von Maltzahn, E. Ruoslahti, S. N. Bhatia, M. J. Sailor, Biodegradable luminescent porous silicon nanoparticles for in vivo applications., *Nature Materials* 8 (2009) 331–6.
- [394] L. Canham, Mechanical properties of porous silicon, in: L. T. Canham (Ed.), *Handbook of Porous Silicon: Second Edition*, 2nd ed., Springer International Publishing, Cham, 2018, pp. 309–318.
- [395] Z. Qin, J. Joo, L. Gu, M. J. Sailor, Size Control of Porous Silicon Nanoparticles by Electrochemical Perforation Etching, *Particle & Particle Systems Characterization* 31 (2014) 252–256.
- [396] C. J. Storey, E. Nekovic, A. Kaplan, W. Theis, L. T. Canham, Preserving surface area and porosity during fabrication of silicon aerocrystal particles from anodized wafers, *Journal of Porous Materials* (2020) 1–6.

- [397] D. Lumen, S. Wang, E. Mäkilä, S. Imlimhan, M. Sarparanta, A. Correia, C. Westerveld Haug, J. Hirvonen, H. A. Santos, A. J. Airaksinen, W. Filtvedt, J. Salonen, Investigation of silicon nanoparticles produced by centrifuge chemical vapor deposition for applications in therapy and diagnostics, *European Journal of Pharmaceutics and Biopharmaceutics* 158 (2021) 254–265.
- [398] D. S. Roberts, D. Estrada, N. Yagi, E. J. Anglin, N. A. Chan, M. J. Sailor, Preparation of Photoluminescent Porous Silicon Nanoparticles by High-Pressure Microfluidization, *Particle & Particle Systems Characterization* 34 (2017) 1600326.
- [399] F. Cunin, T. A. Schmedake, J. R. Link, Y. Y. Li, J. Koh, S. N. Bhatia, M. J. Sailor, Biomolecular screening with encoded porous-silicon photonic crystals., *Nature Materials* 1 (2002) 39–41.
- [400] M. Cohen, K. Melnik, A. Boiarski, M. Ferrari, F. J. Martin, Microfabrication of silicon-based nanoporous particulates for medical applications, *Biomedical Microdevices* 5 (2003) 253–259.
- [401] C. Chiappini, E. Tasciotti, J. R. Fakhoury, D. Fine, L. Pullan, Y.-C. Wang, L. Fu, X. Liu, M. Ferrari, Tailored Porous Silicon Microparticles: Fabrication and Properties, *ChemPhysChem* 11 (2010) 1029–1035.
- [402] B. Godin, C. Chiappini, S. Srinivasan, J. F. Alexander, K. Yokoi, M. Ferrari, P. Decuzzi, X. Liu, Discoidal Porous Silicon Particles: Fabrication and Biodistribution in Breast Cancer Bearing Mice, *Advanced Functional Materials* 22 (2012) 4225–4235.
- [403] H. Alhmod, B. Delalat, R. Elnathan, A. Cifuentes-Rius, A. Chaix, M.-L. Rogers, J.-O. Durand, N. H. Voelcker, Porous Silicon Nanodiscs for Targeted Drug Delivery, *Advanced Functional Materials* 25 (2015) 1137–1145.
- [404] J. W. Mares, J. S. Fain, K. R. Beavers, C. L. Duvall, S. M. Weiss, Shape-Engineered multifunctional porous silicon nanoparticles by direct imprinting, *Nanotechnology* 26 (2015) 271001.
- [405] M.-A. Shahbazi, N. Shrestha, E. Mäkilä, F. Araújo, A. Correia, T. Ramos, B. Sarmento, J. Salonen, J. Hirvonen, H. A. Santos, A prospective cancer chemo-immunotherapy approach mediated by synergistic CD326 targeted porous silicon nanovectors, *Nano Research* 8 (2015) 1505–1521.
- [406] F. Tang, L. Li, D. Chen, Mesoporous silica nanoparticles: Synthesis, biocompatibility and drug delivery, *Advanced Materials* 24 (2012) 1504–1534.
- [407] J. Henstock, L. Canham, S. Anderson, Silicon: The evolution of its use in biomaterials, *Acta Biomaterialia* 11 (2014) 17–26.
- [408] J. G. Croissant, Y. Fatieiev, N. M. Khashab, Degradability and Clearance of Silicon, Organosilica, Silsesquioxane, Silica Mixed Oxide, and Mesoporous Silica Nanoparticles, *Advanced Materials* 29 (2017) 1604634.
- [409] W. Li, Z. Liu, F. Fontana, Y. Ding, D. Liu, J. T. Hirvonen, H. A. Santos, Tailoring Porous Silicon for Biomedical Applications: From Drug Delivery to Cancer Immunotherapy, *Advanced Materials* 30 (2018) 1703740.
- [410] D. Liu, M. A. Shahbazi, L. M. Bimbo, J. Hirvonen, H. A. Santos, Biocompatibility of porous silicon for biomedical applications, in: *Porous Silicon for Biomedical Applications*, Elsevier Ltd., 2014, pp. 129–181.
- [411] S. P. Low, N. H. Voelcker, Biocompatibility of Porous Silicon, in: L. T. Canham (Ed.), *Handbook of Porous Silicon*, 1st ed., Springer International Publishing, Cham, 2014, pp. 381–393.
- [412] Q. Shabir, Biodegradability of porous silicon, in: L. T. Canham (Ed.), *Handbook of Porous Silicon: Second Edition*, 2nd ed., Springer International Publishing, Cham, 2018, pp. 547–554.
- [413] P. Allongue, V. Costa-Kieling, H. Gerischer, Etching of Silicon in NaOH Solutions: II. Electrochemical Studies of n-Si(111) and (100) and Mechanism of the Dissolution, *Journal of the Electrochemical Society* 140 (1993) 1018–1026.
- [414] D. M. Reffitt, R. Jugdaohsingh, R. P. Thompson, J. J. Powell, Silicic acid: its gastrointestinal uptake and urinary excretion in man and effects on aluminium excretion, *Journal of Inorganic Biochemistry* 76 (1999) 141–147.
- [415] P. Uribe, A. Johansson, R. Jugdaohsingh, J. J. Powell, C. Magnusson, M. Davila, A. Westerland, M. Ransjö, Soluble silica stimulates osteogenic differentiation and gap junction communication in human dental follicle cells, *Scientific Reports* 10 (2020).
- [416] A. Tzur-Balter, Z. Shatsberg, M. Beckerman, E. Segal, N. Artzi, Mechanism of erosion of nanostructured porous silicon drug carriers in neoplastic tissues, *Nature Communications* 6 (2015) 6208.
- [417] S. P. Low, N. H. Voelcker, L. T. Canham, K. A. Williams, The biocompatibility of porous silicon in tissues of the eye, *Biomaterials* 30 (2009) 2873–2880.
- [418] S. H. Anderson, H. Elliott, D. J. Wallis, L. T. Canham, J. J. Powell, Dissolution of different forms of partially porous silicon wafers under simulated physiological conditions, *Physica Status Solidi (A): Applications and Materials Science* 197 (2003) 331–335.
- [419] S. Qi, P. Zhang, M. Ma, M. Yao, J. Wu, E. Mäkilä, J. Salonen, H. Ruskoaho, Y. Xu, H. A. Santos, H. Zhang, Cellular Internalization-Induced Aggregation of Porous Silicon Nanoparticles for Ultrasound Imaging and Protein-Mediated Protection of Stem Cells, *Small* 15 (2019) 1804332.
- [420] H. A. Santos, J. Riikonen, J. Salonen, E. Mäkilä, T. Heikkilä, T. Laaksonen, L. Peltonen, V.-P. Lehto, J. Hirvonen, In vitro cytotoxicity of porous silicon microparticles: Effect of the par-

- ticle concentration, surface chemistry and size, *Acta Biomaterialia* 6 (2010) 2721–2731.
- [421] M.-A. Shahbazi, M. Hamidi, E. M. Mäkilä, H. Zhang, P. V. Almeida, M. Kaasalainen, J. J. Salonen, J. T. Hirvonen, H. A. Santos, The mechanisms of surface chemistry effects of mesoporous silicon nanoparticles on immunotoxicity and biocompatibility, *Biomaterials* 34 (2013) 7776–7789.
- [422] B. Xia, W. Zhang, J. Shi, S. J. Xiao, Engineered stealth porous silicon nanoparticles via surface encapsulation of bovine serum albumin for prolonging blood circulation in vivo, *ACS Applied Materials & Interfaces* 5 (2013) 11718–11724.
- [423] T. Nissinen, S. Näkki, H. Laakso, D. Kučiauskas, A. Kaupinis, M. I. Kettunen, T. Liimatainen, M. Hyvönen, M. Valius, O. Gröhn, V.-P. Lehto, Tailored Dual PEGylation of Inorganic Porous Nanocarriers for Extremely Long Blood Circulation in Vivo, *ACS Applied Materials & Interfaces* 8 (2016) 32723–32731.
- [424] L. M. Bimbo, M. Sarparanta, E. Mäkilä, T. Laaksonen, P. Laaksonen, J. Salonen, M. B. Linder, J. Hirvonen, A. J. Airaksinen, H. A. Santos, Cellular interactions of surface modified nanoporous silicon particles, *Nanoscale* 4 (2012) 3184.
- [425] M. P. Sarparanta, L. M. Bimbo, E. M. Mäkilä, J. J. Salonen, P. H. Laaksonen, A. K. Helariutta, M. B. Linder, J. T. Hirvonen, T. J. Laaksonen, H. A. Santos, A. J. Airaksinen, The mucoadhesive and gastroretentive properties of hydrophobin-coated porous silicon nanoparticle oral drug delivery systems, *Biomaterials* 33 (2012) 3353–3362.
- [426] M. Sarparanta, L. M. Bimbo, J. Rytönen, E. Mäkilä, T. J. Laaksonen, P. Laaksonen, M. Nyman, J. Salonen, M. B. Linder, J. Hirvonen, H. A. Santos, A. J. Airaksinen, Intravenous Delivery of Hydrophobin-Functionalized Porous Silicon Nanoparticles: Stability, Plasma Protein Adsorption and Biodistribution, *Molecular Pharmaceutics* 9 (2012) 654–663.
- [427] F. Fontana, M.-A. Shahbazi, D. Liu, H. Zhang, E. Mäkilä, J. Salonen, J. T. Hirvonen, H. A. Santos, Multistaged Nanovaccines Based on Porous Silicon@Acetalated Dextran@Cancer Cell Membrane for Cancer Immunotherapy, *Advanced Materials* 29 (2017) 1603239.
- [428] A. Rahikkala, F. Fontana, T. Bauleth-Ramos, A. Correia, M. Kemell, J. Seitonen, E. Mäkilä, B. Sarmiento, J. Salonen, J. Ruokolainen, J. Hirvonen, H. A. Santos, Hybrid red blood cell membrane coated porous silicon nanoparticles functionalized with cancer antigen induce depletion of T cells, *RSC Advances* 10 (2020) 35198–35205.
- [429] A. Loni, Melt intrusion in porous silicon, in: L. T. Canham (Ed.), *Handbook of Porous Silicon: Second Edition*, 2nd ed., Springer International Publishing, Cham, 2018, pp. 945–950.
- [430] J. Riikonen, Solvent loading of porous silicon, in: L. T. Canham (Ed.), *Handbook of Porous Silicon: Second Edition*, 2nd ed., Springer International Publishing, Cham, 2018, pp. 913–925.
- [431] M. Wang, J. L. Coffey, K. Dorraj, P. S. Hartman, A. Loni, L. T. Canham, Sustained antibacterial activity from triclosan-loaded nanostructured mesoporous silicon., *Molecular Pharmaceutics* 7 (2010) 2232–9.
- [432] L. Tang, A. Saharay, W. Fleischer, P. S. Hartman, A. Loni, L. T. Canham, J. L. Coffey, Sustained Antifungal Activity from a Ketoconazole-Loaded Nanostructured Mesoporous Silicon Platform, *Silicon* 5 (2013) 213–217.
- [433] Y. Tozuka, A. Wongmekiat, K. Kimura, K. Moribe, S. Yamamura, K. Yamamoto, Effect of pore size of FSM-16 on the entrapment of flurbiprofen in mesoporous structures, *Chemical and Pharmaceutical Bulletin* 53 (2005) 974–977.
- [434] R. Mellaerts, J. A. G. Jammaer, M. Van Speybroeck, H. Chen, J. Van Humbeeck, P. Augustijns, G. Van den Mooter, J. A. Martens, Physical state of poorly water soluble therapeutic molecules loaded into SBA-15 ordered mesoporous silica carriers: a case study with itraconazole and ibuprofen., *Langmuir* 24 (2008) 8651–9.
- [435] K. P. Nartowski, J. Tedder, D. E. Braun, L. Fábán, Y. Z. Khimyak, Building solids inside nano-space: from confined amorphous through confined solvate to confined ‘metastable’ polymorph, *Phys. Chem. Chem. Phys.* 17 (2015) 24761–24773.
- [436] T. Konno, Physical and chemical changes of medicinals in mixtures with adsorbents in the solid state. III. Determination of vapor pressure of solid drugs by steam distillation., *Chemical & Pharmaceutical Bulletin* 38 (1990) 1032–1034.
- [437] K. K. Qian, D. E. Wurster, R. H. Bogner, Spontaneous crystalline-to-amorphous phase transformation of organic or medicinal compounds in the presence of porous media, part 3: effect of moisture., *Pharmaceutical Research* 29 (2012) 2698–709.
- [438] K. Trzeciak, S. Kaźmierski, E. Wielgus, M. J. Potrzebowski, DiSupLo - New extremely easy and efficient method for loading of active pharmaceutical ingredients into the pores of MCM-41 mesoporous silica particles, *Microporous and Mesoporous Materials* 308 (2020).
- [439] C. Charnay, S. Bégu, C. Tourné-Péteilh, L. Nicole, D. A. Lerner, J. M. Devoisselle, Inclusion of ibuprofen in mesoporous templated silica: drug loading and release property., *European Journal of Pharmaceutics and Biopharmaceutics* 57 (2004) 533–40.
- [440] A. Tzur-Balter, A. Gilert, N. Massad-Ivanir, E. Segal, Engineering porous silicon nanostructures as tunable carriers for mitoxantrone dihydrochloride., *Acta Biomaterialia* 9 (2013) 6208–17.

- [441] V. Ambrogì, L. Perioli, F. Marmottini, S. Giovagnoli, M. Esposito, C. Rossi, Improvement of dissolution rate of piroxicam by inclusion into MCM-41 mesoporous silicate, *European Journal of Pharmaceutical Sciences* 32 (2007) 216–222.
- [442] M. Kaasalainen, E. Mäkilä, J. Riikonen, M. Kovalainen, K. Järvinen, K.-H. Herzig, V.-P. Lehto, J. Salonen, Effect of isotonic solutions and peptide adsorption on zeta potential of porous silicon nanoparticle drug delivery formulations., *International Journal of Pharmaceutics* 431 (2012) 230–6.
- [443] M. Kaasalainen, J. Rytönen, E. Mäkilä, A. Närvänen, J. Salonen, Electrostatic Interaction on Loading of Therapeutic Peptide GLP-1 into Porous Silicon Nanoparticles, *Langmuir* 31 (2015) 1722–1729.
- [444] K. L. Jarvis, T. J. Barnes, C. A. Prestidge, Thermal oxidation for controlling protein interactions with porous silicon., *Langmuir* 26 (2010) 14316–22.
- [445] J. Lyklema, Adsorption at solid–liquid interfaces with special reference to emulsion systems, *Colloids and Surfaces A: Physicochemical and Engineering Aspects* 91 (1994) 25–38.
- [446] K. A. Fisher, K. D. Huddersman, M. J. Taylor, Comparison of micro- and mesoporous inorganic materials in the uptake and release of the drug model fluorescein and its analogues., *Chemistry - A European Journal* 9 (2003) 5873–8.
- [447] E. Skorupska, A. Jeziorna, P. Paluch, M. J. Potrzebowski, Ibuprofen in mesopores of Mobil Crystalline Material 41 (MCM-41): a deeper understanding., *Molecular Pharmaceutics* 11 (2014) 1512–9.
- [448] M. Fernández-Núñez, D. Zorrilla, A. Montes, M. J. Mosquera, Ibuprofen loading in surfactant-templated silica: role of the solvent according to the polarizable continuum model., *Journal of Physical Chemistry A* 113 (2009) 11367–75.
- [449] M. Šoltys, P. Kovačik, O. Dammer, J. Beránek, F. Štěpánek, Effect of solvent selection on drug loading and amorphisation in mesoporous silica particles, *International Journal of Pharmaceutics* 555 (2019) 19–27.
- [450] A. Daehler, G. W. Stevens, A. J. O'Connor, Bioadsorption and separation with nanoporous materials, in: G. Q. Lu, X. S. Zhao (Eds.), *Nanoporous Materials: Science and Engineering*, World Scientific Publishing, 2004, pp. 812–848.
- [451] E. C. Wu, J.-H. Park, J. Park, E. Segal, F. Cunin, M. J. Sailor, Oxidation-triggered release of fluorescent molecules or drugs from mesoporous Si microparticles., *ACS Nano* 2 (2008) 2401–9.
- [452] C.-F. Wang, E. M. Mäkilä, M. H. Kaasalainen, M. V. Hagström, J. J. Salonen, J. T. Hirvonen, H. A. Santos, Dual-drug delivery by porous silicon nanoparticles for improved cellular uptake, sustained release, and combination therapy, *Acta Biomaterialia* 16 (2015) 206–214.
- [453] J. Riikonen, E. Mäkilä, J. Salonen, V.-P. Lehto, Determination of the Physical State of Drug Molecules in Mesoporous Silicon with Different Surface Chemistries, *Langmuir* 25 (2009) 6137–6142.
- [454] T. Azaïs, C. Tourné-Péteilh, F. Aussenac, N. Bacile, C. Coelho, J.-M. Devoisselle, F. Babonneau, Solid-State NMR Study of Ibuprofen Confined in MCM-41 Material, *Chemistry of Materials* 18 (2006) 6382–6390.
- [455] R. Mellaerts, E. J. Fayad, G. Van den Mooter, P. Augustijns, M. Rivallan, F. Thibault-Starzyk, J. A. Martens, In situ FT-IR investigation of etravirine speciation in pores of SBA-15 ordered mesoporous silica material upon contact with water., *Molecular Pharmaceutics* 10 (2013) 567–73.
- [456] J. Riikonen, A. Correia, M. Kovalainen, S. Näkki, M. Lehtonen, J. Leppänen, J. Rantanen, W. Xu, F. Araújo, J. Hirvonen, K. Järvinen, H. A. Santos, V. P. Lehto, Systematic in vitro and in vivo study on porous silicon to improve the oral bioavailability of celecoxib, *Biomaterials* 52 (2015) 44–55.
- [457] M. V. Speybroeck, V. Barillaro, T. D. Thi, R. Mellaerts, J. Martens, J. V. Humbeek, J. Vermant, P. Annaert, G. V. Den Mooter, P. Augustijns, Ordered Mesoporous Silica Material SBA-15: A Broad-Spectrum Formulation Platform for Poorly Soluble Drugs, *Journal of Pharmaceutical Sciences* 98 (2009) 2648–2658.
- [458] R. Mellaerts, R. Mols, J. A. G. Jammaer, C. A. Aerts, P. Annaert, J. Van Humbeek, G. Van den Mooter, P. Augustijns, J. A. Martens, Increasing the oral bioavailability of the poorly water soluble drug itraconazole with ordered mesoporous silica., *European Journal of Pharmaceutics and Biopharmaceutics* 69 (2008) 223–30.
- [459] I. Smirnova, J. Mamic, W. Arlt, Adsorption of Drugs on Silica Aerogels, *Langmuir* 19 (2003) 8521–8525.
- [460] R. J. Ahern, A. M. Crean, K. B. Ryan, The influence of supercritical carbon dioxide (SC-CO₂) processing conditions on drug loading and physicochemical properties, *International Journal of Pharmaceutics* 439 (2012) 92–99.
- [461] A. Gignone, M. Delle Piane, M. Corno, P. Ugliengo, B. Onida, Simulation and Experiment Reveal a Complex Scenario for the Adsorption of an Antifungal Drug in Ordered Mesoporous Silica, *Journal of Physical Chemistry C* 119 (2015) 13068–13079.
- [462] H. Takeuchi, S. Nagira, H. Yamamoto, Y. Kawashima, Solid dispersion particles of amorphous indomethacin with fine porous silica particles by using spray-drying method, *International Journal of Pharmaceutics* 293 (2005) 155–164.
- [463] T. Limnell, H. A. Santos, E. Mäkilä, T. Heikkilä, J. Salonen, D. Y. Murzin, N. Kumar, T. Laaksonen, L. Peltonen, J. Hirvonen, Drug Delivery

- Formulations of Ordered and Nonordered Mesoporous Silica: Comparison of Three Drug Loading Methods, *Journal of Pharmaceutical Sciences* 100 (2011) 3294–3306.
- [464] K. Nagane, S. Kimura, K. Ukai, N. Ogawa, H. Yamamoto, Practical approach to prepare solid dispersion drug product using spherical silicate, *International Journal of Pharmaceutics* 475 (2014) 364–371.
- [465] Y. C. Hacene, A. Singh, G. Van den Mooter, Drug loaded and ethylcellulose coated mesoporous silica for controlled drug release prepared using a pilot scale fluid bed system, *International Journal of Pharmaceutics* 506 (2016) 138–147.
- [466] C. L. Jackson, G. B. McKenna, The melting behavior of organic materials confined in porous solids, *Journal of Chemical Physics* 93 (1990) 9002.
- [467] C. L. Jackson, G. B. McKenna, Vitrification and Crystallization of Organic Liquids Confined to Nanoscale Pores, *Chemistry of Materials* 8 (1996) 2128–2137.
- [468] S. Cheng, G. B. McKenna, Nanoconfinement Effects on the Glass Transition and Crystallization Behaviors of Nifedipine, *Molecular Pharmaceutics* 16 (2019) 856–866.
- [469] C. J. Ellison, J. M. Torkelson, The distribution of glass-transition temperatures in nanoscopically confined glass formers, *Nature Materials* 2 (2003) 695–700.
- [470] C. Alba-Simionesco, B. Coasne, G. Dosseh, G. Dudziak, K. E. Gubbins, R. Radhakrishnan, M. Sliwinska-Bartkowiak, Effects of confinement on freezing and melting, *Journal of Physics: Condensed Matter* 18 (2006) R15–R68.
- [471] Q. Jiang, M. D. Ward, Crystallization under nanoscale confinement., *Chemical Society Reviews* 43 (2014) 2066–2079.
- [472] T. Linnell, T. Heikkilä, H. A. Santos, S. Sistonen, S. Hellstén, T. Laaksonen, L. Peltonen, N. Kumar, D. Y. Murzin, M. Louhi-Kultanen, J. Salonen, J. Hirvonen, V. P. Lehto, Physicochemical stability of high indomethacin payload ordered mesoporous silica MCM-41 and SBA-15 microparticles, *International Journal of Pharmaceutics* 416 (2011) 242–251.
- [473] K. P. Nartowski, D. Malhotra, L. E. Hawarden, J. Sibik, D. Iuga, J. A. Zeitler, L. Fábíán, Y. Z. Khimiyak, ¹⁹F NMR Spectroscopy as a Highly Sensitive Method for the Direct Monitoring of Confined Crystallization within Nanoporous Materials, *Angewandte Chemie, International Edition* 55 (2016) 8904–8908.
- [474] G. T. Rengarajan, D. Enke, M. Steinhart, M. Beiner, Stabilization of the amorphous state of pharmaceuticals in nanopores, *Journal of Materials Chemistry* 18 (2008) 2537.
- [475] A. R. Brás, I. M. Fonseca, M. Dionísio, A. Schönhals, F. Affouard, N. T. Correia, Influence of Nanoscale Confinement on the Molecular Mobility of Ibuprofen, *Journal of Physical Chemistry C* 118 (2014) 13857–13868.
- [476] M. Beiner, G. T. Rengarajan, S. Pankaj, D. Enke, M. Steinhart, Manipulating the crystalline state of pharmaceuticals by nanoconfinement, *Nano Letters* 7 (2007) 1381–1385.
- [477] B. D. Hamilton, M. A. Hillmyer, M. D. Ward, Glycine polymorphism in nanoscale crystallization chambers, *Crystal Growth & Design* 8 (2008) 3368–3375.
- [478] G. Graubner, G. T. Rengarajan, N. Anders, N. Sonnenberger, D. Enke, M. Beiner, M. Steinhart, Morphology of porous hosts directs preferred polymorph formation and influences kinetics of solid/solid transitions of confined pharmaceuticals, *Crystal Growth & Design* 14 (2014) 78–86.
- [479] K. P. Nartowski, D. Malhotra, L. E. Hawarden, L. Fábíán, Y. Z. Khimiyak, Nanocrystallization of Rare Tolbutamide Form V in Mesoporous MCM-41 Silica, *Molecular Pharmaceutics* 15 (2018) 4926–4932.
- [480] N. E. Chayen, E. Saridakis, R. El-Bahar, Y. Nemirovsky, Porous silicon: an effective nucleation-inducing material for protein crystallization., *Journal of Molecular Biology* 312 (2001) 591–5.
- [481] S. Stolyarova, E. Saridakis, N. E. Chayen, Y. Nemirovsky, A model for enhanced nucleation of protein crystals on a fractal porous substrate., *Biophysical Journal* 91 (2006) 3857–63.
- [482] M. Tahvanainen, T. Rotko, E. Mäkilä, H. A. Santos, D. Neves, T. Laaksonen, A. Kallonen, K. Hämäläinen, M. Peura, R. Serimaa, J. Salonen, J. Hirvonen, L. Peltonen, Tablet preformulations of indomethacin-loaded mesoporous silicon microparticles, *International Journal of Pharmaceutics* 422 (2012) 125–131.
- [483] N. Zilony, A. Tzur-Balter, E. Segal, O. Shefi, Bombarding cancer: biolistic delivery of therapeutics using porous Si carriers., *Scientific Reports* 3 (2013) 2499.
- [484] L. M. Bimbo, E. Mäkilä, T. Laaksonen, V.-P. Lehto, J. Salonen, J. Hirvonen, H. A. Santos, Drug permeation across intestinal epithelial cells using porous silicon nanoparticles, *Biomaterials* 32 (2011) 2625–2633.
- [485] R. E. Serda, B. Godin, E. Blanco, C. Chiappini, M. Ferrari, Multi-stage delivery nano-particle systems for therapeutic applications., *Biochimica et Biophysica Acta* 1810 (2011) 317–29.
- [486] W. Sun, J. E. Puzas, T.-J. Sheu, P. M. Fauchet, Porous silicon as a cell interface for bone tissue engineering, *Physica Status Solidi (A): Applications and Materials Science* 204 (2007) 1429–1433.
- [487] M. A. Whitehead, D. Fan, P. Mukherjee, G. R. Akkaraju, L. T. Canham, J. L. Coffey, High-porosity poly(ϵ -caprolactone)/mesoporous silicon scaffolds: Calcium phosphate deposition and

- biological response to bone precursor cells, *Tissue Engineering: Part A* 14 (2008) 195–206.
- [488] Y. D. Irani, S. Klebe, S. J. McInnes, M. Jasieniak, N. H. Voelcker, K. A. Williams, Oral Mucosal Epithelial Cells Grown on Porous Silicon Membrane for Transfer to the Rat Eye, *Scientific Reports* 7 (2017) 10042.
- [489] L. Gu, J.-H. Park, K. H. Duong, E. Ruoslahti, M. J. Sailor, Magnetic Luminescent Porous Silicon Microparticles for Localized Delivery of Molecular Drug Payloads, *Small* 6 (2010) 2546–2552.
- [490] P. J. Kinnari, M. L. Hyvönen, E. M. Mäkilä, M. H. Kaasalainen, A. Rivinoja, J. J. Salonen, J. T. Hirvonen, P. M. Laakkonen, H. A. Santos, Tumour homing peptide-functionalized porous silicon nanovectors for cancer therapy, *Biomaterials* 34 (2013) 9134–9141.
- [491] C. A. Prestidge, T. J. Barnes, C.-H. Lau, C. Barnett, A. Loni, L. Canham, Mesoporous silicon: a platform for the delivery of therapeutics., *Expert Opinion on Drug Delivery* 4 (2007) 101–10.
- [492] W. Xu, J. Riikonen, V.-P. Lehto, Mesoporous systems for poorly soluble drugs., *International Journal of Pharmaceutics* 453 (2013) 181–97.
- [493] J. Riikonen, W. Xu, V. P. Lehto, Mesoporous systems for poorly soluble drugs – recent trends, *International Journal of Pharmaceutics* 536 (2018) 178–186.
- [494] H. A. Santos, E. Mäkilä, A. J. Airaksinen, L. M. Bimbo, J. Hirvonen, Porous silicon nanoparticles for nanomedicine: preparation and biomedical applications, *Nanomedicine* 9 (2014) 535–554.
- [495] D. X. Zhang, L. Esser, R. B. Vasani, H. Thissen, N. H. Voelcker, Porous silicon nanomaterials: recent advances in surface engineering for controlled drug-delivery applications, *Nanomedicine* 14 (2019) 3213–3230.
- [496] L. Canham, D. Ferguson, Porous silicon in brachytherapy, in: L. T. Canham (Ed.), *Handbook of Porous Silicon: Second Edition*, 2nd ed., Springer International Publishing, Cham, 2018, pp. 1369–1375.
- [497] K. Zhang, S. L. E. Loong, S. Connor, S. W. K. Yu, S. Y. Tan, R. T. H. Ng, K. M. Lee, L. Canham, P. K. H. Chow, Complete tumor response following intratumoral ^{32}P BioSilicon on human hepatocellular and pancreatic carcinoma xenografts in nude mice, *Clinical Cancer Research* 11 (2005) 7532–7537.
- [498] A. S. W. Goh, A. Y. F. Chung, R. H. G. Lo, T. N. Lau, S. W. K. Yu, M. Chng, S. Satchithanatham, S. L. E. Loong, D. C. E. Ng, B. C. Lim, S. Connor, P. K. H. Chow, A novel approach to brachytherapy in hepatocellular carcinoma using a phosphorous 32 (^{32}P) brachytherapy delivery device – a first-in-man study, *International Journal of Radiation Oncology Biology Physics* 67 (2007) 786–792.
- [499] P. J. Ross, H. S. Wasan, D. Croagh, M. Nikfarjam, N. Nguyen, M. Aghmesheh, A. M. Nagrial, D. Bartholomeusz, A. Hendlisz, T. Ajithkumar, C. Iwuiji, N. E. Wilson, D. M. Turner, D. C. James, E. Young, M. T. Harris, Results of a single-arm pilot study of ^{32}P microparticles in unresectable locally advanced pancreatic adenocarcinoma with gemcitabine/nab-paclitaxel or FOLFIRINOX chemotherapy, *ESMO Open* 7 (2022) 100356.
- [500] S. J. P. McInnes, Y. Irani, K. A. Williams, N. H. Voelcker, Controlled drug delivery from composites of nanostructured porous silicon and poly(L-lactide)., *Nanomedicine* 7 (2012) 995–1016.
- [501] D. Liu, E. Mäkilä, H. Zhang, B. Herranz, M. Kaasalainen, P. Kinnari, J. Salonen, J. Hirvonen, H. A. Santos, Nanostructured Porous Silicon-Solid Lipid Nanocomposite: Towards Enhanced Cytocompatibility and Stability, Reduced Cellular Association, and Prolonged Drug Release, *Advanced Functional Materials* 23 (2013) 1893–1902.
- [502] S. Minardi, L. Pandolfi, F. Taraballi, E. De Rosa, I. K. Yazdi, X. Liu, M. Ferrari, E. Tasciotti, PLGA-Mesoporous Silicon Microspheres for the in Vivo Controlled Temporospatial Delivery of Proteins, *ACS Applied Materials & Interfaces* 7 (2015) 16364–16373.
- [503] S. J. P. McInnes, T. D. Michl, B. Delalat, S. A. Al-Bataineh, B. R. Coad, K. Vasilev, H. J. Griesser, N. H. Voelcker, “Thunderstruck”: Plasma-Polymer-Coated Porous Silicon Microparticles As a Controlled Drug Delivery System, *ACS Applied Materials & Interfaces* 8 (2016) 4467–4476.
- [504] X. Li, J. John, J. Coffey, Y. Chen, R. F. Pinizzotto, J. P. Newey, C. Reeves, L. T. Canham, Porosified silicon wafer structures impregnated with platinum anti-tumor compounds: Fabrication, characterization, and diffusion studies, *Biomedical Microdevices* 2 (2000) 265–272.
- [505] J. Kang, J. Joo, E. J. Kwon, M. Skalak, S. Husain, Z.-G. She, E. Ruoslahti, S. N. Bhatia, M. J. Sailor, Self-Sealing Porous Silicon-Calcium Silicate Core-Shell Nanoparticles for Targeted siRNA Delivery to the Injured Brain, *Advanced Materials* 28 (2016) 7962–7969.
- [506] J. Wang, T. Kumeria, M. T. Bezem, J. Wang, M. J. Sailor, Self-Reporting Photoluminescent Porous Silicon Microparticles for Drug Delivery, *ACS Applied Materials & Interfaces* 10 (2018) 3200–3209.
- [507] A. P. Mann, T. Tanaka, A. Somasunderam, X. Liu, D. G. Gorenstein, M. Ferrari, E-Selectin-Targeted Porous Silicon Particle for Nanoparticle Delivery to the Bone Marrow, *Advanced Materials* 23 (2011) H278–H282.
- [508] E. Secret, M. Maynadier, A. Gallud, M. Gary-Bobo, A. Chaix, E. Belamie, P. Maillard, M. J. Sailor, M. Garcia, J.-O. Durand, F. Cunin, Anionic porphyrin-grafted porous silicon nanoparti-

- cles for photodynamic therapy., *Chemical Communications* 49 (2013) 4202–4.
- [509] K. Yokoi, B. Godin, C. J. Oborn, J. F. Alexander, X. Liu, I. J. Fidler, M. Ferrari, Porous silicon nanocarriers for dual targeting tumor associated endothelial cells and macrophages in stroma of orthotopic human pancreatic cancers., *Cancer Letters* 334 (2013) 319–27.
- [510] A. Bertucci, K.-H. Kim, J. Kang, J. M. Zuidema, S. H. Lee, E. J. Kwon, D. Kim, S. B. Howell, F. Ricci, E. Ruoslahti, H.-J. Jang, M. J. Sailor, Tumor-Targeting, MicroRNA-Silencing Porous Silicon Nanoparticles for Ovarian Cancer Therapy, *ACS Applied Materials & Interfaces* 11 (2019) 23926–23937.
- [511] M. Luo, G. Lewik, J. C. Ratcliffe, C. H. J. Choi, E. Mäkilä, W. Y. Tong, N. H. Voelcker, Systematic Evaluation of Transferrin-Modified Porous Silicon Nanoparticles for Targeted Delivery of Doxorubicin to Glioblastoma, *ACS Applied Materials & Interfaces* 11 (2019) 33637–33649.
- [512] S. Sheykhzadeh, M. Luo, B. Peng, J. White, Y. Abdalla, T. Tang, E. Mäkilä, N. H. Voelcker, W. Y. Tong, Transferrin-targeted porous silicon nanoparticles reduce glioblastoma cell migration across tight extracellular space, *Scientific Reports* 10 (2020) 1–16.
- [513] D. X. Zhang, T. Tieu, L. Esser, M. Wojnilowicz, C. H. Lee, A. Cifuentes-Rius, H. Thissen, N. H. Voelcker, Differential Surface Engineering Generates Core-Shell Porous Silicon Nanoparticles for Controlled and Targeted Delivery of an Anticancer Drug, *ACS Applied Materials & Interfaces* 14 (2022) 54539–54549.
- [514] J. Wu, M. J. Sailor, Chitosan Hydrogel-Capped Porous SiO₂ as a pH Responsive Nano-Valve for Triggered Release of Insulin, *Advanced Functional Materials* 19 (2009) 733–741.
- [515] M. Xue, X. Zhong, Z. Shaposhnik, Y. Qu, F. Tamanoi, X. Duan, J. I. Zink, pH-Operated mechanized porous silicon nanoparticles., *Journal of the American Chemical Society* 133 (2011) 8798–801.
- [516] S. J. P. McInnes, E. J. Szili, S. A. Al-Bataineh, J. Xu, M. E. Alf, K. K. Gleason, R. D. Short, N. H. Voelcker, Combination of iCVD and Porous Silicon for the Development of a Controlled Drug Delivery System, *ACS Applied Materials & Interfaces* 4 (2012) 3566–3574.
- [517] R. B. Vasani, S. J. P. McInnes, M. A. Cole, A. M. M. Jani, A. V. Ellis, N. H. Voelcker, Stimulus-Responsiveness and Drug Release from Porous Silicon Films ATRP-Grafted with Poly(N-isopropylacrylamide), *Langmuir* 27 (2011) 7843–7853.
- [518] S. J. P. McInnes, E. J. Szili, S. A. Al-Bataineh, R. B. Vasani, J. Xu, M. E. Alf, K. K. Gleason, R. D. Short, N. H. Voelcker, Fabrication and Characterization of a Porous Silicon Drug Delivery System with an Initiated Chemical Vapor Deposition Temperature-Responsive Coating, *Langmuir* 32 (2016) 301–308.
- [519] S. Müller, A. Cavallaro, K. Vasilev, N. H. Voelcker, H. Schönherr, Temperature-Controlled Antimicrobial Release from Poly(diethylene glycol methylether methacrylate)-Functionalized Bottleneck-Structured Porous Silicon for the Inhibition of Bacterial Growth, *Macromolecular Chemistry and Physics* 217 (2016) 2243–2251.
- [520] S. Bakshi, P. Pandey, Y. Mohammed, J. Wang, M. J. Sailor, A. Papat, H. S. Parekh, T. Kumeria, Porous silicon embedded in a thermoresponsive hydrogel for intranasal delivery of lipophilic drugs to treat rhinosinusitis, *Journal of Controlled Release* 363 (2023) 452–463.
- [521] K. Tamarov, W. Xu, L. Osminkina, S. Zinovyev, P. Soininen, A. Kudryavtsev, M. Gongalsky, A. Gaydarova, A. Närvänen, V. Timoshenko, V.-P. Lehto, Temperature responsive porous silicon nanoparticles for cancer therapy – spatiotemporal triggering through infrared and radiofrequency electromagnetic heating, *Journal of Controlled Release* 241 (2016) 220–228.
- [522] B. Xia, B. Wang, Z. Chen, Q. Zhang, J. Shi, Near-Infrared Light-Triggered Intracellular Delivery of Anticancer Drugs Using Porous Silicon Nanoparticles Conjugated with IR820 Dyes, *Advanced Materials Interfaces* 3 (2016) 1–11.
- [523] H. Zhang, W. Cui, X. Qu, H. Wu, L. Qu, X. Zhang, E. Mäkilä, J. Salonen, Y. Zhu, Z. Yang, D. Chen, H. A. Santos, M. Hai, D. A. Weitz, Photothermal-responsive nanosized hybrid polymersome as versatile therapeutics codeivery nanovehicle for effective tumor suppression, *Proceedings of the National Academy of Sciences* 116 (2019) 201817251.
- [524] A. Chaix, E. Cueto-Diaz, S. Dominguez-Gil, C. Spiteri, L. Lichon, M. Maynadier, X. Du-mail, D. Aggad, A. Delalande, A. Bessière, C. Pichon, C. Chiappini, M. J. Sailor, N. Bettache, M. Gary-Bobo, J. Durand, C. Nguyen, F. Cunin, Two-Photon Light Trigger siRNA Transfection of Cancer Cells Using Non-Toxic Porous Silicon Nanoparticles, *Advanced Healthcare Materials* 12 (2023).
- [525] N. Shrestha, M.-A. Shahbazi, F. Araújo, E. Mäkilä, J. Raula, E. I. Kauppinen, J. Salonen, B. Sarmiento, J. Hirvonen, H. A. Santos, Multi-stage pH-responsive mucoadhesive nanocarriers prepared by aerosol flow reactor technology: A controlled dual protein-drug delivery system, *Biomaterials* 68 (2015) 9–20.
- [526] N. Shrestha, F. Araújo, M.-A. Shahbazi, E. Mäkilä, M. J. Gomes, M. Airavaara, E. I. Kauppinen, J. Raula, J. Salonen, J. Hirvonen, B. Sarmiento, H. A. Santos, Oral hypoglycaemic effect of GLP-1 and DPP4 inhibitor based nanocomposites in a diabetic animal model, *Journal of Controlled Release* 232 (2016) 113–119.

- [527] J. Roine, M. Murtomaa, M. Myllys, J. Salonen, Dual-capillary electroencapsulation of mesoporous silicon drug carrier particles for controlled oral drug delivery, *Journal of Electrostatics* 70 (2012) 428–437.
- [528] J. Roine, M. Kaasalainen, M. Peurla, A. Correia, F. Araújo, H. A. Santos, M. Murtomaa, J. Salonen, Controlled Dissolution of Griseofulvin Solid Dispersions from Electrospayed Enteric Polymer Micromatrix Particles: Physicochemical Characterization and in Vitro Evaluation, *Molecular Pharmaceutics* 12 (2015) 2254–2264.
- [529] T. Kumeria, J. Wang, B. Kim, J. H. Park, J. M. Zuidema, M. Klempner, L. Cavacini, Y. Wang, M. J. Sailor, Enteric Polymer-Coated Porous Silicon Nanoparticles for Site-Specific Oral Delivery of IgA Antibody, *ACS Biomaterials Science and Engineering* 8 (2022) 4140–4152.
- [530] D. Liu, B. Herranz-Blanco, E. Mäkilä, L. R. Arriaga, S. Mirza, D. A. Weitz, N. Sandler, J. Salonen, J. Hirvonen, H. A. Santos, Microfluidic Templated Mesoporous Silicon–Solid Lipid Microcomposites for Sustained Drug Delivery, *ACS Applied Materials & Interfaces* 5 (2013) 12127–12134.
- [531] D. Liu, H. Zhang, B. Herranz-Blanco, E. Mäkilä, V.-P. Lehto, J. Salonen, J. Hirvonen, H. A. Santos, Microfluidic Assembly of Monodisperse Multistage pH-Responsive Polymer/Porous Silicon Composites for Precisely Controlled Multi-Drug Delivery, *Small* 10 (2014) 2029–2038.
- [532] D. Liu, H. Zhang, E. Mäkilä, J. Fan, B. Herranz-Blanco, C.-F. Wang, R. Rosa, A. J. Ribeiro, J. Salonen, J. Hirvonen, H. A. Santos, Microfluidic assisted one-step fabrication of porous silicon@acetalated dextran nanocomposites for precisely controlled combination chemotherapy, *Biomaterials* 39 (2015) 249–259.
- [533] B. Herranz-Blanco, L. R. Arriaga, E. Mäkilä, A. Correia, N. Shrestha, S. Mirza, D. A. Weitz, J. Salonen, J. Hirvonen, H. A. Santos, Microfluidic assembly of multistage porous silicon–lipid vesicles for controlled drug release, *Lab on a Chip* 14 (2014) 1083–1086.
- [534] A. Cifuentes-Rius, A. Ivask, E. Sporleder, I. Kaur, Y. Assan, S. Rao, D. Warther, C. A. Prestidge, J.-O. Durand, N. H. Voelcker, Dual-Action Cancer Therapy with Targeted Porous Silicon Nanovectors, *Small* 13 (2017) 1701201.
- [535] I. Kaur, T. Tieu, V. G. Deepagan, M. A. Ali, F. Alsunaydih, D. Rudd, M. A. Moghaddam, L. Bourgeois, T. E. Adams, K. J. Thurecht, M. Yuce, A. Cifuentes-Rius, N. H. Voelcker, Combination of Chemotherapy and Mild Hyperthermia Using Targeted Nanoparticles: A Potential Treatment Modality for Breast Cancer, *Pharmaceutics* 15 (2023).
- [536] J. Coffey, Porous silicon and tissue engineering scaffolds, in: L. T. Canham (Ed.), *Handbook of Porous Silicon: Second Edition*, 2nd ed., Springer International Publishing, Cham, 2018, pp. 1453–1459.
- [537] P.-Y. Collart-Dutilleul, E. Secret, I. Panayotov, D. Deville de Périère, R. J. Martín-Palma, V. Torres-Costa, M. Martín, C. Gergely, J.-O. Durand, F. Cunin, F. J. Cuisinier, Adhesion and proliferation of human mesenchymal stem cells from dental pulp on porous silicon scaffolds., *ACS Applied Materials & Interfaces* 6 (2014) 1719–28.
- [538] N. Fatima, H. Salehi, E. J. Cueto-Díaz, A. Desoutter, F. Cuisinier, F. Cunin, P. Y. Collart-Dutilleul, Nanostructured Porous Silicon for Bone Tissue Engineering: Kinetics of Particle Degradation and Si-Controlled Release, *Journal of Functional Biomaterials* 14 (2023) 493.
- [539] J. L. Coffey, M. A. Whitehead, D. K. Nagesha, P. Mukherjee, G. Akkaraju, M. Totolici, R. S. Saffie, L. T. Canham, Porous silicon-based scaffolds for tissue engineering and other biomedical applications, *Physica Status Solidi (A) Applications and Materials Science* 202 (2005) 1451–1455.
- [540] D. Fan, E. De Rosa, M. B. Murphy, Y. Peng, C. A. Smid, C. Chiappini, X. Liu, P. Simmons, B. K. Weiner, M. Ferrari, E. Tasciotti, Mesoporous Silicon-PLGA Composite Microspheres for the Double Controlled Release of Biomolecules for Orthopedic Tissue Engineering, *Advanced Functional Materials* 22 (2012) 282–293.
- [541] N. K. Bodiford, S. J. McInnes, N. H. Voelcker, J. L. Coffey, Porous silicon-poly(ϵ -caprolactone) film composites: evaluation of drug release and degradation behavior, *Biomedical Microdevices* 20 (2018) 71.
- [542] J. R. Henstock, U. R. Ruktanonchai, L. T. Canham, S. I. Anderson, Porous silicon confers bioactivity to polycaprolactone composites in vitro., *Journal of Materials Science: Materials in Medicine* 25 (2014) 1087–97.
- [543] M. Rosenberg, D. Shilo, L. Galperin, T. Capucha, K. Tarabieh, A. Rachmiel, E. Segal, Bone morphogenic protein 2-loaded porous silicon carriers for osteoinductive implants, *Pharmaceutics* 11 (2019) 602.
- [544] M. Kaasalainen, R. Zhang, P. Vashisth, A. A. Birjandi, M. S’Ari, D. A. Martella, M. Isaacs, E. Mäkilä, C. Wang, E. Moldenhauer, P. Clarke, A. Pinna, X. Zhang, S. A. Mustfa, V. Caprettini, A. P. Morrell, E. Gentleman, D. S. Brauer, O. Addison, X. Zhang, M. Bergholt, K. Al-Jamal, A. A. Volponi, J. Salonen, N. Hondow, P. Sharpe, C. Chiappini, Lithiated porous silicon nanowires stimulate periodontal regeneration, *Nature Communications* 15 (2024) 487.
- [545] S. Kashanian, F. Harding, Y. Irani, S. Klebe, K. Marshall, A. Loni, L. Canham, D. Fan, K. A. Williams, N. H. Voelcker, J. L. Coffey, Evaluation of mesoporous silicon/polycaprolactone composites as ophthalmic implants, *Acta Biomaterialia* 6 (2010) 3566–3572.

- [546] Y. D. Irani, Y. Tian, M. Wang, S. Klebe, S. J. McInnes, N. H. Voelcker, J. L. Coffer, K. A. Williams, A novel pressed porous silicon-polycaprolactone composite as a dual-purpose implant for the delivery of cells and drugs to the eye, *Experimental Eye Research* 139 (2015) 123–131.
- [547] N. Zanjanzadeh Ezazi, R. Ajdary, A. Correia, E. Mäkilä, J. Salonen, M. Kemell, J. Hirvonen, O. J. Rojas, H. J. Ruskoaho, H. A. Santos, Fabrication and Characterization of Drug-Loaded Conductive Poly(glycerol sebacate)/Nanoparticle-Based Composite Patch for Myocardial Infarction Applications, *ACS Applied Materials & Interfaces* 12 (2020) 6899–6909.
- [548] J. M. Kinsella, S. Ananda, J. S. Andrew, J. F. Grondek, M.-P. Chien, M. Scadeng, N. C. Gianneschi, E. Ruoslahti, M. J. Sailor, Enhanced magnetic resonance contrast of Fe₃O₄ nanoparticles trapped in a porous silicon nanoparticle host., *Advanced Materials* 23 (2011) H248–53.
- [549] K. Tamarov, A. Sviridov, W. Xu, M. Malo, V. Andreev, V. Timoshenko, V. P. Lehto, Nano Air Seeds Trapped in Mesoporous Janus Nanoparticles Facilitate Cavitation and Enhance Ultrasound Imaging, *ACS Applied Materials & Interfaces* 9 (2017) 35234–35243.
- [550] S. Qi, P. Zhang, M. Ma, M. Yao, J. Wu, E. Mäkilä, J. Salonen, H. Ruskoaho, Y. Xu, H. Santos, H. Zhang, Cellular Internalization-Induced Aggregation of Porous Silicon Nanoparticles for Ultrasound Imaging and Protein-Mediated Protection of Stem Cells, *Small* 15 (2019).
- [551] J. Kang, D. Kim, J. Wang, Y. Han, J. M. Zuidema, A. Hariri, J. H. Park, J. V. Jokerst, M. J. Sailor, Enhanced Performance of a Molecular Photoacoustic Imaging Agent by Encapsulation in Mesoporous Silicon Nanoparticles, *Advanced Materials* 30 (2018) 1–8.
- [552] W. Xu, J. Leskinen, J. Tick, E. Happonen, T. Tarvainen, V.-P. Lehto, Black mesoporous silicon as contrast agent for LED-based 3D photoacoustic tomography, *ACS Applied Materials & Interfaces* 12 (2020) 5456–5461.
- [553] H. Kobayashi, M. Ogawa, R. Alford, P. L. Choyke, Y. Urano, New strategies for fluorescent probe design in medical diagnostic imaging, *Chemical Reviews* 110 (2010) 2620–2640.
- [554] J. Joo, J. F. Cruz, S. Vijayakumar, J. Grondek, M. J. Sailor, Photoluminescent Porous Si/SiO₂ Core/Shell Nanoparticles Prepared by Borate Oxidation, *Advanced Functional Materials* 24 (2014) 5688–5694.
- [555] J. Joo, T. Defforge, A. Loni, D. Kim, Z. Y. Li, M. J. Sailor, G. Gautier, L. T. Canham, Enhanced quantum yield of photoluminescent porous silicon prepared by supercritical drying, *Applied Physics Letters* 108 (2016) 153111.
- [556] S. Frohnhoff, R. Arens-Fischer, T. Heinrich, J. Fricke, M. Arntzen, W. Theiss, Characterization of supercritically dried porous silicon, *Thin Solid Films* 255 (1995) 115–118.
- [557] L. Gu, D. J. Hall, Z. Qin, E. Anglin, J. Joo, D. J. Mooney, S. B. Howell, M. J. Sailor, In vivo time-gated fluorescence imaging with biodegradable luminescent porous silicon nanoparticles, *Nature Communications* 4 (2013) 2326.
- [558] J. Joo, X. Liu, V. R. Kotamraju, E. Ruoslahti, Y. Nam, M. J. Sailor, Gated Luminescence Imaging of Silicon Nanoparticles, *ACS Nano* 9 (2015) 6233–6241.
- [559] D. Kim, J. Kang, T. Wang, H. G. Ryu, J. M. Zuidema, J. Joo, M. Kim, Y. Huh, J. Jung, K. H. Ahn, K. H. Kim, M. J. Sailor, Two-Photon In Vivo Imaging with Porous Silicon Nanoparticles, *Advanced Materials* 29 (2017) 1703309.
- [560] X. Chen, F. Wo, Y. Jin, J. Tan, Y. Lai, J. Wu, Drug-Porous Silicon Dual Luminescent System for Monitoring and Inhibition of Wound Infection, *ACS Nano* 11 (2017) 7938–7949.
- [561] J. M. Zuidema, T. Kumeria, D. Kim, J. Kang, J. Wang, G. Hollett, X. Zhang, D. S. Roberts, N. Chan, C. Dowling, E. Blanco-Suarez, N. J. Allen, M. H. Tuszynski, M. J. Sailor, Oriented Nanofibrous Polymer Scaffolds Containing Protein-Loaded Porous Silicon Generated by Spray Nebulization, *Advanced Materials* 1706785 (2018) 1706785.
- [562] A. Chaix, K. El Cheikh, E. Bouffard, M. Maynadier, D. Aggad, V. Stojanovic, N. Knezevic, M. Garcia, P. Maillard, A. Morere, M. Gary-Bobo, L. Raehm, S. Richeter, J.-O. Durand, F. Cunin, Mesoporous silicon nanoparticles for targeted two-photon theranostics of prostate cancer, *Journal of Materials Chemistry B* 4 (2016) 3639–3642.
- [563] E. Secret, M. Maynadier, A. Gallud, A. Chaix, E. Bouffard, M. Gary-Bobo, N. Marcotte, O. Mongin, K. El Cheikh, V. Hugues, M. Auffan, C. Frochot, A. Morère, P. Maillard, M. Blanchard-Desce, M. J. Sailor, M. Garcia, J. Durand, F. Cunin, Two-Photon Excitation of Porphyrin-Functionalized Porous Silicon Nanoparticles for Photodynamic Therapy, *Advanced Materials* 26 (2014) 7643–7648.
- [564] C.-F. Wang, M. P. Sarparanta, E. M. Mäkilä, M. L. K. Hyvönen, P. M. Laakkonen, J. J. Salonen, J. T. Hirvonen, A. J. Airaksinen, H. A. Santos, Multifunctional porous silicon nanoparticles for cancer theranostics., *Biomaterials* 48 (2015) 108–18.
- [565] M. P. A. Ferreira, S. Ranjan, S. Kinnunen, A. Correia, V. Talman, E. Mäkilä, B. Barrios-Lopez, M. Kemell, V. Balasubramanian, J. Salonen, J. Hirvonen, H. Ruskoaho, A. J. Airaksinen, H. A. Santos, Drug-Loaded Multifunctional Nanoparticles Targeted to the Endocardial Layer of the

- Injured Heart Modulate Hypertrophic Signaling, *Small* 13 (2017) 1701276.
- [566] H. A. Santos, E. Mäkilä, L. M. Bimbo, P. Almeida, J. Hirvonen, Porous Silicon Nanoparticles, in: I. F. Uchegbu, A. G. Schätzlein, W. P. Cheng, A. Lalatsa (Eds.), *Fundamentals of Pharmaceutical Nanoscience*, Springer New York, New York, NY, 2013, pp. 235–275.
- [567] A. Loni, Gas Adsorption Analysis of Porous Silicon, in: L. T. Canham (Ed.), *Handbook of Porous Silicon*, 1st ed., Springer International Publishing, Cham, 2014, pp. 431–437.
- [568] S. Brunauer, P. Emmett, E. Teller, Adsorption of gases in multimolecular layers, *Journal of the American Chemical Society* 60 (1938) 309–319.
- [569] E. Barrett, L. Joyner, P. Halenda, The determination of pore volume and area distributions in porous substances. I. Computations from nitrogen isotherms, *Journal of the American Chemical Society* 73 (1951) 373–380.
- [570] D. Giron, Applications of thermal analysis and coupled techniques in pharmaceutical industry, *Journal of Thermal Analysis and Calorimetry* 68 (2002) 335–357.
- [571] P. Griffiths, J. A. De Haseth, *Fourier Transform Infrared Spectrometry*, 2nd ed., Wiley Interscience, New Jersey, 2007.
- [572] J. F. Watts, J. Wolstenholme, *An introduction to Surface Analysis by XPS and AES*, 2nd ed., Wiley, 2003.
- [573] C. V. Cushman, S. Chatterjee, G. H. Major, N. J. Smith, A. Roberts, M. R. Linford, Trends in Advanced XPS Instrumentation. 1. Overview of the Technique, Automation, High Sensitivity, Imaging, Snapshot Spectroscopy, Gas Cluster Ion Beams, and Multiple Analytical Techniques on the Instrument, *Vacuum Technology & Coating* (2016) 20–28.
- [574] G. Neue, C. Dybowski, Determining temperature in a magic-angle spinning probe using the temperature dependence of the isotropic chemical shift of lead nitrate, *Solid State Nuclear Magnetic Resonance* 7 (1997) 333–336.
- [575] N. Shrestha, M.-A. Shahbazi, F. Araújo, H. Zhang, E. M. Mäkilä, J. Kauppila, B. Sarmiento, J. J. Salonen, J. T. Hirvonen, H. A. Santos, Chitosan-modified porous silicon microparticles for enhanced permeability of insulin across intestinal cell monolayers, *Biomaterials* 35 (2014) 7172–7179.
- [576] K. R. Beavers, J. W. Mares, C. M. Swartz, Y. Zhao, S. M. Weiss, C. L. Duvall, In situ synthesis of peptide nucleic acids in porous silicon for drug delivery and biosensing., *Bioconjugate Chemistry* 25 (2014) 1192–7.
- [577] S. Chandrasekaran, T. Nann, N. H. Voelcker, Nanostructured silicon photoelectrodes for solar water electrolysis, *Nano Energy* 17 (2015) 308–322.
- [578] B. Kim, S. Sun, J. A. Varner, S. B. Howell, E. Ruoslahti, M. J. Sailor, Securing the Payload, Finding the Cell, and Avoiding the Endosome: Peptide-Targeted, Fusogenic Porous Silicon Nanoparticles for Delivery of siRNA, *Advanced Materials* 31 (2019) 1–14.
- [579] M. Qin, H. Zong, R. Kopelman, Click Conjugation of Peptide to Hydrogel Nanoparticles for Tumor-Targeted Drug Delivery., *Biomacromolecules* (2014).
- [580] H. Zhang, M. Li, J. Li, A. Agrawal, H. W. Hui, D. Liu, Superiority of Mesoporous Silica-Based Amorphous Formulations over Spray-Dried Solid Dispersions, *Pharmaceutics* 14 (2022).
- [581] C.-F. Wang, E. M. Mäkilä, M. H. Kaasalainen, D. Liu, M. P. Sarparanta, A. J. Airaksinen, J. J. Salonen, J. T. Hirvonen, H. A. Santos, Copper-free azide–alkyne cycloaddition of targeting peptides to porous silicon nanoparticles for intracellular drug uptake, *Biomaterials* 35 (2014) 1257–1266.
- [582] M.-A. Shahbazi, T. D. Fernández, E. M. Mäkilä, X. Le Guével, C. Mayorga, M. H. Kaasalainen, J. J. Salonen, J. T. Hirvonen, H. A. Santos, Surface chemistry dependent immunostimulative potential of porous silicon nanoplateforms, *Biomaterials* 35 (2014) 9224–9235.
- [583] K. Masuda, S. Tabata, H. Kono, Y. Sakata, T. Hayase, E. Yonemochi, K. Terada, Solid-state ^{13}C NMR study of indomethacin polymorphism., *International Journal of Pharmaceutics* 318 (2006) 146–53.



**TURUN
YLIOPISTO**
UNIVERSITY
OF TURKU

ISBN 978-951-29-9723-7 (PRINT)
ISBN 978-951-29-9724-4 (PDF)
ISSN 0082-7002 (Print)
ISSN 2343-3175 (Online)